EVALUATION OF SHEAR STRENGTH CHARACTERISTICS OF UNSATURATED UNDISTURBED VOLCANIC ASH SOIL SUBJECTED TO STATIC AND CYCLIC LOADING FOR SLOPE STABILITY ANALYSIS

オクリ, アスフィノ, プトラ

EVALUATION OF SHEAR STRENGTH CHARACTERISTICS OF UNSATURATED UNDISTURBED VOLCANIC ASH SOIL SUBJECTED TO STATIC AND CYCLIC LOADING FOR SLOPE STABILITY ANALYSIS

OKRI ASFINO PUTRA

SEPTEMBER 2020

EVALUATION OF SHEAR STRENGTH CHARACTERISTICS OF UNSATURATED UNDISTURBED VOLCANIC ASH SOIL SUBJECTED TO STATIC AND CYCLIC LOADING FOR SLOPE STABILITY ANALYSIS

九州大学
KYUSHU UNIVERSITY

A THESIS SUBMITTED

IN PARTIAL FULFILLMENT OF THE REQUIREMENTS

FOR THE DEGREE OF

DOCTOR OF ENGINEERING

BY

OKRI ASFINO PUTRA

TO THE

DEPARTMENT OF CIVIL AND STRUCTURAL ENGINEERING
GRADUATE SCHOOL OF ENGINEERING
KYUSHU UNIVERSITY
FUKUOKA, JAPAN
2020

GEOTECHNICAL ENGINEERING LABORATORY
DEPARTMENT OF CIVIL AND STRUCTURAL ENGINEERING
GRADUATE SCHOOL OF ENGINEERING
KYUSHU UNIVERSITY
FUKUOKA, JAPAN

CERTIFICATE

*The undersigned hereby certify that they have read and recommended to the Graduate School of Engineering for the acceptance of this dissertation entitled, "**EVALUATION OF SHEAR STRENGTH CHARACTERISTICS OF UNSATURATED UNDISTURBED VOLCANIC ASH SOIL SUBJECTED TO STATIC AND CYCLIC LOADING FOR SLOPE STABILITY ANALYSIS**" by **OKRI ASFINO PUTRA** in partial fulfillment of the requirements for the degree of **DOCTOR OF ENGINEERING**.*

Dated: July 2020

Supervisor:

_____
Prof. Noriyuki YASUFUKU, Dr. Eng.

Examining Committee:

_____
Prof. Hideki SHIMADA, Dr. Eng.

_____
Assoc. Prof. Kiyonobu KASAMA, Dr. Eng

ACKNOWLEDGMENT

First of all, I am very grateful to Allah the Almighty for His grace I managed to complete my Doctoral degree. During completing the research and Doctoral degree thesis, I have received invaluable help from many people. I would like to reflect on the people who have supported and helped me so much throughout this period.

I would like to express my special appreciation and sincere gratitude to my supervisor Prof. Noriyuki YASUFUKU, for his patience, enthusiasm, motivation, endless encouragement, immense knowledge, and guide throughout my three years of research. I'm so lucky to have a supervisor who is very kind and knowledgeable as he was. He has always been available to advise me even he is busy with daily routine work, make him a great mentor. Thank you for your kindness and for accepting me three years ago to experience your extensive knowledge in Geotechnical Engineering. Besides my advisor, I would like to express my gratefulness to members of the examining committee, Prof. Hideki SHIMADA, and Assoc. Prof. Kiyonobu KASAMA for their treasured time, attentive evaluation, and valuable comments on my works.

I would also like to address my thanks to Assoc. Prof. Ryohei ISHIKURA for his worth guidance and valuable advice during my research and writing of this dissertation. My grateful appreciation is also addressed to Assoc. Prof. Ahmad RIFA'I for patient and kindness in guiding me and precious advice during my research works.

My thousand of appreciation also goes to Research Assistant Prof. Adel ALOWAISY for his crucial contribution, worth guidance and valuable advice during my research work. I would also like to thank and acknowledge with much appreciation

to the academic and technical staff in Geotechnical Engineering Laboratory, both past and present, Mrs. Aki ITO and Mrs. Shinobu SATO. Special thanks and appreciation goes to Mr. Michio NAKASHIMA for his great assistance and technical support in the laboratory testing. My special gratitude is given to present and past research college members in Geotechnical Engineering Laboratory for their friendship and support throughout my time at Kyushu University.

Finally, special appreciation and sincere gratitude from my deep heart to my beloved parents, ZAINAL ARIFIN, S.Pd, and ASNIARLIS, for their continuous support through every step of my life, where without them I would not have made it through my Doctoral degree. Special thanks also go to my brother ONI ASFINO MENDRA, S.Pd, and OTTRIALDO ASFINO WENDRA. In addition, I would like to thank and acknowledge with much appreciation to my fiancée DINNA PUSPITA, S.E., M.M, and “Mimi” IMELDA, S.H for their great support and efforts where without their contribution I would not have been able to reach this point.

ABSTRACT

Major direct triggering factors of slope failures are rainfall and earthquake load which change pore pressure or stress in the slope and directly reduce the soil shear strength. There is a possibility for a combination of rainfall and earthquake load attack the same area especially Indonesia and Japan which has high annual precipitation and high intensity of earthquake event. However, a few studies discussed the combined factor between rainfall and earthquake load induced slope failures.

Recently in April 2016 an earthquake with a magnitude of 7.0 has struck the Kumamoto area and induced several slope cracks and failures. Where one of the massive failures occurred around the Aso mountain area. In addition, after the Kumamoto earthquake, the rainy season followed. Consequently, it will trigger a secondary disaster. Therefore, the investigation of soil shear strength behavior around the Aso mountain area is strongly needed. It was reported that orange-colored pumice deposits and the black volcanic ash soil are dominant in the affected area. Many researchers have studied the Kumamoto slope failures especially the orange-colored pumice. However, small attention was given to the black volcanic ash soil. In Japan, the black volcanic ash soil which is also known as Kuro-boku soil is a problematic type of soil and generally located in the top layer of the natural slopes above the groundwater table with degrees of saturation less than 100 %, which can be classified as an unsaturated state. In addition, for simplicity, the black volcanic ash in this research will be referred to as volcanic ash.

A key parameter in the soil slope stability analysis is estimating the strength of the soil. Reliable analysis can only be performed if the provided shear strength

properties are reliable for the considered soil and representative for the investigated location. Extensive and detailed analysis for both the soil mechanical and hydrological properties is required to acquire a better understanding of slope stability when considering rainfall infiltration. Generally, the existing conventional approaches for soil mechanics are not enough to analyze such kind of complex problem. The limitations can be generally attributed to the simplified assumptions where the soil pore is assumed to be fully saturated with water. Adopting those methods lead to inaccurate estimation of the safety factor and the slip surface location. Therefore, an advanced analysis that incorporates unsaturated soil mechanics is strongly needed. Several approaches and techniques to obtain unsaturated shear strength properties of soil were developed. Laboratory testing for unsaturated soils is difficult, high cost, and time-consuming. Consequently, researchers have been trying to propose empirical and theoretical formulas to predict the unsaturated shear strength properties. However, the accuracy of the obtained data is relatively low in comparison to the data directly determined in the laboratory.

This thesis aims at evaluating the shear strength characteristics of unsaturated undisturbed volcanic ash subjected to static and cyclic loading for slope stability analysis. In order to achieve the aim of this thesis, four main objectives were delineated, starting with identifying the shear strength behavior of the collected unsaturated undisturbed volcanic ash soil under static and cyclic loading. To identify the effect of the soil structure disturbance on the shear strength of the volcanic ash soil by reflecting the pore size distribution differences of undisturbed and disturbed samples. To develop a new suction controlled unsaturated direct shear box apparatus. The developed apparatus differs in its features and testing procedure in comparison to the

conventional testing apparatus. Finally, application of the experimental results in the unsaturated slopes stability analysis subjected to rainfall infiltration and earthquake loading. The thesis was divided into 7 chapters as follows:

Chapter 1 provides an introduction to this research, the current problems, and the motivation to conduct this research. The proposed aim, objectives, and scopes of this thesis are illustrated.

Chapter 2 includes a brief literature review illustrating the research that has been carried out in relation to the scopes considered in this thesis. This chapter starts with the elements of unsaturated soils, and methods to impose the suction before reviewing the existing laboratory testing techniques of unsaturated shear strength of soils. Next, a review of the conventional slope stability analysis is presented.

Chapter 3 presents the shear strength behavior of unsaturated undisturbed volcanic ash soil subjected to static and cyclic loading using the conventional direct shear box apparatus. It was found that under static shearing, unsaturated undisturbed volcanic ash soil samples exhibit a higher apparent cohesion and friction angle in comparison to the saturated samples. Furthermore, the normalized shear stress under cyclic loading of the unsaturated undisturbed sample was found to be relatively larger.

Chapter 4 provides the necessity to evaluate the effect of degree of disturbance on the volcanic ash soil which is directly related to the soil structure characteristics. It was found that the chemical composition of the volcanic ash soil is comprised mainly from allophane which accounts for as high as about 94%. The undisturbed samples exhibit a unimodal pore structure, while the disturbed samples exhibit a bimodal pore structure. Since the pore structure of the disturbed sample is unstable, the static shear strength tends to be lower, and the degradation index value is around 20 % higher than

that of the undisturbed sample. It can be said that disturbed samples do not properly represent the field conditions with significant discrepancies that should be carefully considered when conducting slope stability analysis.

Chapter 5 focuses on the development of a new suction controlled unsaturated direct shear box apparatus. Using the standard soil, the suction-controlled system was confirmed. Furthermore, the shear strength and stiffness of the volcanic ash soil increase with the increase in the soil suction. The soil exhibits more dilative volumetric behavior as the suction increases. The internal friction angle (ϕ) of the volcanic ash soil is relatively constant, and the apparent cohesion (c) increases with increasing the suction value.

Chapter 6 presents the slope stability analysis considering reflecting the obtained experimental results. It was found that the discrepancies of the soil shear strength and the reduction of vertical stress under cyclic loading as represented by the degradation index between undisturbed and disturbed samples affected the safety factor of slope. Furthermore, the safety factor of the slope decreases with increasing the soil layer thickness. However, during precipitation events, the smaller the layer's thickness results in a higher average reduction in the safety factor. In addition, the safety factor of slope in the higher suction value significantly larger. It can be concluded that the suction value provides more resistance to the slope stability.

Chapter 7 summarizes the main findings of this dissertation and delineates the future work

TABLE OF CONTENTS

LIST OF FIGURES

LIST OF TABLES

LIST OF NOMENCLATURE

Nomenclature	Meaning
CD	Consolidated Drained
CU	Consolidated Undrained
d	Soil pore diameter
HAEV	High Air Entry Value
LSF	Local Safety Factor
MIP	Mercury Intrusion Porosimetry
N	Number of cycles
NC	Normally consolidated
OC	Over-consolidated
OCR	Over-Consolidated Ratio
P	Applied pressure
PEG	Polyethylene glycol
PSD	Pore-size distribution
Pc	Yield stress
SEM	Scanning Electron Microscope
SWCC	Soil-water characteristic curve
S_1	Initial normalized vertical stress

S_N	Normalized vertical stress after N cycles
Ts	Surface tension
XRF	X-ray fluorescence analysis
α	Contact angle between the soil particles and the fluid
τ	Shear stress
σ	Vertical stress
δ	Degradation index
δ_{avg}	Average degradation index
τ_p	Peak static shear stress ratio
k_r	The relative permeability
u_w	Pore water pressure
u_a	Pore air pressure
σ'	Effective stress
χ	A soil parameter related to degree of saturation from 0 to 1
ψ	Total suction
π	Osmotic suction
ρ_w	Density of water,
R	Universal (molar) gas constant (R= 8.31432 J/(mol K)
T	Absolute temperature
ω_v	Molecular mass of water vapour

x_w	Molecular fraction of water in the solution
c'	Effective cohesion
ϕ'	Effective internal friction angle
$\sigma - u_w$	Efective normal stress
$u_a - u_w$	Matric suction
ϕ^b	The shear strength contribution due to matric suction
r_1	The small radius of this doughnut-shaped torus
r_2	The distance from the center to the inside wall of the torus
γ_t	The unit weight of soil
H	The soil thickness
β	The slope inclination angle
k_h	The horizontal seismic intensity
k_v	The vertical seismic intensity
σ^s	Suction stress

CHAPTER I

INTRODUCTION

1.1 Introduction

Evaluating the stability of slopes is an important, interesting, and challenging aspect of geotechnical engineering. Concerns with slope stability have driven some of the most important advances in our understanding of the complex behavior of soils. Extensive engineering and research studies were performed over the past 80 years that have provided a sound set of soil mechanics principles with which to face the practical problems of slope stability (Duncan, 2014).

In general, the major direct triggering factors of slope failures can be classified into three types of triggering factors which are rainfall events, earthquake load, and human activity. These triggering factors change the pore pressure or stress in the slope and directly reduce the soil shear strength. Futhermore, the triggering factors from the natural process can be categorized by rainfall events and earthquake load. Fig. 1.1 shows the slope failure in Hita July 2017 which the main triggering factor is the infiltration of rainfall. On the other hand, Fig. 1.2 illustartes the slope failure in Kumamoto April 2016 after an earthquake with a magnitude of 7.0 has struck the Kumamoto area and induced several slope failures around Aso mountain area.

There is a possibility for a combination of rainfall and earthquake load attack the same area especially Indonesia and Japan which has high annual precipitation and high intensity of earthquake event. However, a few studies discussed the combined factor between rainfall and earthquake load induced slope failures.

Fig. 1.1 Slope failure after the torrential rain on July, 2017 in Hita, Oita (The Asahi Shimbun July, 2017)

Fig. 1.2 Slope failure after Kumamoto earthquake April 2016, Japan (https://mainichi.jp/)

1.2 Kumamoto slope failures

Recently in April 2016 an earthquake with a magnitude of 7.0 has struck the Kumamoto area and induced several slope cracks and failures. Where one of the massive failures occurred around the Aso mountain area. In addition, after the Kumamoto earthquake, the rainy season followed. Consequently, it will trigger a secondary disaster. Therefore, the investigation of soil shear strength behavior around the Aso mountain area is strongly needed. It was reported that orange-colored pumice deposits and the black volcanic ash soil are dominant in the affected area. According to (Miyabuchi, 2016; Mukonoki et al., 2016; Kiyota et al., 2017; Chiaro et al., 2018), the critical factor that has led to those failures is the reduction in the total shear strength of the volcanic soil due to the earthquake load. Many researchers have studied the volcanic ash soil in Kumamoto slope failures especially the orange-colored pumice. They investigated the shear strength by a series of static and cyclic triaxial tests. However, small attention was given to the shear strength and characteristic of the black volcanic ash soil.

Black volcanic ash soil which is also known as Kuro-boku soil in Japan is a problematic type of soil (Kitazono et al., 1987; Mshana et al., 1993). Kuro-boku (organic cohesive volcanic ash soil) is usually rich with the allophane minerals, which are characterized by unique problematic properties. As reported by several researchers, black volcanic ash soil has high natural moisture content varying between 65-160% (Kodani et al., 1975; Japan soil inventory, 2016).

The black volcanic ash soil is generally located in the top layer of natural slopes above the groundwater table with degrees of saturation less than 100 % which can be classified as an unsaturated state. It is well known that soil under unsaturated

conditions has higher strength and shear resistance in comparison to the saturated condition. However, under heavy rainfall events, the pore water pressure increases leading to the loss of shear strength and slope instability. The black volcanic ash soil covers approximately 31% of the total area of Japan, mainly within the volcanic zones (Yamauchi, 1983). In Kyushu Island, the black volcanic ash soil is generally found in the Aso mountain area, Kumamoto city. Fig. 1.3 illustrates the distribution of the black volcanic ash soil in Japan. In addition, for simplicity, the black volcanic ash in this research will be called as volcanic ash.

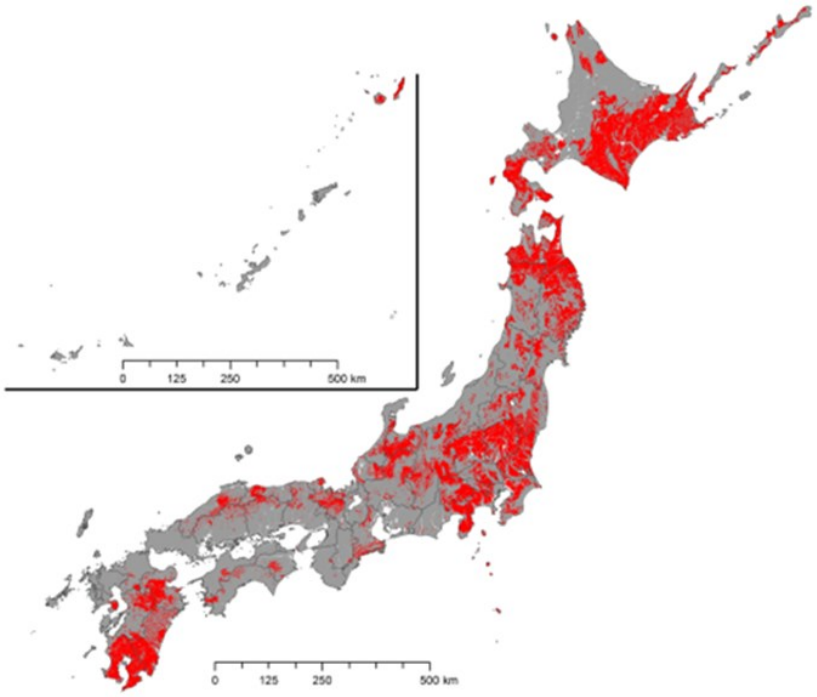

Fig. 1.3 Distribution of the black volcanic ash soil in Japan (Yamauchi, 1983)

A key step in the soil slope stability analysis is measuring or estimating the strengths of the soils. Reliable analysis can only be performed if the provided shear strength properties are appropriate for the considered soil and representative for the investigated location. Extensive and detailed analysis for both the soil mechanical and hydrological properties is required to acquire a better understanding of slope stability

when considering rainfall infiltration. The existing conventional approaches for soil mechanics are not enough to analyze such kind of complex problem. The limitations can be generally attributed to the simplified assumptions where the soil pore is assumed to be either fully saturated with air (dry state) or fully saturated with water. Those methods also ignore the negative pore water pressure above the ground-water table level. Adopting those methods result inaccurate estimation of the safety factor and the slip surface location. Therefore, an advanced analysis that incorporates unsaturated soil mechanics is strongly needed.

Several approaches and techniques to obtain unsaturated shear strength properties of soil were developed. The most reliable and accurate properties can be obtained by conducting direct laboratory testing. Many laboratory testing apparatus for unsaturated shear strength have been developed, such as the unsaturated triaxial and direct shear box apparatus (Ho and Fredlund, 1982, Tom et al., 2008 and Luky 2012). Laboratory testing for unsaturated soils is difficult, high cost, and time-consuming. Consequently, researchers have been trying to propose empirical and theoretical formulas to predict unsaturated shear strength properties, where such an approach is relatively easier than laboratory testing, cheaper and can be done in a relatively short time. However, the accuracy and reliability ot the obtained data are reltively low in comparison to the directly obtained in laboratory data.

1.3 Research Objectives and Original Contributions

This thesis aims at the evaluation of shear strength characteristics of unsaturated-undisturbed volcanic ash soil subjected to static and cyclic loading for slope stability analysis. Furthermore, in this study, the soil was collected at Kumamoto slope failure

2016. In order to achieve the aim of this thesis, the following objectives were delineated:

1. To identify the shear strength behavior of the collected unsaturated undisturbed volcanic ash soil under static and cyclic loading.
2. To identify the effect of the soil structure disturbance on the shear strength of the volcanic ash soil by reflecting the pore size distribution differences of undisturbed and disturbed samples.
3. To develop the new suction controlled unsaturated direct shear box apparatus. The developed apparatus differs in its features and testing procedure in comparison to the conventional testing apparatus. The proposed procedure and apparatus configuration ensure easy testing, relatively short time, and low cost.
4. To analyze the stability of unsaturated slopes subjected to rainfall infiltration and earthquake loading. The analysis considers various loading and rainfall patterns and their influence on the slope stability adopting several slope stability evaluation methods.

Furrthemore, Fig. 1.4 illustrates some new finding is obtained to which are considered as the originality of this research

1.4 Framework and outlines of the thesis

To achieve the above-mentioned objective and scopes, this dissertation is organized in seven chapters following the framework presented in Fig. 1.5. The outlines of each chapter are briefly described as follows:

Chapter 1 presents an introduction to this research, the current problems, and the motivation to conduct this research. The proposed aim, objectives, and scopes of this

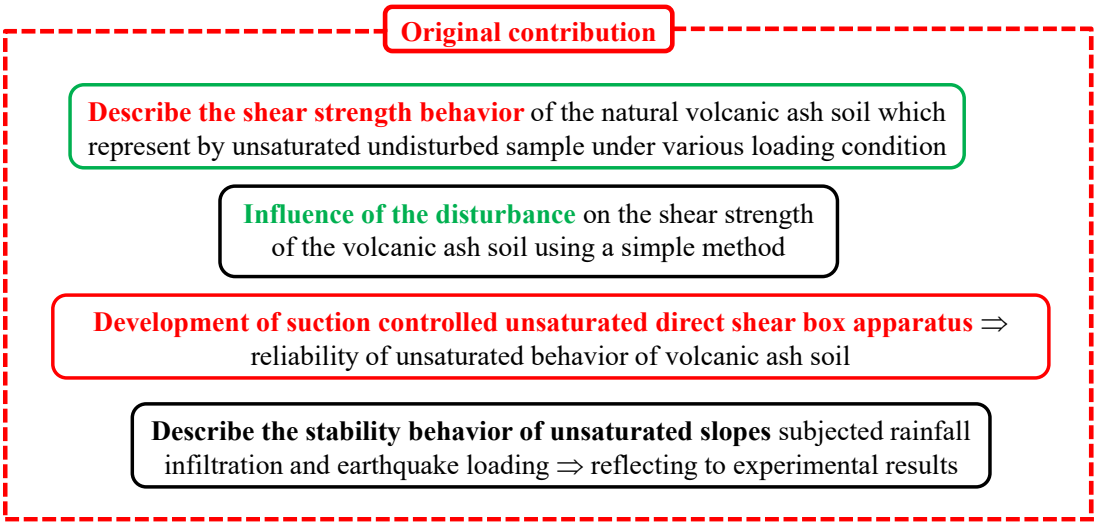

Fig. 1.4 Original contribution

thesis are illustrated. Besides, the original contributions of this study and the framework of the thesis are presented.

Chapter 2 briefly describes the present state of knowledge on unsaturated soils, especially related to the shear strength of unsaturated soils. This chapter starts with the elements of unsaturated soils, then proceeds to define the suction, and methods to impose the suction before reviewing the existing laboratory testing techniques of unsaturated shear strength of soils. Next, a review of the slope stability analysis considering infinite and circular slope is presented. The slope stability subjected to static and earthquake loading is described.

Through Chapter 3, the shear strength behavior of unsaturated undisturbed volcanic ash soil subjected to static and cyclic loading using the conventional direct shear box apparatus are discussed. The principle of direct shear box apparatus including limitations and advantages are explained. Finally, the static shear strength and cyclic shear strength of the black volcanic ash soil are discussed.

Chapter 4 discusses the effect of soil structure disturbance on the shear strength of the volcanic ash soil. The effect of soil structure disturbance on the shear strength

characteristics of the volcanic ash was evaluated using a simple methodology where the disturbance on soil micro-structure was indirectly considered by studying the pore size distribution variations which was reflected from the Soil Water Characteris Curve (SWCC) corresponding to disturbed and undisturbed samples. In addition, the chemical composition of the volcanic ash soil confirmed. The static shear strength of both undisturbed and disturbed samples was evaluated. In addition, the degradation index under cyclic loading and the post cyclic behavior is discussed.

Chapter 5 presents the newly developed suction controlled unsaturated direct shear box apparatus and testing procedure. The principle of new suction controlled direct shear box apparatus including the limitations and advantages are explained. In addition, the unsaturated shear strength results of standard soil are presented as a validation of the developed device. Finally, the unsaturated shear strength of volcanic ash soil with different suction values under the drying process [along the SWCC] was determined.

Chapter 6 discusses the unsaturated slope stability analysis of the volcanic ash soil. In order to get representative results, the Aso mountain area, Kumamoto slope properties was adopted. The infinite slope and circular slope stability were presented under static and earthquake load. Furthermore, the unsaturated shear strength results experimentally obtained using the conventional and the newly developed direct shear box apparatus were used to analyze. Finally, the effect of the rainfall infiltration on the slope stability using HYDRUS FEM software analysis is presented.

Chapter 7 summarizes the main findings of this dissertation, delineates the remaining issues to be solved, and defines goals for future research issues and scopes that need to be investigated in relation to this research main theme.

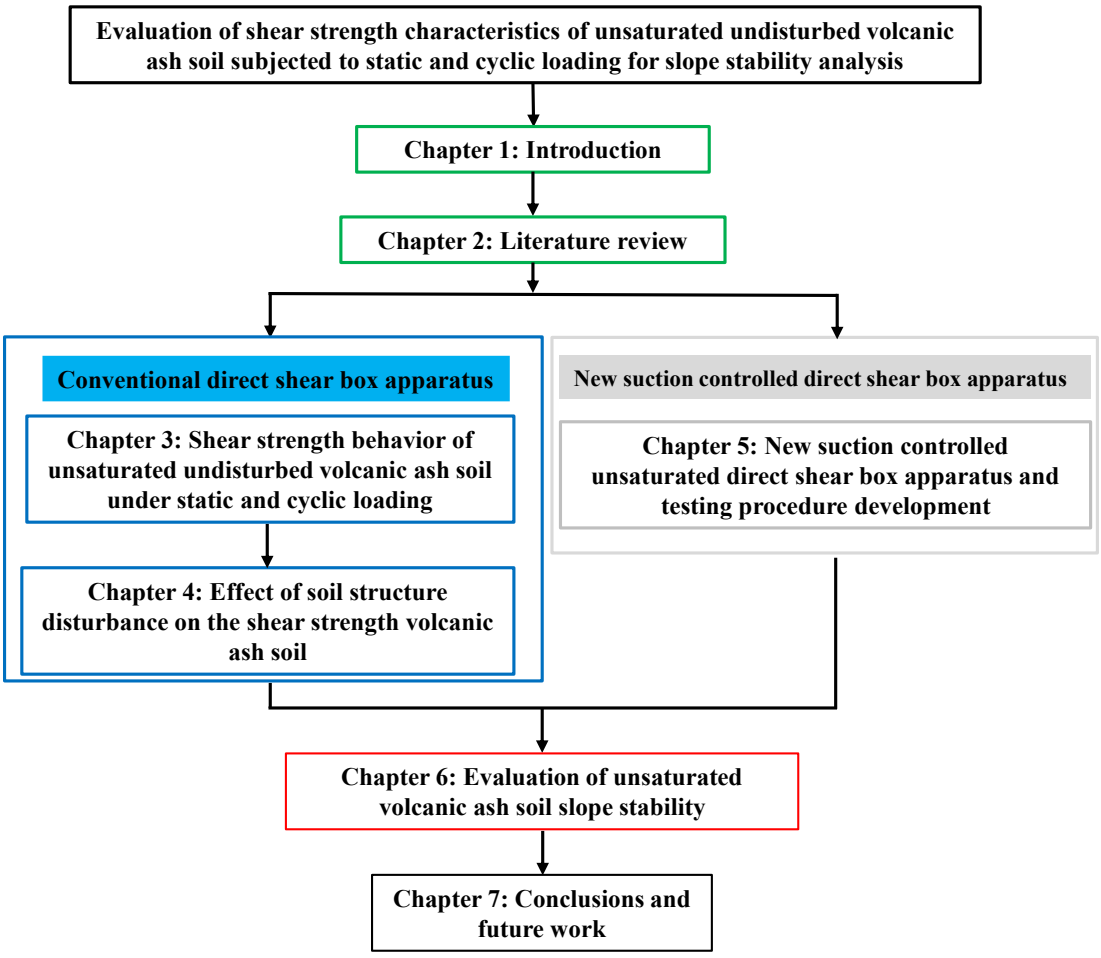

Fig. 1.5 Framework and thesis organization. (Flow chart)

References

Berti, M., Simoni, A., 2012. Observation and analysis of near surface pore pressure measurement in clay-shales slopes. Hydrological Process, 26: 2817-2205

Chiaro, G., Umar, M., Kiyota, T., Massey, C., 2018. The Takanodai landslide, Kumamoto, Japan: insights from post-earthquake field observations, laboratory tests, and numerical analyses. Proc. Geotechnical Earthquake Engineering and Soil Dynamics V, June 10-13, 2018, Austin, Texas: 98-111

Duncan, J.M., Wright, S.G., Brandon, T.L., 2014. Soil strength and slope stability. Wiley

Froude, M.J., Petley, D.N., 2018. Global fatal landslide occurrence from 2004 to 2016. Natural Hazards and Earth System Sciences, 18: 2161-2181

Ho, D.Y.F., fredlund, D.G., 1982. A multistage triaxial test for unsaturated soils. Geotechnical Testing Journal, 5 (1): 18-25

Handoko, L., 2012. Evaluation of hydro-mechanical properties of unsaturated soils and non-woven geotextile under low confining pressure. Kyushu University.

Kitazono, Y., Suzuki, A., Kajiwara, M., Aramaki, S., 1987. Contribution of microstructure to repeated loading effect on compacted allophaneous volcanic ash soil. Soils and Foundations, 27 (4): 23-33

Kiyota, T., Ikeda, T., Konagai, K., Shiga, M., 2017. Geotechnical damaged caused by the 2016 Kumamoto earthquake, Japan. International of Journal Geoengineering Case Histories, 4 (2): 78-95

Kodani, Y., Kuono, S., Uchida, K., 1975. Relation between Organic Matter, Content and Physical Properties of Kuroboku Soil. The Japanese Society of Irrigation, Drainage and Reclamation Engineering, 60: 7-13

Miyabuchi, Y., 2016. Landslide disaster triggered by the 2016 earthquake in and around Minamiaso village, western part of Aso caldera, southwestern Japan. Journal of Geography, 125 (3): 421-429

Mshana, N.S., Suzuki, A., Kitazono, Y., 1993. Effect of weathering on stability of natural slopes in north-central Kumamoto. Soils and Foundations, 33 (4): 74-87

Mukonoki, T., Kasama, K., Murakami, S., Ikemi, H., Ishikura, R., Fujikawa, T., Yasufuku, N., Kitazono, Y., 2016. Reconnaissance report on geotechnical damage caused by an earthquake with JMA seismic intensity 7 twice in 28 h, Kumamoto, Japan. Soils and Foundations, 56 (6): 947-964

Santolo, A.S., Nicotera, M.V., Evangelista, A., 2005. Monitoring matric suction profiles in partially saturated pyroclastic topsoil slopes in Tarantino. Advanced Experimental Unsaturated Soil Mechanics. Taylor and Francis Group.

Thom, R., Shivakumar, V., Brown, J., Hughes, D., 2008. A simple triaxial system for evaluating the performance of unsaturated soils under repeated loading. Geotechnical Testing Journal, 31 (2): 107-114.

Tu, X.B., Kwong, A.K.L., Dai, F.C., Tham, L.G., Min, H., 2009. Field monitoring of rainfall infiltration in a loess slope and analysis of failure mechanism of rainfall induced landslides. Engineering Geology, 105: 134-150

Yamauchi, Y., 1983. Kyushu University Press, in Japanese

CHAPTER II

LITERATURE REVIEW

2.1 Introduction

Soil can be divided into saturated and unsaturated soils in the general field of soil mechanics. Saturated soils are two-phase materials (solid and liquid). Unsaturated soils have three phases, consisting of soil particles, water and air (solid, liquid and gas). The pore spaces are filled with a mixture of two or more media, most commonly water and air in unsaturated soils. The presence of air along with water in the soil voids gives rise to two types of pore pressures: pore air pressure, u_a and pore water pressure, u_w. Interaction between the solid, liquid and gas phases produces the complex hydro-mechanical behavior of unsaturated soils.

This chapter briefly describes the present state of knowledge on unsaturated soils, especially related to the shear strength of unsaturated soils. This chapter starts with the elements of unsaturated soils, then continues by defining suction and methods to impose the suction and reviewing measurements of unsaturated shear strength for laboratory testing. Next, a review of the unsaturated slope stability analysis considering infinite and circular slope is presented. The slope stability under static and earthquake load is described.

2.2 Element of unsaturated soils

The development of soil mechanics for unsaturated soils began about two to three decades after the commencement of study of soil mechanics for saturated soils.

The basic principles related to the understanding of unsaturated soil mechanics were formulated mainly in the 1970s. The development of classical soil mechanics has led to an emphasis on particular types of soils. The common soil types are saturated sands, silts and clays, and dry sands. The general field of soil mechanics can be subdivided into that portion dealing with saturated soils and that portion dealing with unsaturated soils Fig. 2.1. The differentiation between saturated and unsaturated soils becomes necessary due to basic differences in their nature and engineering behavior. An unsaturated soil has more than two phases, and the pore-water pressure is negative relative to the pore-air pressure. Any soil near the ground surface, present in a relatively dry environment, will be subjected to negative pore-water pressures and possible desaturation.

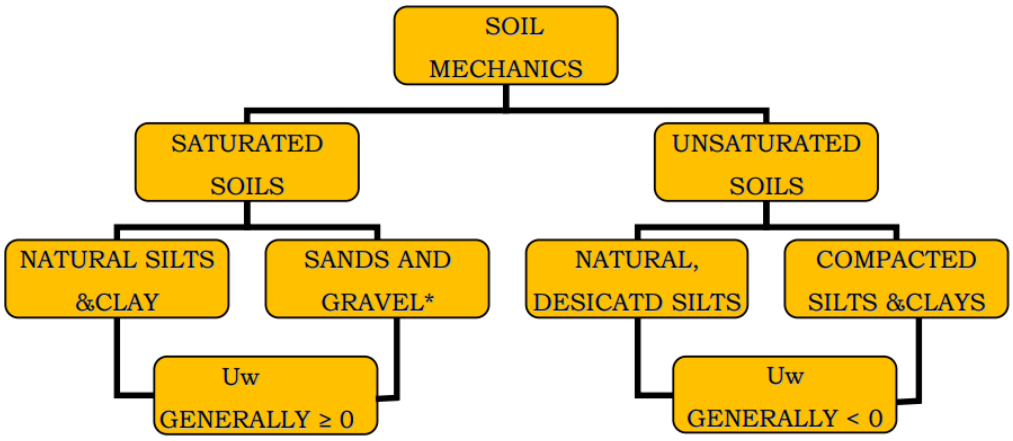

Fig. 2.1 Categorization of soil mechanics (Fredlund and Rahardjo, 1993)

Unsaturated soils have recently gained widespread attention in many studies and construction works all over the world, since many soils near the ground surface are considered unsaturated and also those compacted soils comprising the many earthworks constructed all over the world are most appropriately considered from an

unsaturated soils framework. Classical soil mechanics simply assumed that soil is either fully saturated with water or fully saturated with air (dry soils). Those, classical soil mechanics is also called as saturated soil mechanics. This simplicity considers that soil has two phases only: solid particle and water, or solid particle and air. Ground water table is a boundary to separate those two divisions. Water-saturated soil is located at below ground water table, while at above ground water table, soil is considered as air-saturated (or dry soils).

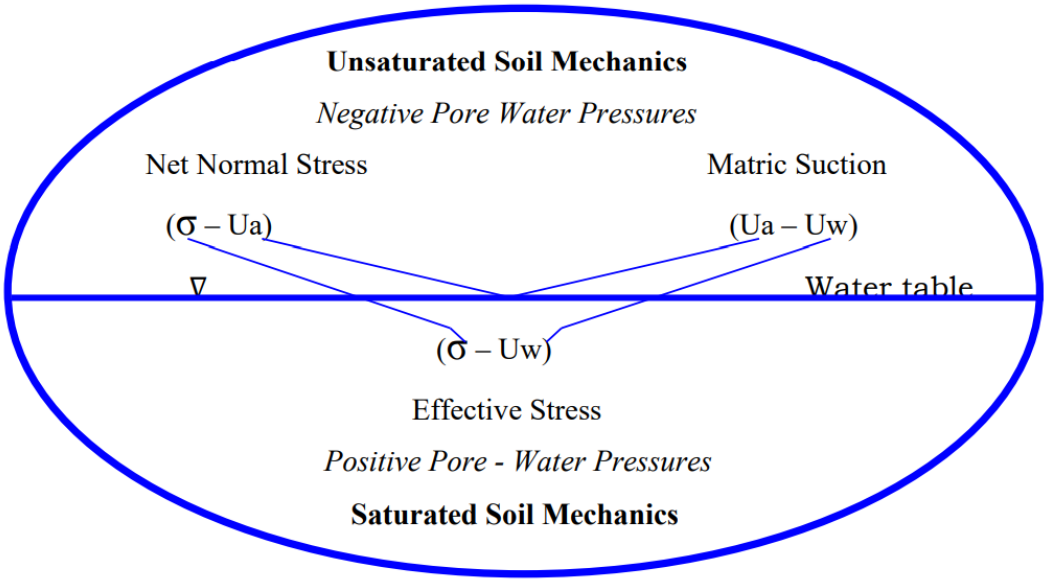

Fig. 2.2 Division of soil mechanics (After Fredlund 1995)

Nowadays, researchers realize that classical two-phase approach is not enough to describe some phenomena in geotechnical engineering problems. In real condition, soil at above ground water table is not air-saturated. Its pore does not consist of air only, but also water. A better approach has been developed recently, which consider soil to have more than two phases. Fredlund (1995) divides soil mechanics into two divisions. One is dealing with saturated soil condition and the other is dealing with unsaturated soil condition. Their nature and engineering behavior are the main factors

that distinguish them. Those two divisions are separated with ground water table as shown in Fig 2.2.

Saturated soil is located below the ground water level. It has two phases and subjected to positive pore water pressure. The soil pore is fully filled with water; thus, it has degree of saturation 100%. The unsaturated soil is located between the ground water table and the ground surface; it has more than two phases and subjected to negative pore pressure. The degree of saturation of an unsaturated soil is ranging from 0 to 100%.

According to Fredlund (1979), an unsaturated soil is consisted of three phases. More recently, the realization of the important role of the air-water interface (i.e., the contractile skin) has warranted its inclusion as an additional phase when considering certain physical mechanisms (Fredlund and Rahardjo, 1993). It is because the air-water interface or contractile skin qualifies as a phase since it has (i) differing properties from that of the contiguous materials and (ii) definite bounding surfaces.

Lu and Likos (2004) divide the unsaturated soil zone into 3 regimes: (i) capillary fringe, which is remain in saturated condition but dealing with negative pore pressure, (ii) funicular regime, which is characterized by continuous water phase and (iii) residual or pendular regime which is characterized by discontinuous water phase. Figure 2.3 describes the condition of air and water of each region in an unsaturated soil. The moisture content of unsaturated soils near surface for certain depth is depended on the climate change, i.e. precipitation and evaporation. Due to precipitation, the moisture content becomes higher and will decrease the negative pore water pressure, while due to evaporation, the effect is at the vice versa.

Fig 2.3 illustrates the type of structure of an unsaturated soil and Fig 2.4

describes a classification of the regions within soil profile together with the evolution of degree of saturation Sr and pore water pressure u_w with depth.

The types of structures of an unsaturated soil can be grouped into three (3) categories depending on the air and water phase continuities (Wroth and Houlsby 1985) Rifa'i 2002, as shown in Fig 2.3. Fig 2.3(a) describes the continuous water and discontinuous air phases. The air phase exists in an occluded form. This category is found in narrow transition zone in natural soil, above the saturated soil with lower degree of saturation Sr and negative pore water pressure uw as shown in Fig 2.4, region (a). The relative permeability k_r of air is zero and k_r of water is almost 1. In other words, this zone is found in unsaturated soils having a very high degree of saturation ("almost saturated").

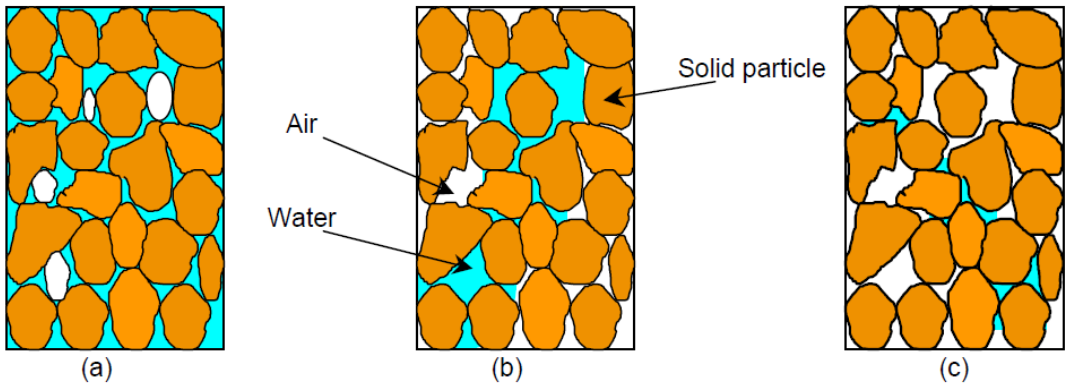

Fig 2.3 Structure types of an unsaturated soil (Wroth & Houlsby 1985): (a) Continuous water and discontinuous air phases; (b) continuous water and air phases; and (c) discontinuous water and continuous air phases.

The second category corresponds to continuous water and air phases (Fig 2.3(b)). This type is found in natural soil above the previously mentioned zone as shown in region (b) of Figure 2.4. This phase has an intermediate degree of saturation and also a negative pore water pressure. The relative permeability of both air and water changes depending on the degree of saturation. The relative permeability of air increases and

the relative permeability of water decreases as the degree of saturation decreases. The pore air pressure may be zero if the continuous air phase is vented to the atmosphere.

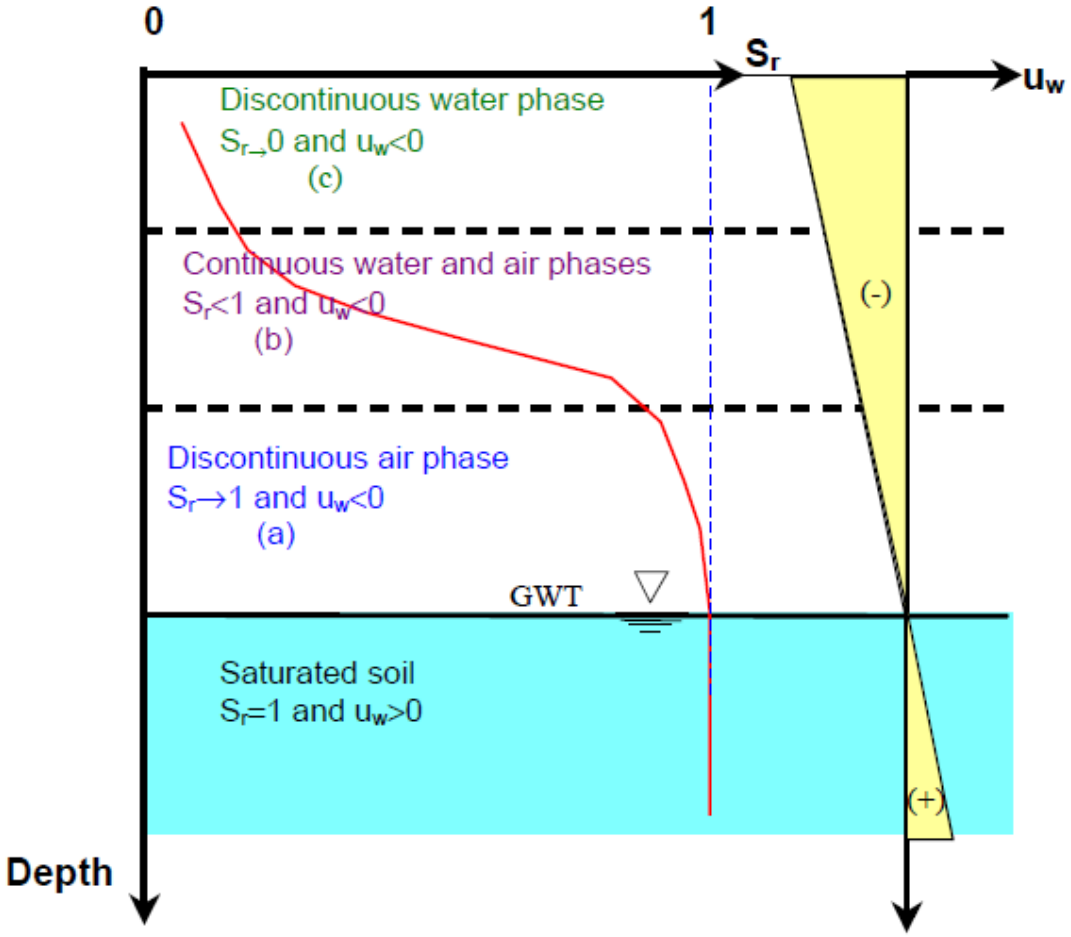

Fig 2.4 Classification of the regions within soil profile.

The last category corresponds to discontinuous water and continuous air phases as illustrated in Fig 2.3(c). In this category, the soil has a very low degree of saturation (see region (c) of Figure 2.4) and the coefficient of permeability of water is almost zero. This situation is commonly found in the top layer at the ground surface in natural soil, but may be strongly influenced by rain infiltration.

2.3 Variables of unsaturated soils

The effective stress variable $\sigma - u_w$ commonly used in saturated soil mechanics is a stress state variable to which saturated soil behavior can be related. The effective stress variable is applicable to sands, silts, or clays and it is independent of the soil properties. The volume change process and the shear strength characteristics of a saturated soil are both controlled by effective stress variables. The effective stress state variable can be independently applied in each of the three Cartesian coordinate directions. In so doing, effective stress takes on the form of a stress tensor (i.e., a 3×3 matrix).

Soil mechanics as a science has been successfully applied to many geotechnical problems involving saturated soils. The success of the stress state variables is largely due to the ability of engineers to uniquely relate observed soil behavior to stress conditions in the soil. Terzaghi (1936) described the stress state variables controlling the behavior of saturated soils as follows: “The stresses in any point of a section through a mass of soil can be computed from the total principal stresses, σ_1, σ_2, σ_3, which act at this point. If the voids of the soil are filled with water under a stress, u_w, the total principal stresses consist of two parts. One part, u_w, acts in the water and in the solid in every direction with equal intensity.

The effective stress concept provides a fundamental basis for studying saturated soil mechanics. The effective stress concept states that all mechanical behavior in a saturated soil is governed by effective stresses (and shear stresses) in each of the three Cartesian coordinate directions. Changes in volume and shear strength are controlled by changes in effective stress. An effective stress change (i.e., a change in pore-water pressure or a change in total stresses) will alter the equilibrium state of a saturated soil.

Consequently, the effective stress variables qualify as stress state variables.

In 1941, Biot proposed a general theory of consolidation for an unsaturated soil with occluded air bubbles. The constitutive equations relating stress and strain were formulated in terms of two independent stress state variables, namely, effective stress $(\sigma - u_w)$ and pore-water pressure, u_w. It was recognized that there needed to be a separation between the effects of total stress changes and pore-water pressure changes when attempting to describe unsaturated soil constitutive behavior.

In 1963, Bishop and Blight reevaluated their previously proposed effective stress equation for unsaturated soils and noted that a variation in matric suction $(u_a - u_w)$ did not result in the same change in soil behavior as did a change in the net normal stress $(\sigma - u_a)$. Laboratory test results were presented using three-dimensional graphical plots with matric suction and net normal stress forming independent orthogonal axes. In other words, net normal stress and matric suction were presented as independent stress variables.

In the 1970s (Fredlund, 1973; Fredlund and Morgenstern, 1977), a theoretical equilibrium analysis was formulated for an unsaturated soil element using concepts consistent with multiphase continuum mechanics. An unsaturated soil had generally been viewed as a three-phase system; however, it was shown that the contractile skin (i.e., the air-water interface) should be introduced as a fourth and independent phase when studying the equilibrium conditions for each phase. The equilibrium analysis on an unsaturated soil element provided justification for the use of independent stress state variables for an unsaturated soil. The soil particles were assumed to be incompressible and the soil was treated as being chemically inert. These assumptions have been historically applied in saturated soil mechanics.

The analysis concluded that any two of three possible stress state variables can be used to describe the stress state of an unsaturated soil. The three possible combinations which can be justified as stress state variables for an unsaturated soil are (1) $(\sigma - u_a)$ and $(u_a - u_w)$, (2) $(\sigma - u_w)$. and $(u_a - u_w)$, and (3) $(\sigma - u_a)$ and $(\sigma - u_w)$. Out of the three possible combinations of stress state variables that can be justified, it is the $(\sigma - u_a)$ and $(u_a - u_w)$ combination that received the widest acceptance in formulating unsaturated soil mechanics problems.

The stress state variables for an unsaturated soil take on the form of two independent stress tensors when considering a three-dimensional Cartesian coordinate system. The proposed stress state variables for unsaturated soils were experimentally tested by Fredlund (1973a) and subsequently used to formulate constitutive equations to describe shear strength behavior and volume change behavior.

Stress tensors that contain stress state variables form the basis for developing a science for both saturated and unsaturated soils. It is possible to write first, second, and third stress invariants for each stress tensor. While it is not imperative that the stress invariants be used in developing constitutive models, the stress invariants should be given consideration because all three Cartesian coordinates are independently taken into consideration.

In summary, it is the two independent stress tensors containing stress state variables [e.g., net normal stress $(\sigma - u_a)$, matric suction $(u_a - u_w)$, and shear stresses] that form a fundamental basis for the development of a science for unsaturated soil mechanics. Constitutive relationships connecting various state variables can then be used in conjunction with soil properties (and soil property functions) to solve practical engineering problems. All proposed constitutive

relationships must be tested for uniqueness in the laboratory on a variety of soil types. The laboratory equipment must be able to independently control each stress component of the stress state variables.

There are theoretical and formulation limitations associated with the use of effective stress equations. Little attention is given to these equations; however, a brief summary is given of effective stress equations that have been proposed.

The oldest and most-often-referred-to single-valued effective stress relationship is that proposed by Bishop (1959). The equation is commonly referred to as Bishop's effective stress equation for unsaturated soils and has the form

$$\sigma' = (\sigma - u_a) + \chi (u_a - u_w) \quad (2.1)$$

Where:

σ' = effective stress

χ = a soil parameter related to degree of saturation and ranging from 0 to 1.

Bishop's equation relates net normal stress to matric suction through the incorporation of a single-valued soil property, χ . Bishop's equation should not be referred to as a fundamental description of stress state for an unsaturated soil. The equation contains a soil property and should be referred to as a constitutive equation. Within the context of continuum mechanics it is not proper to elevate the Bishop equation to the status of a stress state variable for an unsaturated soil.

Morgenstern (1979) explained the limitations of Bishop's effective stress equation as follows: Bishop's effective stress equation "proved to have little impact on practice. The parameter, χ, when determined for volume change behavior was found to differ when determined for shear strength. While originally thought to be a function

of degree of saturation and hence bounded by 0 and 1, experiments were conducted in which χ was found to go beyond these bounds. The effective stress is a stress variable and hence related to equilibrium considerations alone."

Morgenstern (1979) went on to explain: Bishop's effective stress equation "contains the parameter, χ, that bears on constitutive behavior. This parameter is found by assuming that the behavior of a soil can be expressed uniquely in terms of a single effective stress variable and by matching unsaturated soil behavior with saturated soil behavior in order to calculate χ. Normally, we link equilibrium considerations to deformations through constitutive behavior and do not introduce constitutive behavior into the stress state."

Edlefsen and Anderson (1943) referred soil suction as the free energy state of soil water (Fredlund and Rahardjo, 1993). Soil suction or total suction has two components, namely, matric suction and osmotic suction. Matric suction is defined as the difference between the pore-air pressure, u_a, and the pore-water pressure, u_w, while the osmotic suction is a function of the amount of dissolved salts in the pore fluid. The relation of total, matric and osmotic suction is described in Equation 2.2.

$$\psi = (u_a - u_w) + \pi \qquad (2.2)$$

Where:

ψ = effective stress.

π = osmotic suction.

The definition of matric suction is identical with the capillary pressure u_c, so notations of capillary pressure and matric suction are equivalent. The matric suction component is commonly associated with the capillary phenomenon of the surface

tension of water. The value of capillary pressure u_c is dependent on the surface tension *Ts* and the radius of curvature of the meniscus *R*. The radius of curvature of the meniscus *R* depends on the radius of the capillary tube *r* and the contact angle α (Fig 2.5). The relationship between the surface tension and the capillary pressure, u_c is written with Laplace's equation as follows, for the case of a capillary tube:

$$s \equiv u_c = (u_a - u_w) = \frac{2T_s cos\alpha}{r} \tag{2.3}$$

Where:

u_a = the pore air pressure,

u_w = the pore water pressure,

T_s = surface tension of water,

r = radius of the capillary tube,

α = contact angle.

The capillary height rise is defined as:

$$h_c = (u_a - u_w) = \frac{2T_s cos\alpha}{r\gamma_w} \tag{2.4}$$

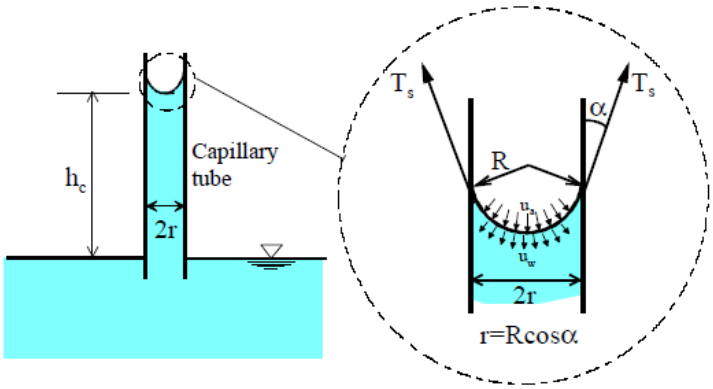

Fig 2.5 Physical model and capillary phenomenon.

According to equation (2.3) the matric suction is inversely proportional to the radius of the capillary tube. In other words, the matric suction increases with smaller pore spaces (voids). So a higher matric suction can develop in clay soils than in granular soils.

The osmotic suction (or osmotic pressure) π, is a function of dissolved salt concentration in the pore fluid. Equation of osmotic suction is written as (Li 2000):

$$\pi = -\frac{\rho_w RT}{\omega_v} \ln x_w \qquad (2.5)$$

Where:

ρ_w = density of water,

R = universal (molar) gas constant (R= 8.31432 J/(mol K)),

T = absolute temperature,

ω_v = molecular mass of water vapour,

x_w = molecular fraction of water in the solution.

A change in osmotic suction is generally less significant than a change in matric suction (Fredlund et al. 2001). In other words, a change in the total suction is essentially caused by a change in the matric suction. In the case where the soil salt content is altered by chemical contamination, however, the effect of the osmotic suction on the soil behaviour may become significant. The change in osmotic suction must be taken into account in this type of problems.

As it is an important parameter, several devises and methods are developed to measure both total and matric suction. Several methods can be used to measure both total and matric suction.

2.3.1 Methods of Applying Suction: Axis-Translation and Osmotic Techniques

The methods for applying matric suction in laboratory testing of unsaturated soils can be divided into two groups: axis-translation and osmotic techniques. Both techniques are briefly presented as follows.

Axis-Translation Technique

The basic principle of the axis-translation technique is to elevate the total stress, the pore air pressure and the pore water pressure by an equal amount so that the pore water pressure is raised to a positive value (relative to atmospheric pressure) and can then be controlled or measured.

The axis translation technique is by far the most common method used in geotechnical engineering for applying controlled value of suction to a soil sample. This technique was first developed by Hilf (1956). Subsequently several researchers have reported successful use of the axis translation technique for the study of soil behavior during shearing tests and also of the variation of volumetric behaviour (e.g. Matyas and Radhakrishna 1968, Escario and Saez 1986, Bishop and Donald 1961, Ho and Fredlund 1982).

In order to keep a constant matric suction, the axis-translation technique can be applied in different ways: increase the air pressure u_a while the pore water pressure u_w is kept constant or lower the pore water pressure while keeping the air pressure constant. Lowering the pore water pressure is limited, since the cavitation effect will appear when the pore water pressure approaches –1 atm (i.e. –101.3 kPa) (Fredlund and Rahardjo, 1993). So, it is easier to impose suction by rising the air pressure with respect to the pore water pressure. This method is usually called the imposed air pressure method.

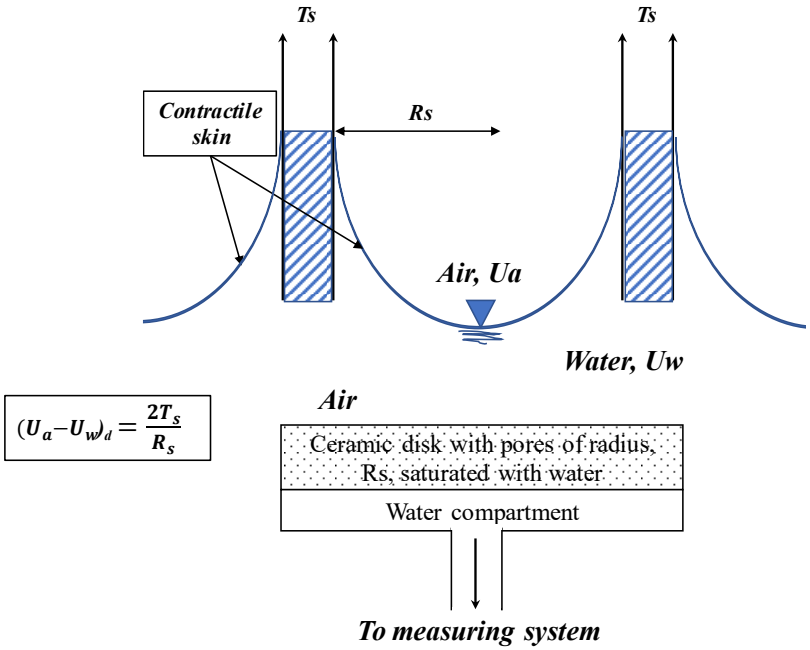

Fig 2.6 Scheme of operating principle of a high air entry ceramic disk (after Fredlund and Rahardjo 1993).

The use of the axis translation technique requires the control of the pore air pressure through a saturated high air-entry ceramic disk. The high air-entry ceramic disks have small pores of relatively uniform size. They act as a membrane between air and water as shown in Figure 2.6. They are used to prevent air getting into the pore water measuring system. The contractile skin acts like a thin membrane joining the small pores of radius of curvature *Rs* on the surface of the high air-entry ceramic disk. The difference between the air pressure u_a above the contractile skin and the water pressure u_w below the contractile skin is defined as matric suction *s*.

Once the ceramic disk is saturated with water, air cannot pass through the ceramic disk due to the ability of the contractile skin to resist the flow of air. Continuity between the water in the soil and the water in the ceramic disk is necessary in order to correctly establish the matric suction. The matric suction in the soil sample must not exceed the air-entry value of the ceramic disk.

The axis-translation method has a limitation since the maximum value of suction that can be achieved is less than 1500 kPa, due to the capacity of the testing equipment. Another limitation is that the applied air pressure must not exceed the capacity of the air entry value of the ceramic disk (properties of high air-entry ceramic disk). However, the smaller the pore size of the ceramic disk, the greater the capacity of the air entry value, and of course, the longer the time to reach equalization.

Osmotic Techniques

The osmotic technique was first developed by Kassif and Ben Shalom (1971) in geotechnical engineering. Subsequently, it has been used by the CERMES research group in Paris on Jossigny silt (Cui and Delage 1996). The osmotic technique of applying suction involves the use of an aqueous solution such as Polyethylene glycol (PEG) separated from the soil sample by a semi permeable membrane. The semi permeable membrane allows the passage of small molecules such as water but is impermeable to larger molecules such as PEG.

The sample is put in contact on both the bottom and top surfaces with the semi-permeable membrane. The PEG solution in the reservoir is circulated around both bases of the cell and the top cap by a closed-circuit system.

The osmotic technique is used to control the matric suction, rather than the osmotic suction, within the soil. The value of the suction depends on the concentration of the solution. The concentration of dissolved ions in the prepared solution is different from the concentration in the soil water. This leads to a concentration gradient across the membrane. The concentration gradient causes water to flow from the lower concentration side to the higher concentration side, but this in turn gives rise to lower hydrostatic pressure in the soil water. The flow of water continues until equilibrium is

established between the concentration imbalance and the imbalance of pressure head, and therefore, the matric suction is equal to the difference of the osmotic suction between the chemical solution and the soil water.

The most commonly used chemical for preparation of the chemical solution is Polyethylene glycol (PEG), primarily because of its large molecule-size. The desired value of suction can be applied by using different concentration of PEG, i.e. PEG6000 and PEG20000.

The main advantage of the osmotic technique is to prevent cavitation within the soil pores as the pore water pressure within the soil is maintained at a negative value. The limitation of this method is that, in its current form, it cannot be used for varying suction in a continuous manner, since suction changes are applied in step by exchanging containers of PEG solution with different concentrations. Another limitation is possible migration of soil salts dissolved in the soil water from the soil sample to the PEG solution and the impact of this change in soil water chemistry on the soil properties (Dineen and Burland 1995).

2.3.2 Methods of Measuring Suction: Filter Paper and Tensiometer

Several methods for suction measurement have been developed over the past few years. This section presents the most commonly used instruments to measure soil suction: the filter paper and the tensiometer.

Filter Paper

The filter paper is allowed to absorb moisture taken from a soil sample and when equilibrium is reached, the suction in the filter paper will be equal to the suction in the soil. Two types of filter paper commonly used are Whatman No.42 and Scheicher and

Schuell No.589 (Ridley and Wray 1995).

The advantage of this method is its simplicity. A variety of equipment exists for making in contact filter paper for the laboratory (Ridley 1995). In the field, the only acceptable method of using the filter paper is the no contact filter paper, thereby only the total suction is measured (Crilly et. al 1991). More details on this method can be found in American standard ASTM D5298 (1994).

Tensiometer

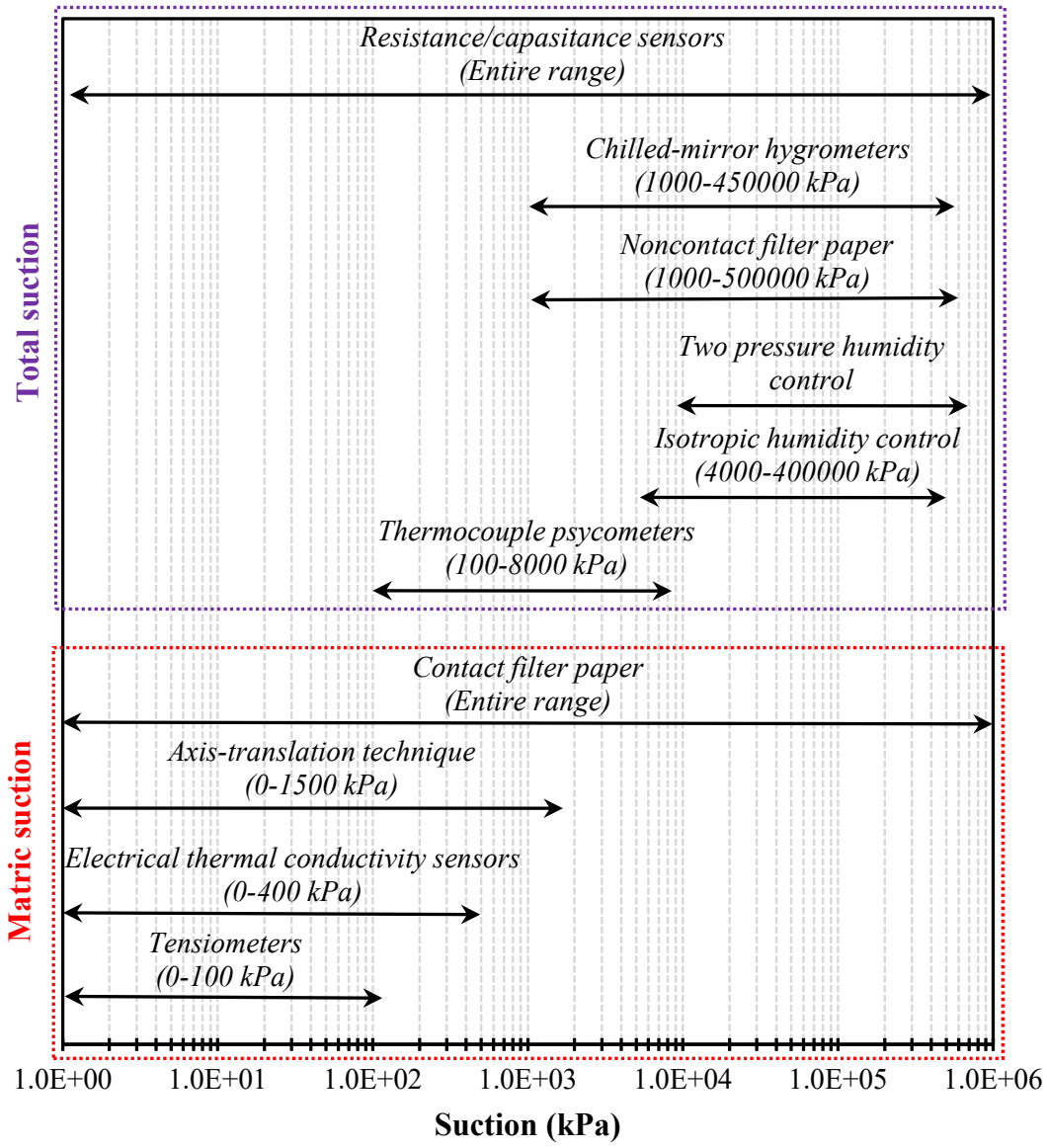

Fig 2.7 Approximation of suction range of various methods (Lu and Likos, 2004)

A tensiometer measures the negative pore water pressure in the soil. It is principally used in the field but has found some application in the laboratory (Tadepalli and Fredlund, 1991). It consists of a high air entry porous ceramic cup connected to a pressure-measuring device through a small bore tube. The tube and the cup are filled with de-aired water. At equilibrium, no further flow of water will occur between the soil and the tensiometer. The water in the tensiometer will have the same negative pressure as the pore water in the soil. The maximum range of operation of the tensiometer is between zero and approximately −100kPa (cavitation effect). Lu and Likos (2004) summarize the approximation of suction range of various methods presented in Fig 2.7.

2.4 Unsaturated soils shear strength

The shear strength of a saturated soil can be described using the Mohr-Coulomb failure criterion and the effective stress variable (Terzaghi, 1936)

$$\tau = c' + (\sigma - u_w) \tan \phi' \quad (2.6)$$

Where:

τ = the shear strength of saturated soil

c' = effective cohesion

ϕ' = effective internal friction angle

$\sigma - u_w$ = effective normal stress

The line tangent to the Mohr circles is commonly referred to as a failure envelope since it represents possible combinations of shear stress and effective normal stress on the failure plane at failure.

The pore-water pressure is isotropic and therefore acts equally on all planes. The shear stress described by the failure envelope indicates the shear strength of the soil for each effective normal stress. The failure envelope for a saturated soil is obtained by plotting a line tangent to a series of Mohr circles representing the stress state at failure. The slope of the line defines the effective angle of internal friction, ϕ', and its intercept on the ordinate is called the effective cohesion, c'. The direction of the failure plane in the soil is obtained by joining the pole point to the point of tangency between the Mohr circle and the failure envelope. The tangent point on the Mohr circle at failure represents the stress state on the failure plane at failure.

The empirical equation containing the material parameters together with the effective stress define the failure conditions of the saturated soils. As it was noted, the pore water pressure in a saturated soil is compressive and isotropic. The pore pressure in saturated soils totally contributes to decrease in the total stress according to the Terzaghi's effective stress principle. However, the pore water pressure is negative in the pores of unsaturated soils due to the solid-water-air interface effects. The behavior of unsaturated soils is highly complex due to the interfacial effects between different phases in soil. The relative amount pore water or pore air and corresponding pressures have direct bearing on the state of stress acting at particle level.

The contribution of this negative pore water pressure on the total stress is less than the contribution of positive pore-water pressure in saturated soils. Terzaghi's stress state variable, therefore, cannot capture the shear strength behavior of unsaturated soils for the same reason. Therefore, the stress state in unsaturated soils is more complex. A simple conceptual analysis of stress distribution in the soil is described here considering different cases to understand the effect of degree of

moisture content on the stress state.

Bishop (1959) proposed an effective stress equation for unsaturated soils and suggested that it can be used for interpreting the shear strength of unsaturated soil extending the same philosophy as Terzaghi (1943) used for the shear strength of saturated soil.

$$\tau = c' + [(\sigma_n - u_a) + \chi(u_a - u_w)] \tan \phi' \quad (2.7)$$

Where:

τ = the shear strength of unsaturated soil

c' = effective cohesion

ϕ' = effective internal friction angle

$\sigma_n - u_a$ = net normal stress

$u_a - u_w$ = matric suction

χ = parameter dependent on the degree of saturation (between 0 and 1)

Bishop et al. (1960) and Bishop & Donald (1961) determined the shear strength of unsaturated soil and interpreted them using Equation 2.7. Jennings & Burland (1962) suggested that Equation 2.7 may pose some limitations to simultaneously interpret the mechanical behavior of unsaturated soils (i.e. for explaining both the shear strength and volume change behavior). Bishop & Blight (1963) reevaluated the proposed effective stress equation (i.e. Equation 2.7) and noted that, "*a variation in matric suction,* $(u_a - u_w)$ *did not result in the same change in effective stress as did a change in net normal stress,* $(\sigma - u_a)$*"*. Several investigators realized that the influence of $(\sigma - u_a)$and $(u_a - u_w)$ should be considered as independent stress

state variables for interpreting the engineering behavior of unsaturated soils (Bishop & Blight 1963, Burland 1964, 1965, Matyas & Radhakrishna 1968).

Fredlund et al., 1978 formulated a linear form of the shear strength for an unsaturated soil in terms of independent stress state variables. Any two of three possible stress state variables can be used to write an appropriate shear strength equation. The stress state variables $(\sigma - u_a)$ and $(u_a - u_w)$ have been found to be the most practical combination of stress state variables for solving practical engineering problems. The linear form of the shear strength equation can be written as follows when using $(\sigma - u_a)$ and $(u_a - u_w)$ as the stress state variables:

$$\tau = c' + (\sigma_n - u_a) \tan \phi' + (u_a - u_w) \tan \phi^b \quad (2.8)$$

τ = the shear strength of unsaturated soil

c' = effective cohesion

ϕ' = effective internal friction angle

$\sigma_n - u_a$ = net normal stress

$u_a - u_w$ = matric suction

ϕ^b = the shear strength contribution due to matric suction

The shear strength contribution due to matric suction, ϕ^b was initially assumed to be linear based on the analysis of experimental results published in the literature prior to 1978, which were mostly conducted on clayey type of soils over a limited range of suction (i.e. typically lower than 200 kPa). As many fine grained soils do not significantly desaturate nonlinearly in this suction range, a reasonable approximation was made and the variation of shear strength with respect to matric suction was represented by an average constant slope, tan ϕ^b. This concept was similar to using a

constant slope, tan ϕ^b for interpreting the saturated shear strength. The tan ϕ^b value was found to be lower than tan ϕ' for many tested unsaturated soils. Comprehensive experimental studies by several investigators conducted over a large suction range using more elaborate testing equipments have shown that the shear strength variation with respect to suction beyond a certain value was nonlinear (Escario & Sáez 1987, Gan & Fredlund 1988). The shear strength increases at the same rate as for an increase in total stress up to a certain suction value (i.e. $\phi^b = \phi'$), which from later studies was recognized to be equal to the air-entry value of the soil (Fredlund & Rahardjo 1993). Soils begin to desaturate when the suction values are greater than the air-entry value and the shear strength contribution due to suction becomes less than ϕ' (i.e. $\phi^b < \phi'$).

The extended Mohr-Coulomb failure envelope may be a planar surface or it may be somewhat curved. The theory is first presented with the assumption that the failure envelope is planar and can be described by Equation 2.8. A curved failure envelope can also be described by Equation 2.8 for limited changes of the stress state variables.

Furthermore, Fig 2.8 shows a planar failure envelope that intersects the shear stress axis, giving a cohesion intercept c'. The envelope has slope angles of ϕ' and ϕ^b with respect to $(\sigma - u_a)$ and $(u_a - u_w)$ axes, respectively. Both angles are assumed to be constants. The cohesion intercept c' and the slope angles ϕ' and ϕ^b are the strength parameters used to relate shear strength to the stress state variables. The shear strength parameters represent many factors which have influenced the results of the shear strength test. Some of these factors are density, void ratio, degree of saturation, mineral composition, stress history, and strain rate. In other words, these factors have been combined and are expressed mathematically in terms of the shear

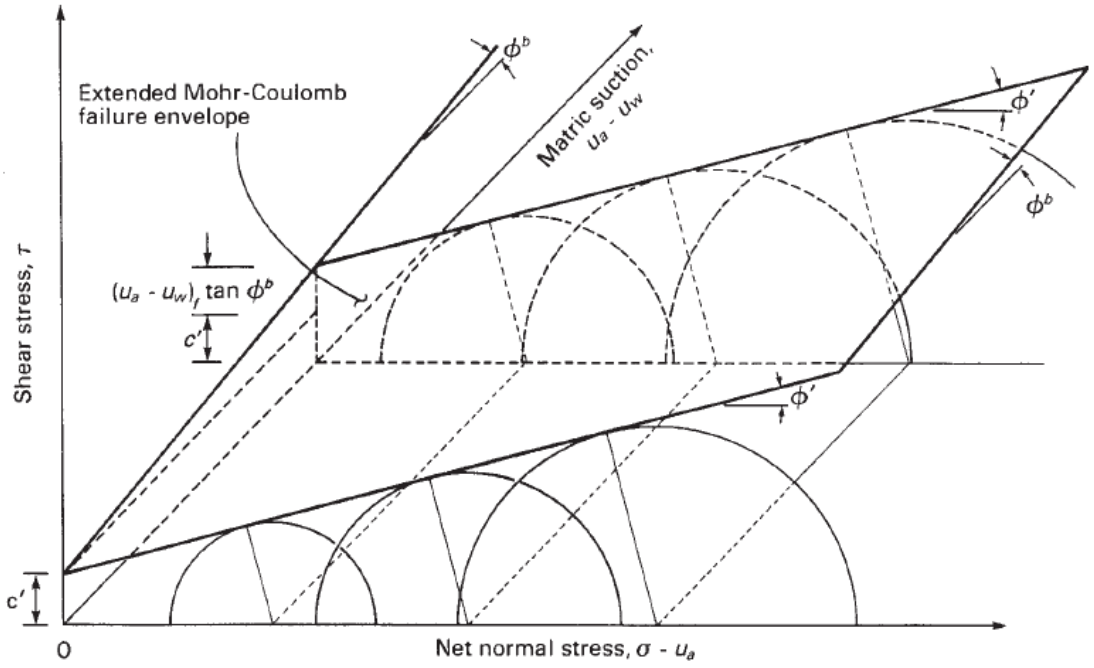

Fig 2.8 The extended Mohr-Coulomb failure envelope for unsaturated soil

strength parameters. The mechanical behavior of an unsaturated soil is affected differently by changes in net normal stress than by changes in matric suction (Jennings and Burland, 1962). The increase in shear strength due to an increase in net normal stress is characterized by the friction angle ϕ'. The increase in shear strength caused by an increase in matric suction is characterized by the angle ϕ^b when assuming linear failure conditions.

2.5 Measurement unsaturated soil shear strength

Shear strength determination of unsaturated soils in laboratory has been the subject matter in geotechnical engineering for several decades. However, the measurement and analysis of strength of field soils is highly complex. Furthermore, the shear strength of unsaturated soils has been studied in the laboratory using both triaxial and direct shear testing equipment. Conventional triaxial and direct shear equipment requires that a number of modifications be made to the equipment prior to

attempting to test unsaturated soils. Several factors related to the nature of an unsaturated soil must be considered when modifying the equipment. The presence of air and water in the pores of the soil causes the testing procedures and techniques to be considerably more complex than when testing saturated soils. The primary modifications are associated with the independent measurement and/or control of the pore-air and pore-water pressures. The pore-water pressure is usually negative (gauge) and can result in cavitation of the water in the measuring system when the water pressures are too low.

2.5.1 Triaxial test on unsaturated soils

Triaxial test is the common test used to measure the shear strength of unsaturated soils in the laboratory. The triaxial test is usually conducted on a cylindrical soil sample enclosed in a rubber membrane, placed in the triaxial cell. The commonly known technique to control the suction in triaxial is axis-translation technique. Osmotic method is used as an alternative to axis-translation technique for controlling matric suction in triaxial device.

Hoyos et al. (2008) has reported that in most existed literature, proposed triaxial apparatus for unsaturated soils features High Air Entry Value (HAEV) ceramic disk at the pedestal and a coarse porous stone at the top cap. This configuration is mainly used for independently applying pore water pressure and pore air pressure using axis translation technique (Hilf, 1956). In this technique, positive water and air pressure is applied to maintain matric suction of the specimen. Matric suction is defined as the difference between pore air pressure and pore water pressure. Ho and Fredlund (1982) modified conventional triaxial apparatus in order to be able to conduct unsaturated

soils test. Fig 2.9 shows the Ho and Fredlund (1982) modified conventional triaxial apparatus.

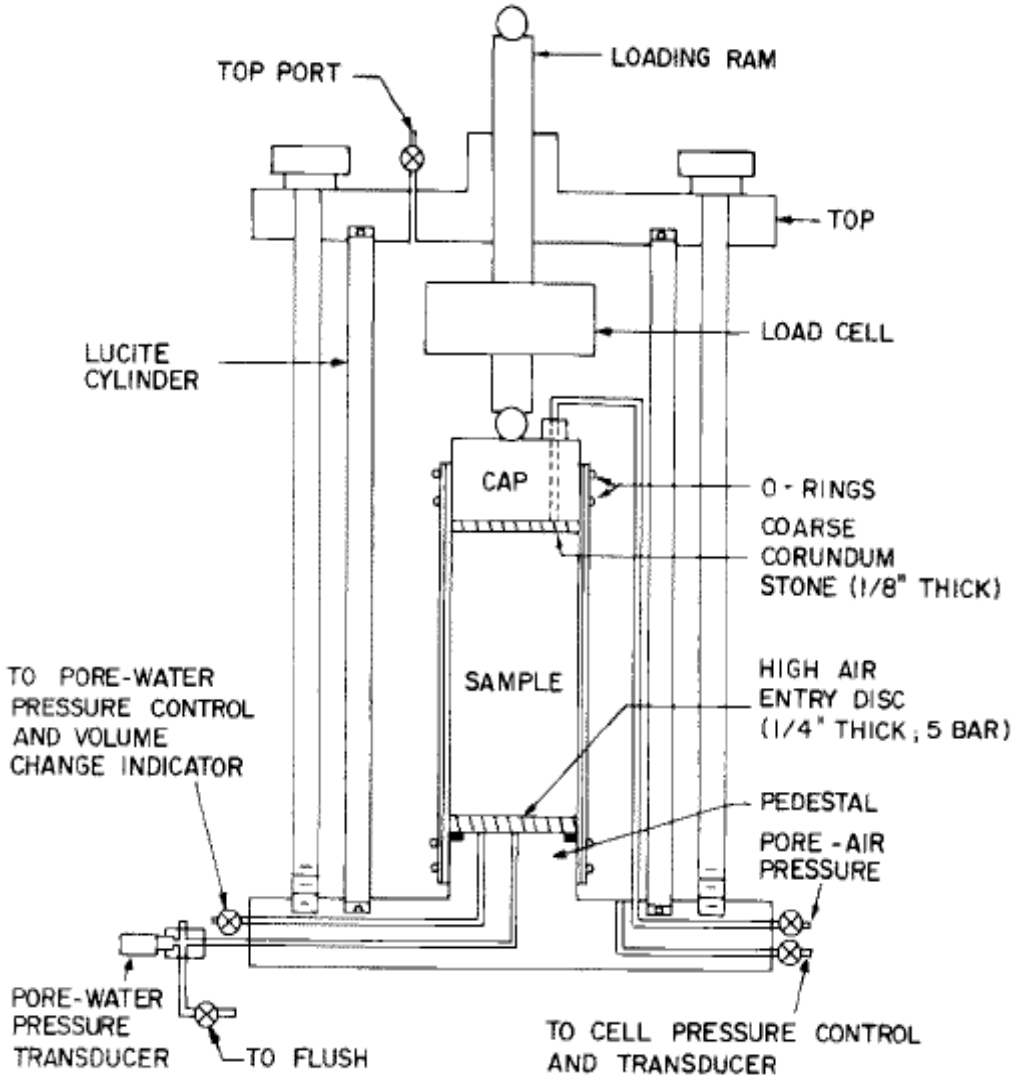

Fig 2.9 Modification of conventional triaxial apparatus for unsaturated soil test (Ho and Fredlund, 1982)

In addition, the triaxial device for unsaturated soil testing consists of conventional triaxial cell, pressure controllers, transducers, total volume change measuring system, and an indicator to measure (Ng and Menzies, 2007). The pressure controllers are used for controlling triaxial cell pressure, pore air pressure, back pressure, and axial stress independently. The transducers are required for measuring

axial force by internal load cell, axial displacement by LVDT, total volume change by differential pressure transducer, cell pressure, pore water pressure, and pore air pressure. These controllers are connected to computer by an interface card. The shear strength of the soil under various stress paths and drainage conditions can be established at any given matric suction and normal stress values using the attached controllers and transducers to the conventional triaxial cell apparatus.

The cylindrical unsaturated soil sample is seated in good contact with HAE disk for establishing external hydraulic connection with soil pore water to the water compartment, provided at the bottom of the pedestal. The water compartment also serves as a channel for flushing trapped air bubbles due to air diffusion. On the top of the soil sample, i.e. between the soil sample and the top cap, for establishing external connection with soil pore air. The soil sample may be consolidated under isotropic effective confining pressure, if required. Desired matric suction is applied to the soil sample by controlling the pore water and pore-air pressures through HAE disk and coarse porous disk respectively, prior to shearing process. The established matric suction is measured at equilibrium as the difference between the applied air pressure and the pore water pressure.

On the other hand, osmotic technique is an alternative to the axis-translation technique to control matric suction for testing unsaturated soil strength in triaxial apparatus. Osmotic technique is gaining popularity to circumvent the problems associated with axis-translation technique. Fig 2.10 provides the schematic diagram of triaxial apparatus using osmotic method for controlling the suction.

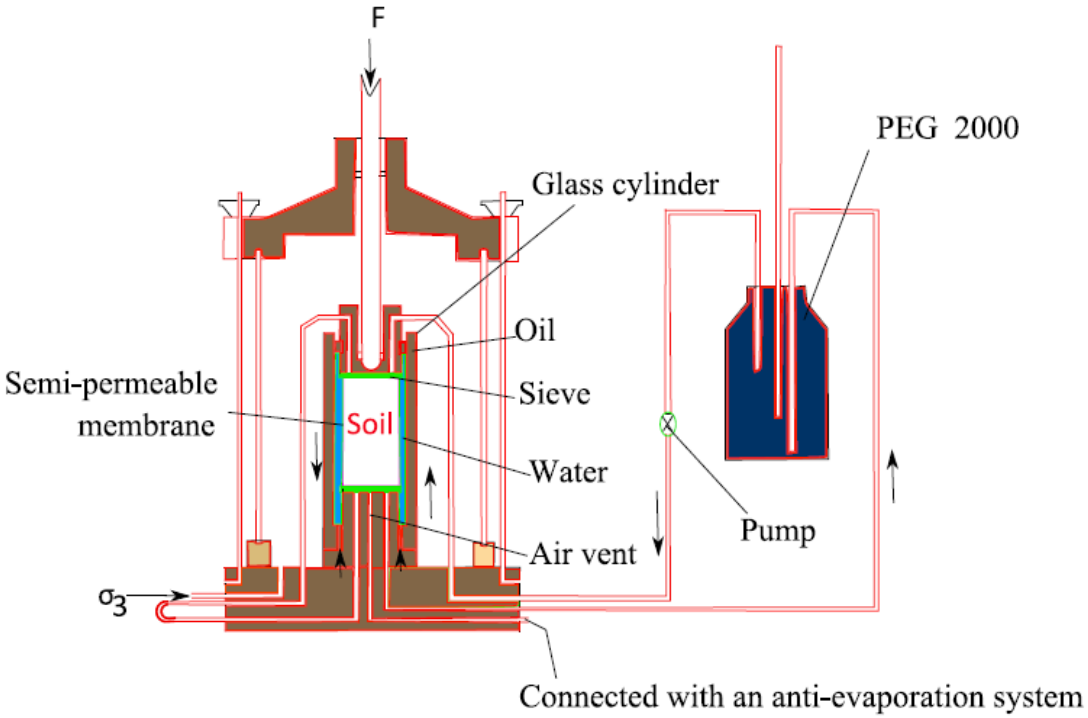

Fig 2.10 Modification of conventional triaxial apparatus osmotic technique for unsaturated soil test (Ng and Chen, 2005 and 2006)

A semi-permeable membrane separates the soil specimen and osmotic solution as shown in the figure. Semi-permeable membranes permeate water molecules but prevent the permeation of larger solute molecules and soil particles. It develops an osmotic suction across the membrane. The difference of osmotic suction across the membrane is equal to the difference of matric suction on both sides of membrane. The maximum applied matric suction depends on the concentration of the solute, type of solute, and performance of semi-permeable membranes. Polyethylene glycol (PEG) is the commonly used solute in geotechnical testing due to its simplicity.

The advantage of osmotic method to control matric suction is that the pore air can be at equilibrium with the atmosphere which simulates soil condition in the field. The maximum applied suction is limited by the performance of semi-permeable membrane. Further, it requires scrupulous calibration of the osmotic pressure/matric

suction with different concentrations of solute using psychrometer or a osmotic pressure cell. It has been recently observed that the maximum matric suction that can be controlled by osmotic techniques is equal to the air-entry suction value. Therefore, the test results are limited by the air-entry value of the soil in this method.

The triaxial types of tests are usually given a two-word designation or abbreviated to a letter symbol. The designations are

a. Consolidated drained or CD test,
b. Constant water content or CW test,
c. Consolidated undrained or CU test with pore pressure measurement,
d. Unconsolidated undrained or UU test, and
e. Unconfined compression or UC test.

In the case of CD and CU test, the first letter refers to the drainage condition prior to shear, while the second letter refers to the drainage condition during shearing. The constant water content test is a special case where only the pore air is kept in a drained mode, while the pore water phases is kept undrained during shearing. The pore air and pore water are not allowed to drain throughout the test for undrained triaxial test. The unconfined compression test is a special loading condition of the undrained triaxial test.

2.5.2 Direct shear box test on unsaturated soils

Direct shear box is a simple testing apparatus to measure the shear strength of the soil in less time. The length of the drainage path associated with pore-water pressure equalization is considerably shorter in the direct shear test than in the triaxial test. Consequently, direct shear strength testing of an unsaturated soil can considerably

expedite shear strength testing.

In general, two types of test were conducted using direct shear box apparatus to measure the shear strength of unsaturated soils. The first type is using conventional direct shear box apparatus and the second type is using modified direct shear box apparatus. In this study, both of them are using to determine unsaturated shear strength properties.

In the first type using conventional direct shear box apparatus, the water content of sample will measure prior to the shearing test. After that, sample will install in the direct shear box apparatus. Then, the undrained test condition will apply during shearing test to keep the water content of sample. On the other hand, the consolidated drained direct shear test on an unsaturated soil specimen was conducted using the modified direct shear apparatus.

Gan and Fredlund, 1988 has been modified a direct shear apparatus for testing unsaturated soils. The cross-sectional view of unsaturated direct shear box illustrated in Fig 2.11. The direct shear test apparatus consists of a top and bottom parts. The soil specimen is sheared by moving the lower part of the shear box relative to the upper part of the box. The test procedure is similar to that used for a conventional direct shear apparatus.

Similar to the modified triaxial apparatus using axis-translation technique, the soil sample is installed between coarser porous disk and high air entry discs for controlling the matric suction. The high air entry disc beneath the soil sample is connected to water compartment. The pore-air and porewater pressures are brought into equilibrium with the applied pressures. There are several transducers for application of shear force, water pressure, and air pressure; and for measurement of

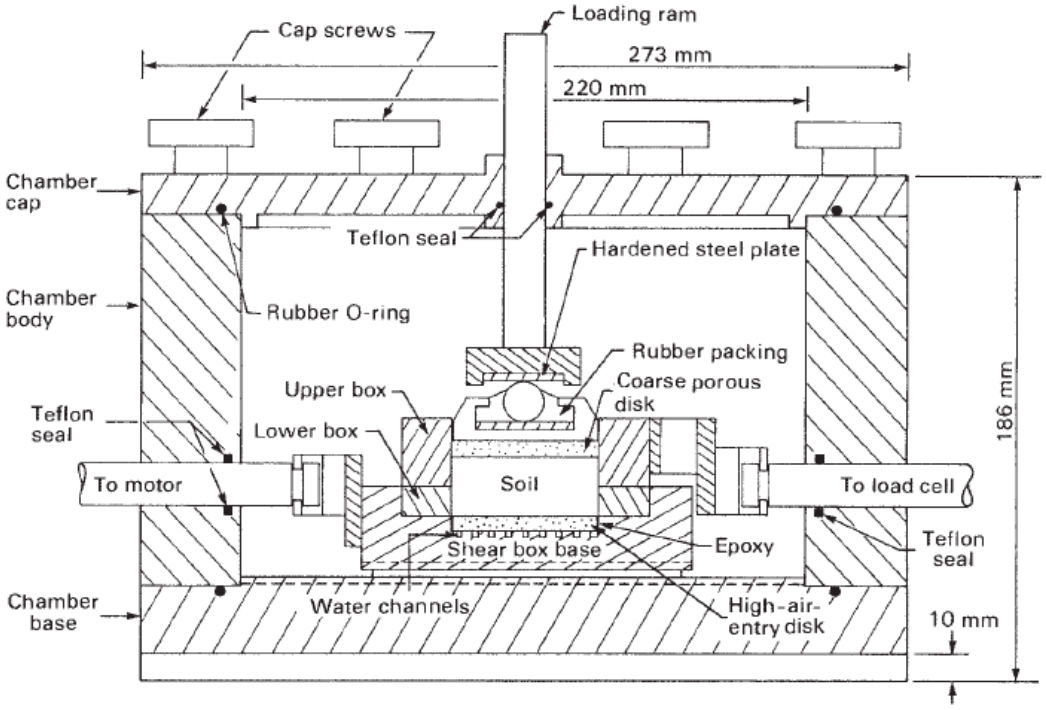

Fig 2.11 Modified direct shear apparatus for testing unsaturated soils (from Gan and Fredlund, 1988)

horizontal and vertical displacements, and water volume changes. The soil sample is initially saturated and then consolidated under a normal stress. The matric suction is increased to a required value prior to shear testing and is measured at equilibrium. Shear stress is induced along the predefined plan at a constant strain rate.

The tests are generally performed as consolidated drained direct shear tests. The soil specimen is usually given access to water after being placed into the direct shear box. It is important to ensure there are no leaks in the system. the leakage of air from the chamber surrounding the soil specimen will cause a continuous water vapor loss from the specimen.

2.6 Slope stability analysis

In this study, the limit equilibrium method was using for the slope stability

analysis. Most of the limit equilibrium analysis in literature discusses only for saturated soil condition. Thus, for the unsaturated condition modifying from the basic formula is needed. In this part the basic formula for the limit equilibrium method was explained.

In the limit equilibrium methods to investigate the equilibrium of a soil mass tending to slide down under the influence of gravity. Transitional or rotational movement is considered on an assumed or known potential slip surface below the soil According to Duncan, 2014 the factor of safety, F, is defined with respect to the shear strength of the soil as

$$F = \frac{s}{\tau} \tag{2.9}$$

Where s is the available shear strength and τ is the equilibrium shear stress. The equilibrium shear stress is the shear stress required to maintain a just-stable slope and from Equation 2.10 may be expressed as

$$\tau = \frac{s}{F} \tag{2.10}$$

The equilibrium shear stress is equal to the available shear strength divided (factored) by the factor of safety. The factor of safety represents the factor by which the shear strength must be divided so that the reduced strength is just in equilibrium with the shear stress (τ) (i.e., the slope is in a state of just-stable limiting equilibrium). The procedures used to perform such computations are known as limit equilibrium procedures.

The shear strength can be expressed by the Mohr-Coulomb equation. If the shear strength is expressed in terms of total stresses, Equation 2.11 is written as

$$\tau = \frac{c+\sigma \tan \phi}{F} \quad (2.11)$$

Where c and ϕ are the cohesion and friction angle for the soil, respectively, and σ is the total normal stress on the shear plane. If the shear strength is expressed in terms of effective stresses (e.g., drained shear strengths are being used), the only change from the above is that Equation 2.12 is written in terms of effective stresses as

$$\tau = \frac{c\prime+(\sigma-u) \tan \phi\prime}{F} \quad (2.12)$$

Where c' and ϕ' represent the shear strength parameters in terms of effective stresses, and u is the pore water pressure.

To calculate the factor of safety, a slip surface is assumed and one or more equations of static equilibrium are used to calculate the stresses and factor of safety for each surface assumed. The term slip surface is used here to refer to an assumed surface along which sliding or rupture might occur. However, it is the intent of slope stability calculations that sliding and rupture not occur along such surfaces if the slope is designed adequately.

The factor of safety is assumed to be the same at all points along the slip surface. Thus, the value represents an average or overall value for the assumed slip surface. If failure was to occur, the shear stress would be equal to the shear strength at all points along the failure surface, and the assumption that the factor of safety is constant would be valid. If, instead, the slope is stable, the factor of safety probably varies along the slip surface (e.g., Wright et al., 1973). However, this should not be of significant consequence as long as the overall factor of safety is suitably greater than 1.0 and the assumed shear strengths can be mobilized along the entire slip surface.

2.6.1 Static load slope stability

2.6.1.1 Infinite slope stability

In the infinite slope analysis, the slope is assumed to be infinite in extent, and sliding is assumed to occur along a plane parallel to the face of the slope (Taylor, 1948). Because the slope is infinite, the stresses will be the same on any two planes that are perpendicular to the slope, such as the planes A − A′ and B − B′ in Fig 2.12.

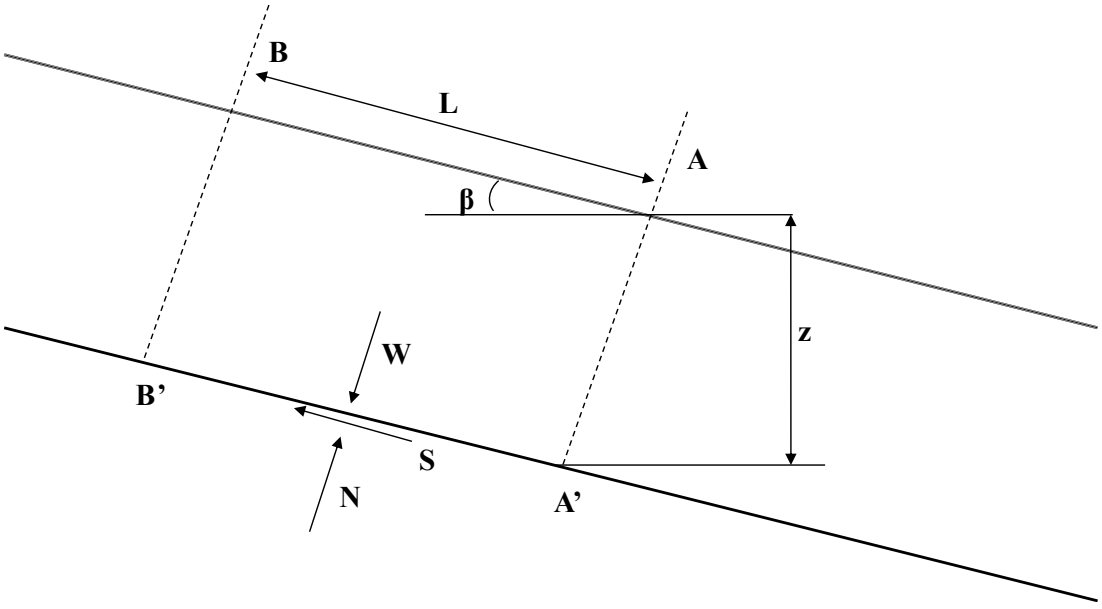

Fig 2.12 Infinite slope and plane slip surface.

Summing forces in directions perpendicular and parallel to the slip plane gives the following expressions for the shear force, S, and normal force, N, on the plane:

$$S = W \sin \beta \tag{2.13}$$

$$N = W \cos \beta \tag{2.14}$$

where β is the angle of inclination of the slope and slip plane, measured from the horizontal, and W is the weight of the block. For a block of unit thickness in the direction perpendicular to the plane of the cross section in Fig 2.12, the weight is

expressed as

$$W = \gamma LZ \cos\beta \tag{2.15}$$

where γ is the total unit weight of the soil, L is the distance between the two ends of the block, measured parallel to the slope, and Z is the depth of the shear plane, measured vertically. Substituting Equation (2.15) into Equations (2.13) and (2.14) gives

$$S = \gamma LZ \cos\beta \sin\beta \tag{2.16}$$

$$N = \gamma LZ \cos^2\beta \tag{2.17}$$

Substituting these expressions for the stresses into Equation 2.11 for the factor of safety for total stresses gives

$$F = \frac{c+\gamma Z \cos^2\beta \tan\phi}{\gamma Z \cos\beta \sin\beta} \tag{2.18}$$

2.6.1.2 Circular slope

In this study, the Bishop simplified method was using for analysis slope stability with the circular slip surface. This method is a more refined solution and explanation to the ordinary method of slices. Ordinary method of slices is the method to find the factor of safety FS of critical circle, through several trials by changing the center of the trial circles. In Bishop's method, the effect of force on every slice is accounted to some degree. The resultant forces on the slice sides are assumed to be horizontal.

There are two main assumptions in the simplified Bishop method: (1) the slip surface is circular, and (2) interslice forces are horizontal, in other words, shear forces are ignored between slices. Fig 2.13 shows a slope with a circular slip surface. The factor of safety is obtained from the following equation

$$F = \frac{\sum_{i=1}^{i=n}\{c' b_i + (W_i - u_i b_i)\tan\phi'\}\left(\frac{1}{\cos\alpha_i (1+\tan\alpha_i \tan\phi'/F)}\right)}{\sum_{i=1}^{i=n} W_i \sin\alpha_i} \quad (2.19)$$

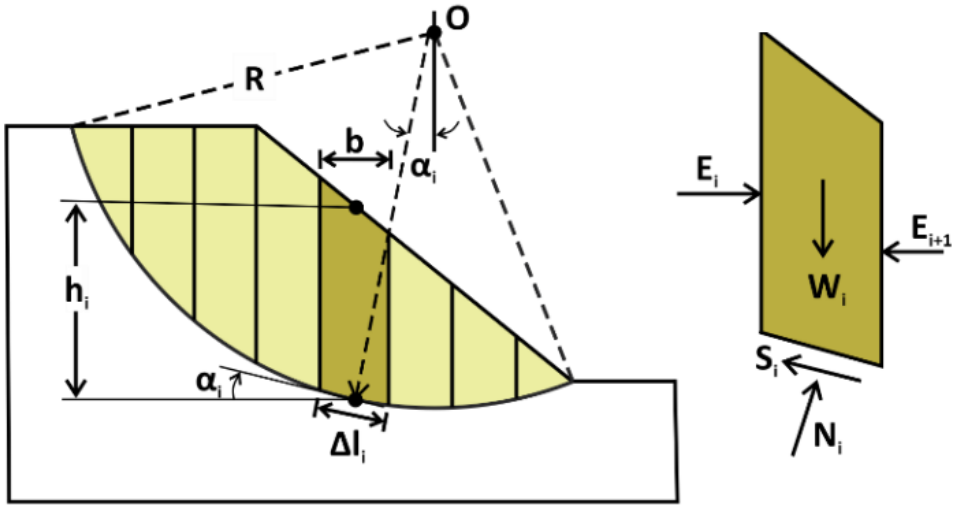

Fig 2.13 Circular slip surface to a slice in the simplified Bishop method.

2.6.2 Slope stability analysis with earthquake load

2.6.2.1 Newmark method

The Newmark method was used to evaluate the effect of earthquake load on the infinite slope stability. If the inertial forces acting on a potential failure mass becomes large enough that the total (static plus dynamic) driving forces exceed the available resisting forces, the factor of safety will drop below 1.0. Newmark (1965) considered the behavior of a slope under such conditions. When the factor of safety is less than 1.0, the potential failure mass is no longer in equilibrium consequently, it will be accelerated by the unbalanced force.

Under static conditions, equilibrium of the block (in the direction parallel to the plane) requires that the available static resting force, exceed the static driving force, (2.14). Assuming that the block's resistance to sliding is purely frictional ($c = 0$).

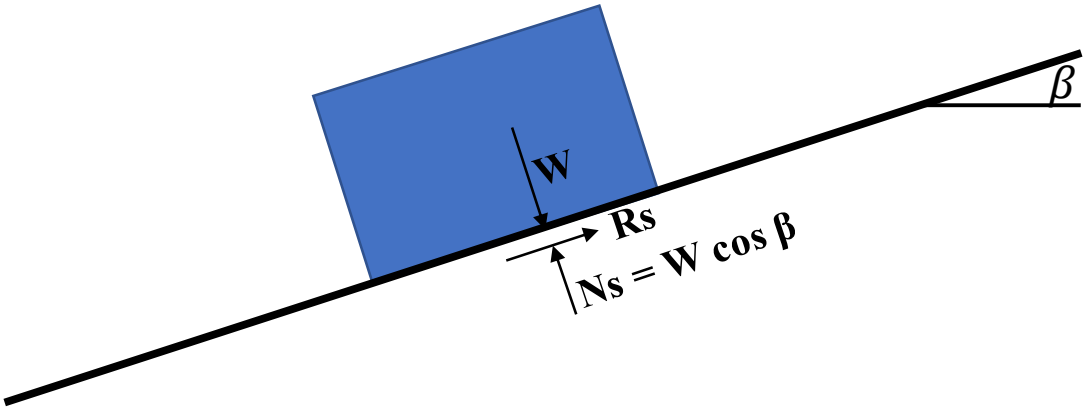

Fig 2.14 Forces acting on a block resting on an inclined plane static condition

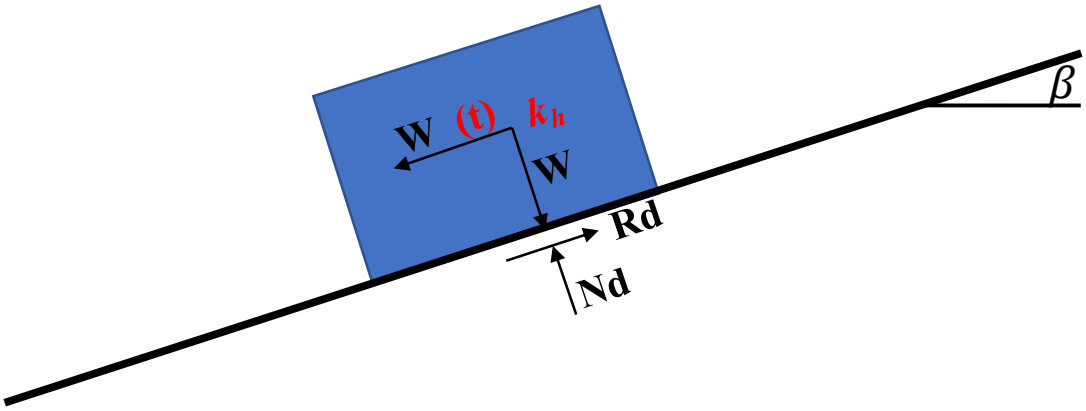

Fig 2.15 Forces acting on a block resting on an inclined plane dynamic condition

$$FS = \frac{Resisting\ force}{Static\ driving\ force} = \frac{R_s}{D_s} = \frac{W\cos\beta\tan\phi}{W\sin\beta} = \frac{\tan\phi}{\tan\beta} \tag{2.20}$$

Where ϕ is the angle of friction between the block and the plane. Now consider the effect of inertial forces transmitted to the block by horizontal vibration of the inclined plane with acceleration, $a_h\ (t) = k_h\ (t)$ g (the effect of vertical accelerations will be neglected for simplicity). At a particular instant of time, horizontal acceleration of the block will induce a horizontal inertial force, khW in Fig 2.15. When the inertial force acts in the downslope direction, resolving forces perpendicular to the inclined plane gives as

$$FSd = \frac{Resisting\ force}{Pseudostatic\ driving\ force} = \frac{R_d(t)}{D_d(t)} = \frac{\cos\beta - k_h(t)\sin\beta\tan\phi}{\sin\beta + k_h(t)\cos\beta} = \frac{\tan\phi}{\tan\beta} \tag{2.21}$$

Obviously the dynamic factor of safety decrease as k_h increases and there will be (for a statically stable block) some positive value of k_h that will produce a factor of safety of 1.0. This coefficient, termed the yield coefficient, k_y corresponds to the yield acceleration, $a_y=k_yg$. The yield acceleration is the minimum pseudostatic acceleration required to produce instability of the block.

$$k_y = \tan(\phi - \beta) \tag{2.22}$$

For sliding in the downslope direction. For sliding in the uphill direction (which can occur when ϕ and β are small

$$k_y = \frac{\tan\phi + \tan\beta}{1 + \tan\phi \tan\beta} \tag{2.23}$$

2.6.2.2 Pseudostatic analysis

The pseudostatic analysis was used to evaluate the effect of earthquake load on the circular slip surface slope stability. The first explicit application of the pseudostatic approach to the analysis of seismic slope stability has been attributed to Terzaghi 1950.

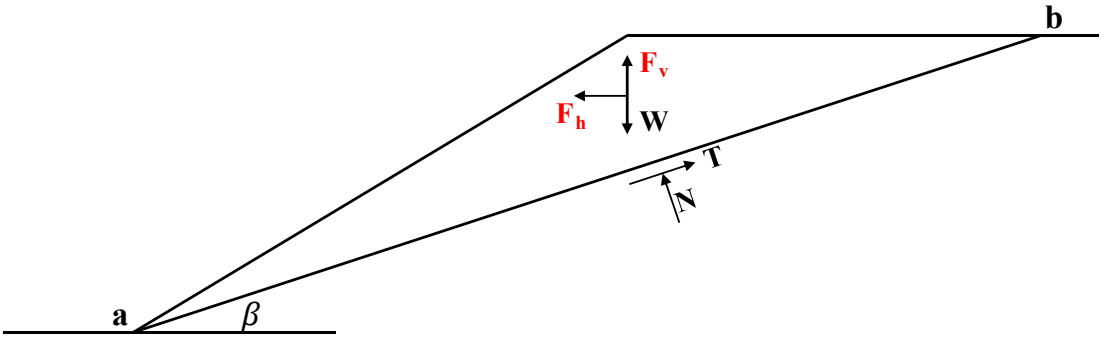

Fig 2.16 Forces acting on triangular wedge of soil in pseudostatic analysis

$$F = \frac{a_h W}{g} = k_h W \tag{2.24}$$

$$F = \frac{a_v W}{g} = k_v W \tag{2.25}$$

In their most common form, pseudosatic analyses represent the effects of earthquake shaking by pseudostatic accelerations that produce inertial forces, F_h and F_v, which act through the centroid of the failure mass (Fig 2.16). The magnitudes of the pseudostatic forces are a_h and a_v where are horizontal and vertical pseudostatic accelerations, k_h and k_v are dimensionless horizontal and vertical presudostatic coefficients, and W is the weight of the failure mass.

The magnitudes of the pseudostatic accelerations should be related to the severity of the anticipated ground motion. Resolving the forces on the potential failure mass in a direction parallel to the failure surface.

$$F = \frac{Resisting\ force}{Driving\ force} = \frac{cl_{ab} + [(W - F_v)\cos\beta - F_h \sin\beta]\tan\phi}{(W - F_v)\sin\beta + F_h \cos\beta} \quad (2.26)$$

References

Biot, M. A. 1941. General theory for three-dimensional consolidation, Journal of Applied Physics, 12 (2): 155–164.

Bishop, A. W. 1959. The principle of effective stress, Teknisk Ukeblad, Norwegian Geotechnical Institute, 106 (39): 859–863.

Bishop, A. W., and Donald, I. B. 1961. The experimental study of partly saturated soil in the triaxial apparatus, Proceedings of the Fifth International Conference on Soil Mechanics and Foundation Engineering, Paris, 1: 13–21.

Bishop, A. W., and Blight, G. E. 1963. Some aspects of effective stress in saturated and unsaturated soils, Geotechnique, 13 (3): 177–197.

Crilly, M. S., Schreiner, H. D., and Gourley, C. S. 1991. A simple field suction measurement probe, Proceedings of the Tenth African Regional Conference on Soil Mechanics and Foundation Engineering, Maseru, Lesotho, 291–298.

Cui, Y., and Delage, P. 1996. Yielding and plastic behaviour of an unsaturated compacted silt, Geotechnique, 46 (2): 291–311.

Dineen, K., and Burland, J. 1995. A new approach to osmotically controlled oedometer

testing, in E. E. Alonso and P. Delage (Eds.), Unsaturated Soils, Proceedings of the First International Conference on Unsaturated Soils, Balkema, Rotterdam, Paris, 2: 459–465.

Duncan, J.M., Wright, S.G., Brandon, T.L., 2014. Soil strength and slope stability. Wiley

Edlefsen, N. E., and Anderson, A. B. C. 1943. Thermodynamics of soil moisture, Hilgardia, 15: 31–298

Escario, V., and Saez, J. 1986. The shear strength of partly saturated soils, Geotechnique, 36 (3): 453–456.

Fredlund, D. G., and Morgenstern, N. R., 1977, Stress State Variables for Unsaturated Soils: Journal of the Geotechnical Engineering Division-Asce, 104 (11): 447-466.

Fredlund, D. G., and Rahardjo, H., 1993, Soil Mechanics for Unsaturated Soil, New York, John Wiley & Sons.

Fredlund, D. G., Rahardjo, H., and Ng, T. 1993. Effect of pore-air and negative pore-water pressures on stability at the end-ofconstruction, Proceedings of International Conference on Dam Engineering, Johor Bahru, Malaysia, 43–51.

Fredlund, D. G., 1995, The Scope of unsaturated soil mechanics, An overview, Proceedings of the 1st International Conference on Unsaturated Soils, Paris, France, 3: 1155-1177.

Fredlund, D. G. 2001. Ensuring a sound scientific basis for geotechnical engineering in developing and developed countries, Proceedings of the International Conference on Management of the Land and Water Resources, Hanoi, 3–20.

Gan, J. K.-M., and Fredlund, D. G. 1988. Multistage direct shear testing of unsaturated soils, Geotechnical Testing Journal, ASTM, 11 (2): 132–138.

Hilf, J. W. 1956. An investigation of pore-water pressure in compacted cohesive soils, PhD Thesis, Technical Memorandum. No. 654, U.S. Department of the Interior, Bureau of Reclamation, Design and Construction Division, Denver, CO.

Ho, D. Y. F., and Fredlund, D. G. 1982. A multi-stage triaxial test for unsaturated soils, Geotechnical Testing Journal, ASTM, 5 (1): 18–25.

Jennings, J. E. B., and Burland, J. B. 1962. Limitations to the use of effective stresses in partly saturated soils, Geotechnique, 12 (2): 125–144.

Kassif, G., and Ben Shalom, A. 1971. Experimental relationships between swell pressure and suction, Geotechnique, 21 (3): 245–255.

Lu, N., and Likos, W. J., 2004, Unsaturated Soil Mechanics, New Jersey, John Wiley & Sons.

Matyas, E. L., and Radhakrishna, H. S. 1968. Volume change characteristics of partially saturated soils, Geotechnique, 18 (4): 432–448.

Morgenstern, N. R. 1979. Properties of compacted soils, Proceedings of the Sixth Pan American Conference on Soil Mechanics and Foundation Engineering, Lima, 3: 349–354.

Newmark., M. N., 1965. Effect of earthquakes on dams and embankments, Geotechnique, 15 (2): 139-160

Ng, C. W. W., Cui, Y. J., Chen, R., and Delage, P. 2007. The axis translation and osmotic techniques in shear testing of unsaturated soils: A comparison, Soils and Foundations, 47 (4): 678–684.

Rifa'i, A., 2002, Mechanical Testing and Modelling of an Unsaturated Silt, with Engineering Applications: The Swiss Federal Institute of Technology Lausanne (EPFL), Switzerland.

Ridley, A. M., and Wray, W. K. 1995. Suction measurements: A review of current theory and practices, in E. E. Alonso and P. Delage (Eds.), Unsaturated Soils: Proceedings of the First International Conference on Unsaturated Soils, Paris, Balkema, Rotterdam, Presse des Ponts et Chaussees, 1293–1322.

Tadepalli, R., and Fredlund, D. G. 1991. The collapse behaviour of a compacted soil during inundation, Canadian Geotechnical Journal, 28: 477–488.

Taylor, D. W., 1948. Fundamentals of Soil Mechanics, Wiley, New York.

Terzaghi, K. 1936. The shear strength of saturated soils, Proceedings of the First International Conference on Soil Mechanics and Foundation Engineering, Cambridge, MA, 1.

Terzaghi, K., 1950. Mechanisms of Landslides, Engineering Geology (Berkeley)Volume, Geological Society of America, Boulder, CO, November, 83–123.

Wright, S. G., Kulhawy, F. H., and Duncan, J. M., 1973. Accuracy of equilibrium slope stability analyses, Journal of the Soil Mechanics and Foundation Division, 99: 783–791.

CHAPTER III

SHEAR STRENGTH BEHAVIOR OF UNSATURATED UNDISTURBED VOLCANIC ASH SOIL UNDER STATIC AND CYCLIC LOADING

3.1 Introduction

Recently Kumamoto earthquake 2016 triggered many slope failures around the Aso area. In general, the slope surface in the Aso area consists of volcanic ash soil and commonly overconsolidated due to the environmental effects. The volcanic ash soils and orange-colored pumice deposits are the most common types of soils that experienced failure in the Aso area. The key factor in slope failures was to be the shear strength of the volcanic soils before and after the earthquake (Miyabuchi, 2016; Mukonoki et al., 2016; Kiyota et al., 2017; Chiaro et al., 2018)

Many researchers have studied the Kumamoto slope failures especially the orange-colored pumice. They investigated the shear strength by a series of static and cyclic triaxial tests. However, small attention was given to the shear strength and characteristic of the volcanic ash soil.

In this chapter to enhance understanding of the volcanic ash soil behavior same as natural condition, the unsaturated undisturbed samples were tested under various loading condition. A series of static and cyclic tests using the constant volume conventional direct shear box were performed. Furthermore, the post cyclic behavior of the volcanic ash soil was evaluated.

3.2 Principle of direct shear box apparatus

In the principle of direct shear box test, soil is made to slide along another by the action of a steadily increasing horizontal shearing force, while a constant load is applied normal to plane of relative movement. These conditions are achieved by placing the soil in the rigid metal box, circle in plane, consisting of two halves. While, applying a vertical pressure, the upper half of the box is driven by a motor to slide in and out relative to the lower half.

The direct shear box test is the simplest, the oldest and the most straightforward procedure for measuring the shear strength of soils in terms of total stress. It is also easiest to understand.

To deal with unsaturated soils, some of disadvantages of conventional direct shear box apparatus need to be modified for measuring the water content and matric suction with a slowly shearing procedure in order to accommodate independent measurement or control of the pore air pressure and the pore water pressure. However, many researchers conducted the unsaturated test with the conventional direct shear box apparatus. They assumed the unsaturated condition based on the water content before shearing. Thus, in this chapter the conventional direct shear box was using to evaluate the unsaturated condition based on water content under static and cyclic test.

3.2.1 Limitation of conventional direct shear box

In order to compare with other methods to define the shear strength (i.e., triaxial testing) the conventional direct shear box testing has mainly limitation as following:

- The soil specimen is constrained to fail along a predetermined plane of

shear.

- The distribution of stresses on their surface is not uniform.
- The actual stress pattern is complex and the directions of the planes of principle stresses rotate as the shear strain is increased.
- No control can be exercised over drainage, except by varying the rate of shear displacement.
- Pore water pressure cannot be measured
- The area of contact between the soil in the two halves of the shear box test decreases, as the test proceeds but its effects is small. It affects the shear stress and normal stress is equal proportion, and the effect on the Coulomb envelope is usually negligible, so it is generally ignored.

3.2.2 Advantages of conventional direct shear box

Notwithstanding the above limitations, the shear box apparatus has certain merits for routine shear strength testing, as summarized:

- The test is relatively quick and simple to carry out.
- The basic principle is easily to understood.
- Preparation of recompacted test specimens is not difficult.
- The principle can be extended to gravelly soils and other materials containing large particles, which would be more expensive to test by other means.
- Friction between rocks and the angle of friction between soils and many other engineering materials can be measured.
- The apparatus can be used for drained test and for the measurement of

residual shear strength by multi-reversal process.

3.3 Materials

3.3.1 Sampling methodology

The undisturbed sampling methodology and molds used for collecting undisturbed volcanic ash soil samples are illustrated in Fig 3.1. Sampling was carried out using 6 cm in diameter and 4 cm in height acrylic cylindrical molds. Before sampling, the inner surface of the acrylic mold and the cutter ring were covered with grease oil to reduce the friction and therefore minimize the disturbance. Samples were collected 10-20 cm below the ground surface in order to avoid the inclusion of plants and roots in the collected samples.

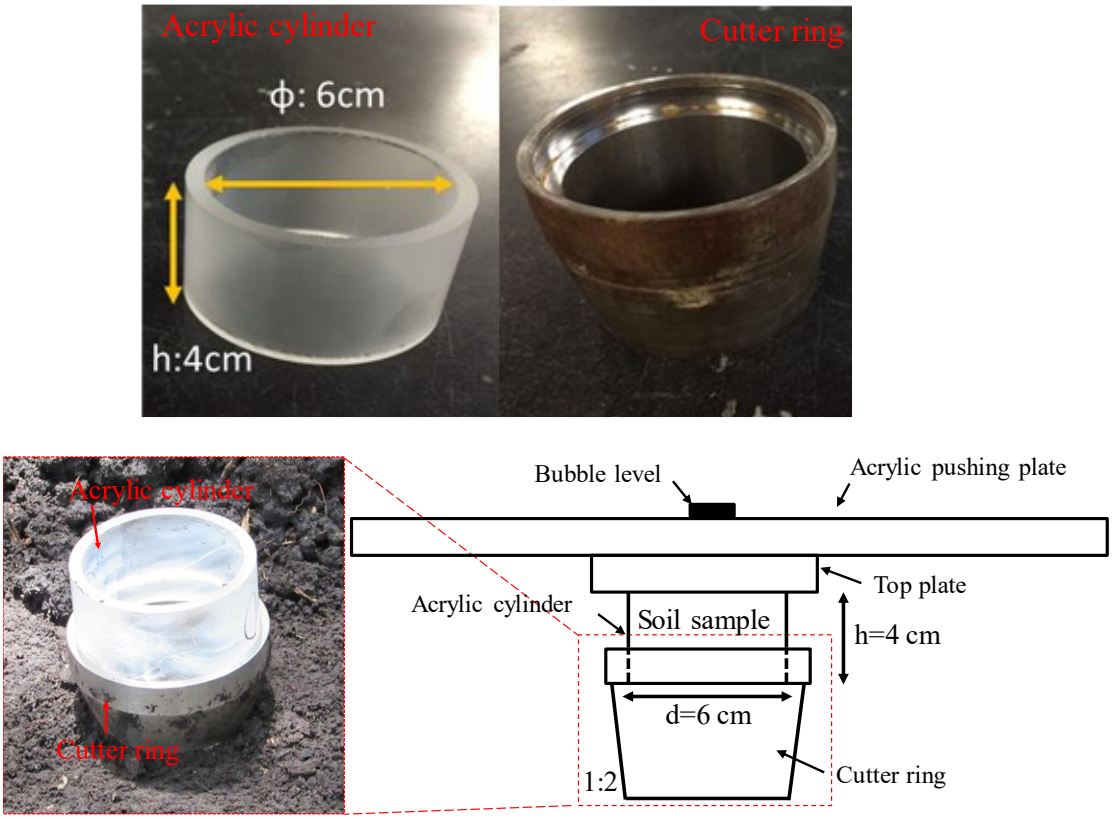

Fig 3.1 Sampling setup for undisturbed sample

The acrylic containing mold attached to the cutter ring was pushed using a plate equipped with a bubble level into the ground. After that, the sample's upper and lower surfaces were trimmed using a spatula. In order to prevent any water loss due to evaporation, samples were kept in sealed plastic bags

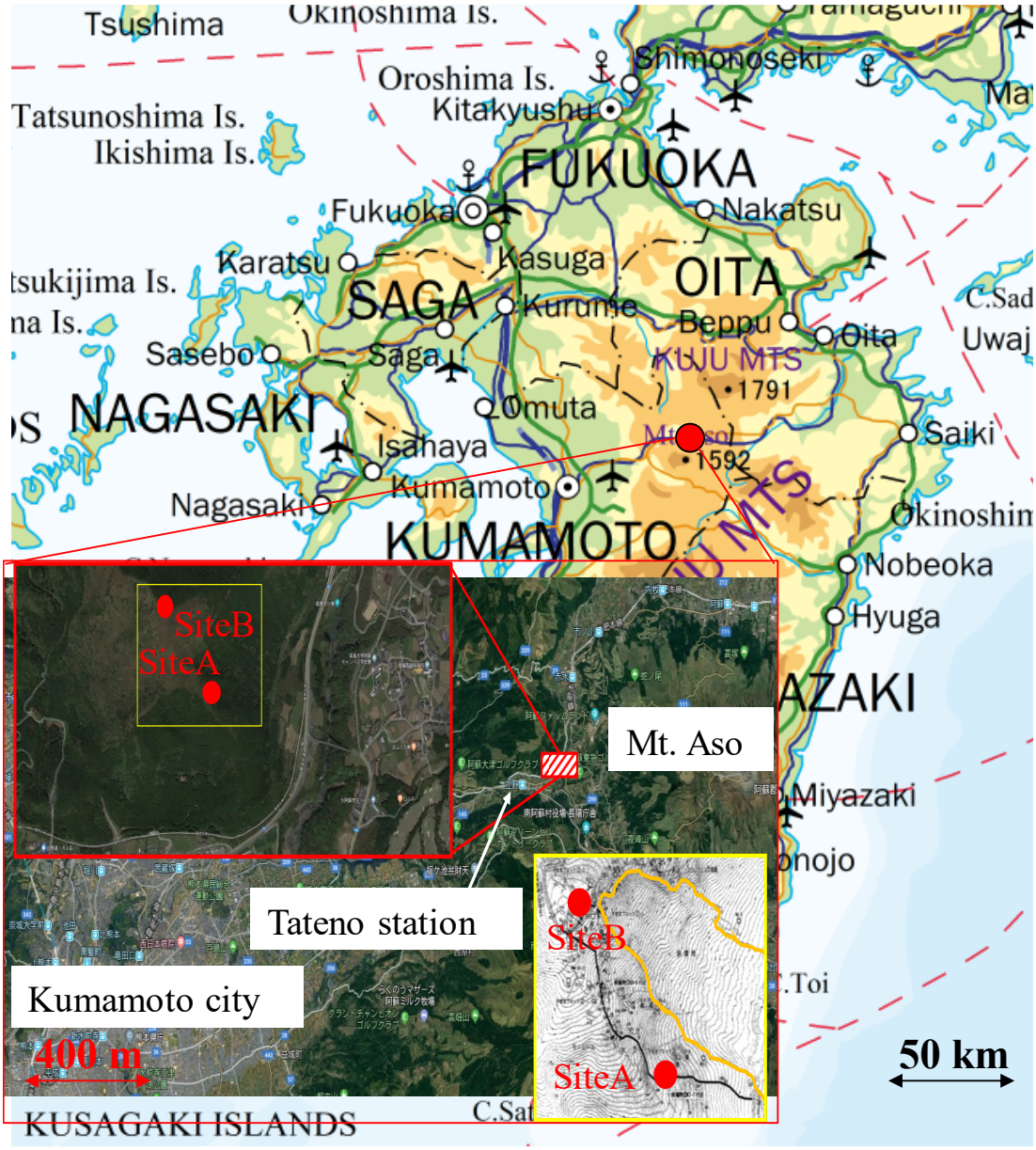

Fig 3.2 Sampling location for undisturbed sample

3.3.2 Sampling location

Tests were conducted using undisturbed unsaturated and saturated samples. After Kumamoto earthquake 2016 many slope failures around Aso area occurred. Samples were collected at the middle and the top boundaries of a large slope failure zone as illustrated in Fig 3.2. The sampling points were located 1.5 m next to the failure zone boundaries where the cross-section mainly comprised of volcanic ash.

3.3.3 Basic properties of the volcanic ash soil

The physical properties of the collected volcanic ash are listed in Table 3.1. It can be seen the organic matter content ranges from 22.9 % - 28.2 %. The particle size distribution is shown in Fig 3.3. it can be seen that the median grain size D_{50} is approximately 0.012 mm. Consequently, the volcanic ash soil in this research can be classified as volcanic cohesive soil type II (VH2) according to the Japanese Geotechnical Society standards (JGS 0051, 2009).

Table 3.1. Physical properties of the volcanic ash

Physical properties		Volcanic ash
Water content	(%)	111-159
Dry density, ρ_d	(g/cm^3)	0.56-0.58
Bulk density, ρ_t	(g/cm^3)	1.18-1.25
Liquid limit	(%)	154-214
Plastic limit	(%)	112-139
Organic matter	(%)	22.9-28.2
Specific gravity	Gs	2.28-2.34
Coefficient of uniformity	U_c	4.33
D_{50}	mm	0.012
Classification by JGS	Volcanic cohesive soil type II (VH_2)	

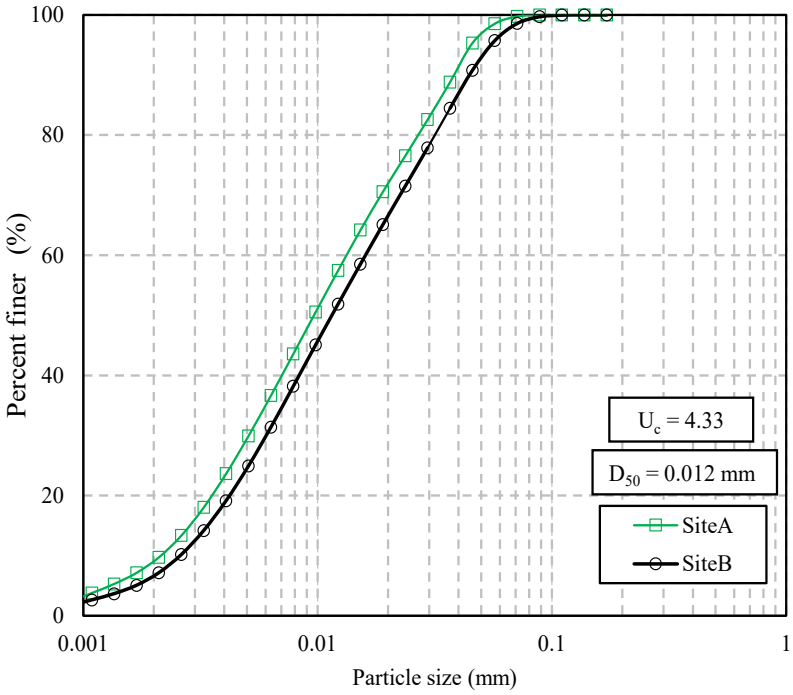

Fig 3.3 Particle size distribution

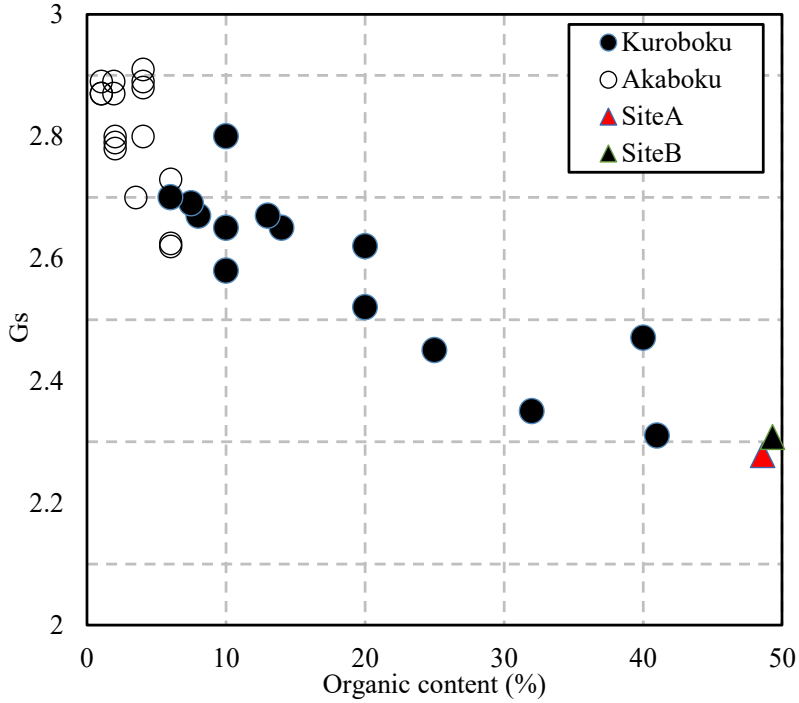

Fig 3.4 Relationship of specific gravity and organic content

Fig 3.4 shows the relationship between organic matter content and specific gravity. It can be seen that the comparison with the previous study. It was found that among the volcanic ash soil in the Kyushu region, the samples of this study have a high organic matter content.

On the other hand, the plasticity diagram in Fig 3.5 shows the plasticity index of volcanic ash soil in this study seems to be relatively cohesive. It can be seen that both the liquid limit and the plasticity index tend to be relatively high. The volcanic ash soil in Hokkaido also tends to be close. On the other hand, it was found that the volcanic ash soil in Tottori prefecture has lower liquid limit and plasticity index.

The consolidation test results of the saturated and unsaturated volcanic ash are indicated in Fig 3.6. The yield stress corresponding to the unsaturated undisturbed sample was 105 kN/m^2 on average. Based on the consolidation test results, the

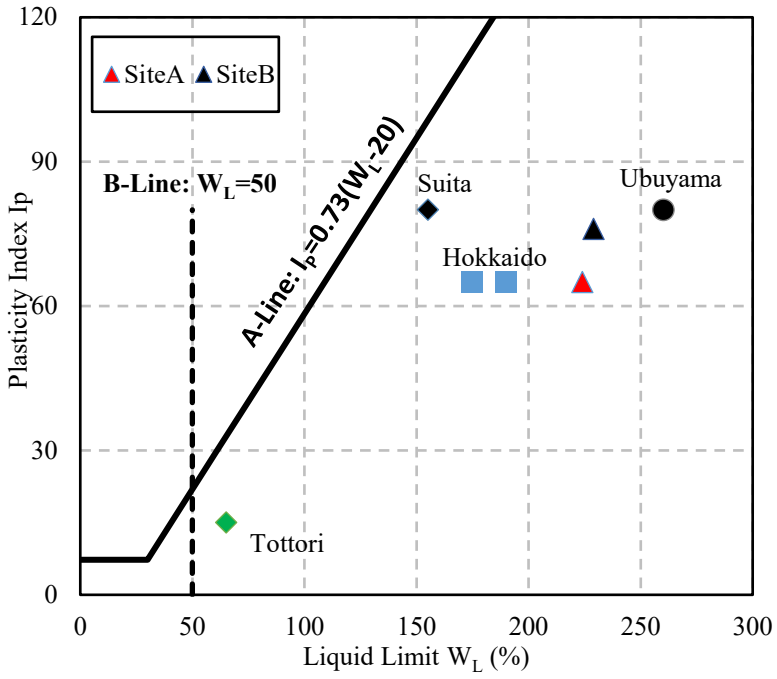

Fig 3.5 Relationship of plasticity index and liquid limit

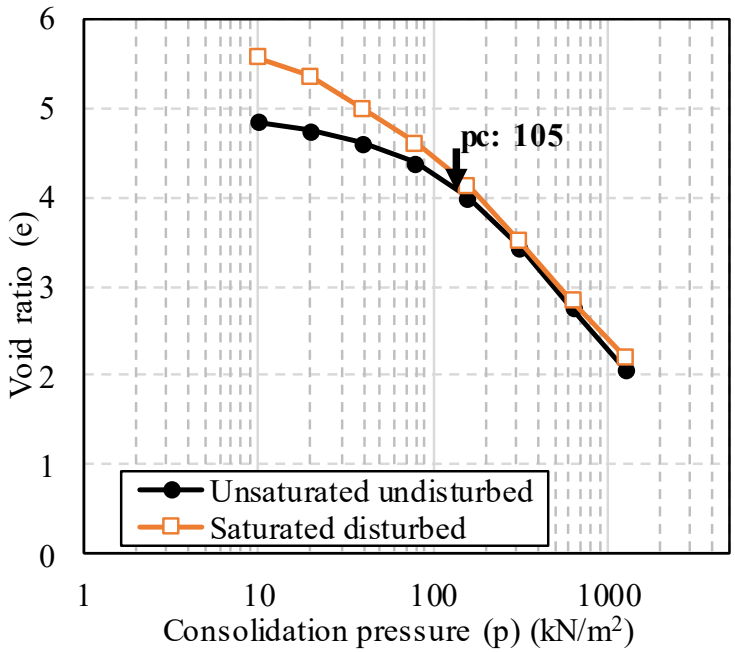

Fig 3.6 Consolidation test result of the volcanic ash soil

collected volcanic ash in this research is considered as over-consolidated soil, where the sampling depth was around 1.5 m, therefore the soil was subjected to an overburden pressure less than 105 kPa

3.4 Methodology

In order to examine the shear strength properties of the volcanic ash soil, a series of constant volume direct shear box tests were carried out considering both unsaturated and saturated samples. During shearing, the specimen volume was maintained constant or not allowed to change in volume. A schematic diagram of direct shear box test is illustrated in Fig. 3.7. The box is divided into upper and lower parts. While the bottom fixed and the top movable. 2 cm in height circular sample were prepared for test. In a static test for overconsolidated sample, 10 and 50 kPa vertical stress was applied. On the other hand, for normally consolidated sample 200 kPa vertical stress was adopted.

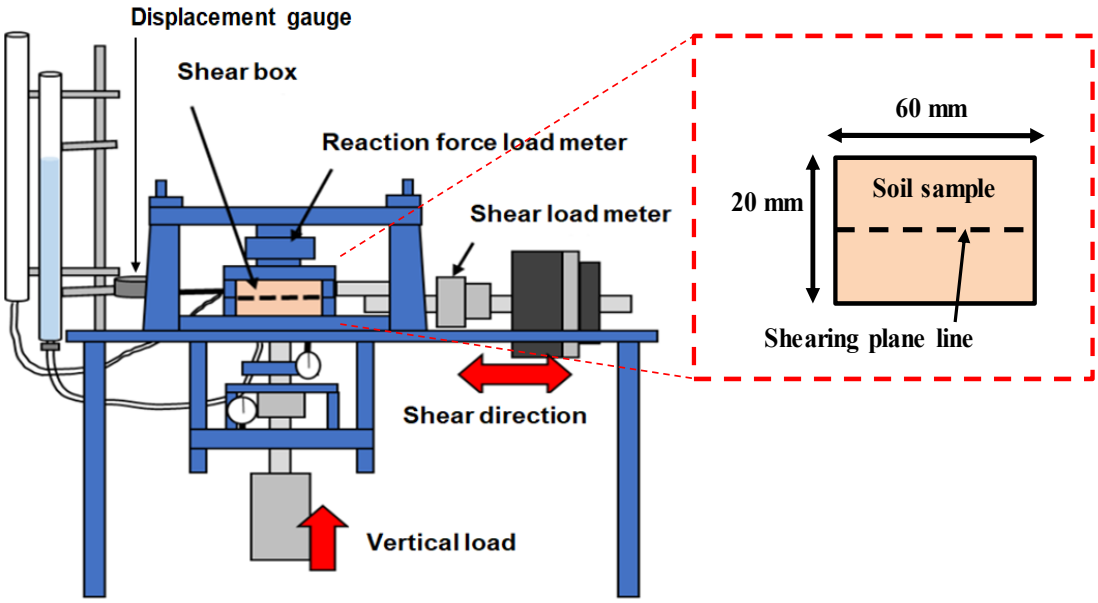

Fig 3.7 Schematic diagram of conventional direct shear box apparatus

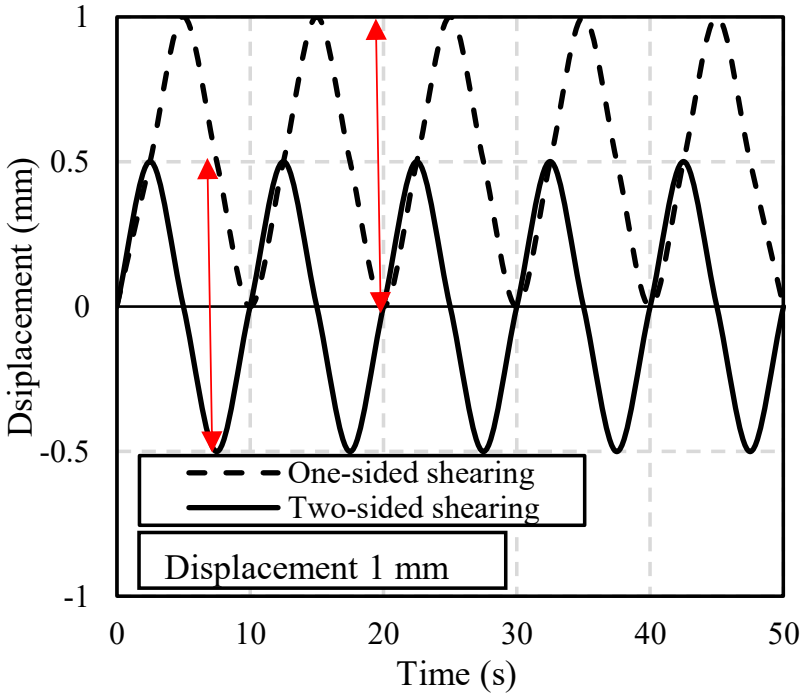

Fig 3.8 Schematic of (one-sided and two-sided) cyclic loading

Before the shearing start, specimens were consolidated under the designated vertical stress each condition for 1 hour. Then, sheared with the undrained condition up to 7 mm at a shear rate of 0.2 mm/min according to the JGS standards.

In order to examine the shear strength of the volcanic ash soil under the earthquake shakes, a series of cyclic direct shear box test using both unsaturated and saturated samples was carried out. The cyclic test under two patterns with displacement 1 mm were adopted.

First type of pattern, cyclic one-sided shearing was applied as represent the slope condition. Where shearing was started from 0.5 mm to 1 mm, from 1 mm moving back to 0 mm and again to 0.5 mm. The total of displacement for one cycle was 2 mm. On the other hand, for the second type of pattern two-sided shearing was conducted. Two-sided shearing pattern represent the flat condition. Where shearing was started from 0 mm to 0.5 mm, then from 0.5 mm moving back to -0.5 mm and again to 0 mm. The total of displacement for one cycle was also 2 mm. For each pattern, a total number of cyclic was 10 times. Then, the shearing was terminated when the displacement reached 7 mm. Based on that, the cumulative displacement for both pattern for one times test was 27 mm. A schematic diagram adopted pattern is shown Fig 3.8. The 50 kPa vertical stress was applied for the overconsolidated sample and 200 kPa for the normally consolidated sample was used. The initial suction before shearing (Alowaisy et al, 2017) is shown in Table 3.2.

Table 3.2. Test program for static and cyclic.

Test ID	Sample	Void Ratio (e_0)	Sr_0 (%)	Initial Suction* (kN/m^2)	Vertical stress (kN/m^2)
Static test					
S01	Unsaturated	4.70	65.5	100	10
S02	Unsaturated	5.16	68.0	100	50
S03	Unsaturated	4.95	72.5	97	200
S04	Saturated	4.60	99.7	0.1	10
S05	Saturated	4.77	99.3	0.1	50
S06	Saturated	4.72	100	0.1	200
One-sided cyclic					
C101	Unsaturated	4.03	67.8	100	50
C102	Unsaturated	4.01	69.5	100	200
C103	Saturated	4.41	99.5	0.1	50
C104	Saturated	4.45	96.8	0.2	200
Two-sided cyclic					
C201	Unsaturated	4.73	74.1	97	50
C202	Unsaturated	4.96	82.9	8	200
C203	Saturated	4.43	100	0.1	50
C204	Saturated	4.77	100	0.1	200
Post cyclic					
PC01	Unsaturated	4.03	67.8	100	50
PC02	Unsaturated	4.01	69.5	100	200
PC03	Saturated	4.41	99.5	0.1	50
PC04	Saturated	4.45	96.8	0.2	200

* Initial suction before shearing

3.5 Static shearing behavior

The relationship between the shear displacement and the shear stress is shown in Fig 3.9. It can be seen in unsaturated condition, for the normally consolidated sample the shear stress converges to a constant value with a shear displacement of 1.5

mm. While, for the overconsolidated sample, the shear stress dramatically increases and converges to a constant value at shear displacement about 0.5 mm.

The relationship between the vertical and shear stress for the unsaturated and saturated sample is illustrated in Fig 3.10. It can be observed that for the normally consolidated condition, the vertical stress increases dramatically till achieving the peak shear stress. Then, slightly decreases regardless of the saturation condition. On the other hand, for the overconsolidated condition both vertical stress and shear stress increases without distinct peak value. The observed behaviour is similar to the clayey soil behaviour under undrained triaxial test (Atkinson et al., 1987).

For the overconsolidated condition, the monotonical increases in the vertical stress can be justified to be a result of the pore water pressure reduction under shearing. On the other hand, for the normally consolidated condition increases in the pore water pressure during shearing leads to decreasing of the vertical stress.

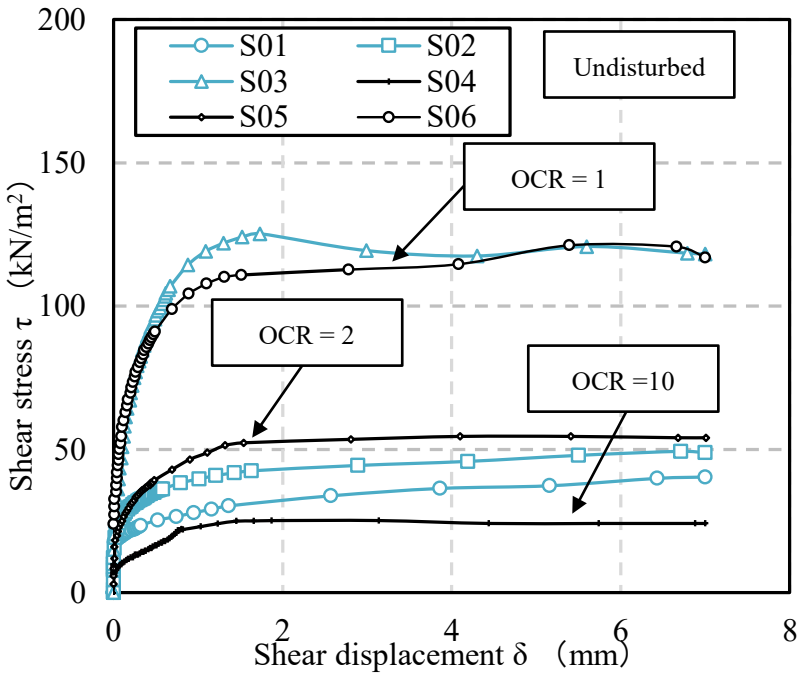

Fig 3.9 Relationship of shear stress and shear displacement

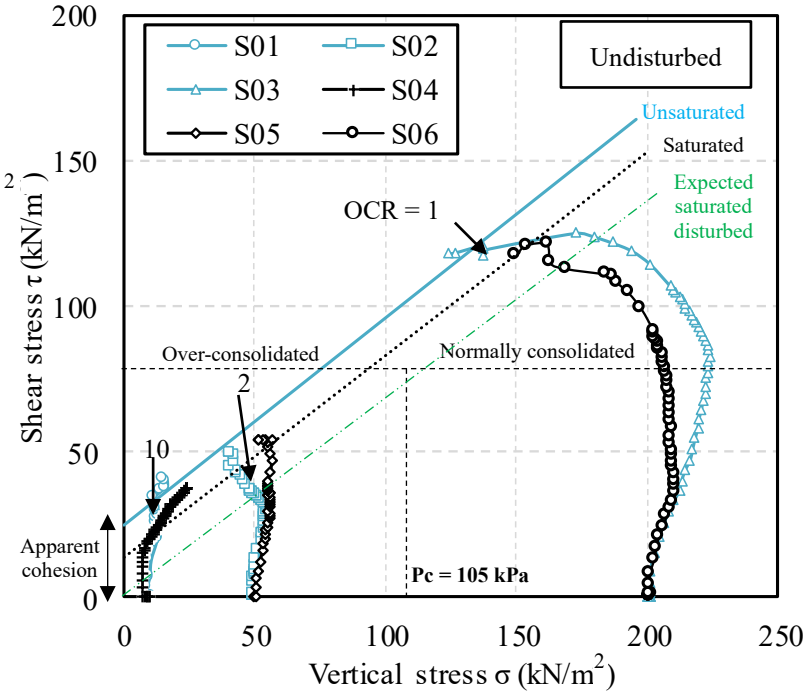

Fig 3.10 Stress path static test unsaturated and saturated sample

The apparent cohesion decreases from 24.6 kN/m^2 under unsaturated condition to 13 kN/m^2 for saturated condition. In addition the apparent friction angle slightly reduced from 35.5° under unsaturated condition to 35.1° for saturated condition. Finally it can be concluded that the shear strength strongly depend on soil water content, within translate into suction force which contributed to the total shear strength of the soil.

An empirical relationship of the overconsolidation ratio and the shear stress ratio was developed (Mayne, 1984). The relationship for the volcanic ash soil is shown in Fig. 3.11. The line represents an empirical model, while the scatter represents the experimental data. For OCR = 1 the shear stress ratio was 0.55, and the shear stress ratio increases as the increasing number of OCR.

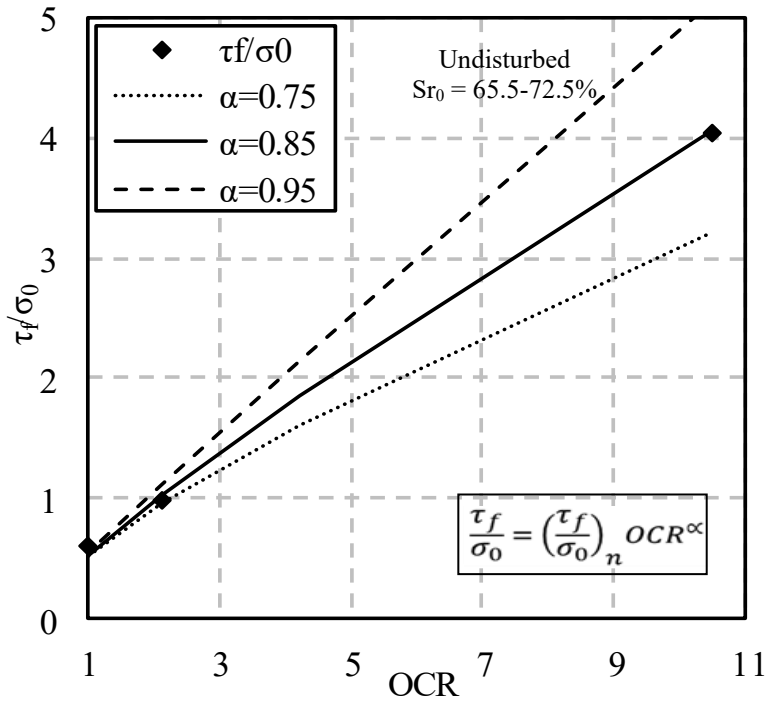

Fig 3.11 Relationship of normalized shear stress at the end of shearing and overconsolidation ratio

3.6 Cyclic (one sided and two sided) shearing

The stress path of the cyclic one-sided and two-sided shearing illustrated in Fig 3.12 and Fig 3.13. It can be seen that the vertical stress significantly decreases in both overconsolidated and normally consolidated samples for one-sided shearing. On the other hand, the vertical stress increases in both overconsolidated and normally consolidated samples for two-sided shearing. Furthermore, in order to clearly understand the vertical stress trend, the cumulative shear displacement and the normalized vertical stress were plotted as indicated in Fig 3.14 and Fig 3.15. In general, the normalized vertical stress decreases by increasing the number of cyclic. When the

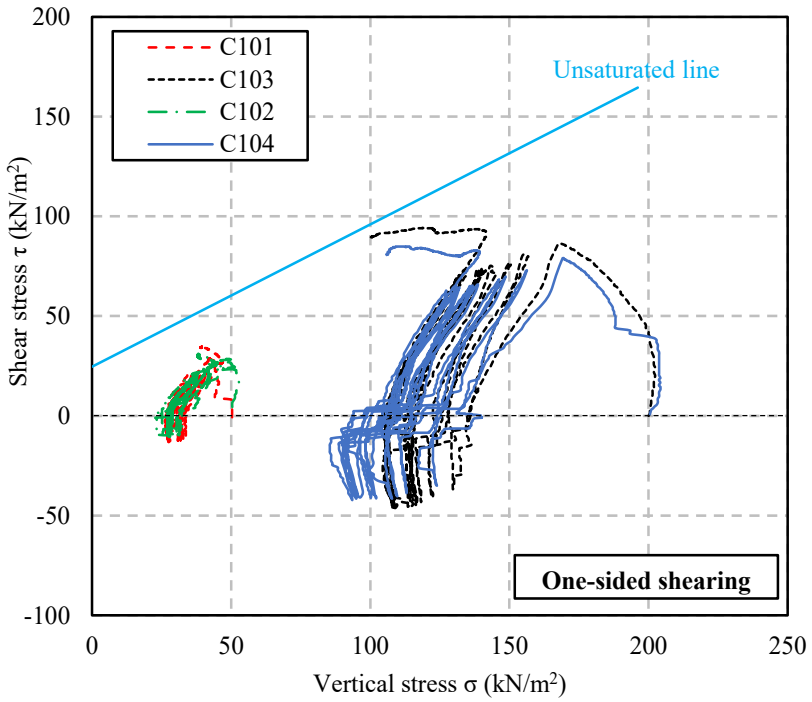

Fig 3.12 Stress path cyclic one-sided shearing

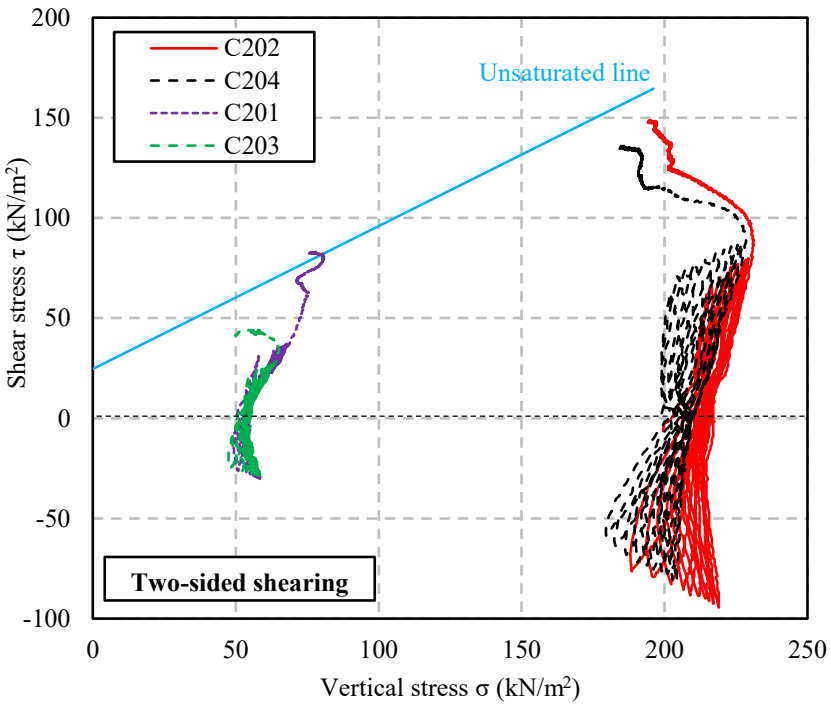

Fig 3.13 Stress path cyclic two-sided shearing

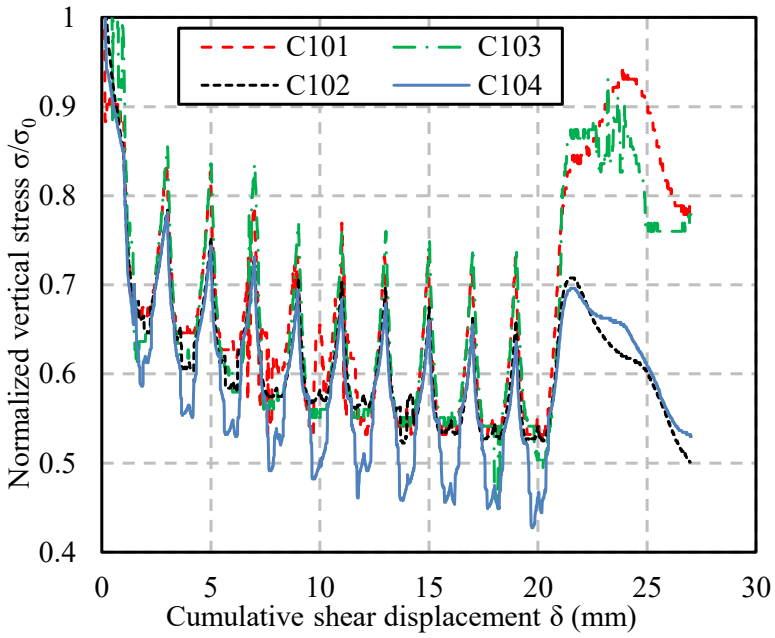

Fig 3.14 Relationship between the vertical stress ratio and cumulative shear displacement one-sided shearing

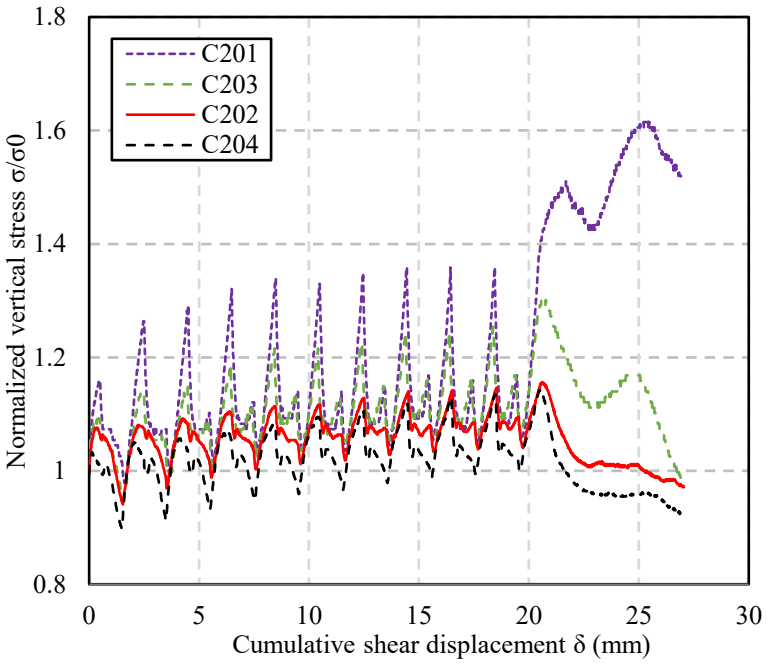

Fig 3.15 Relationship between the vertical stress ratio and cumulative shear displacement two-sided shearing

normalized vertical stress decreases, it is mean affects the shear strength of soil (Matsuda et al, 2011). The normalized vertical stress reduction might be attributed to increase of the pore water pressure during shearing. It must be noted that for both normally consolidated condition and overconsolidated condition, the normalized vertical stress exhibited similar reduction tendency and value. The normalized vertical stress decreases rapidly at the beginning of shearing. However, for the overconsolidated condition the normalized vertical stress decreases till reaching 0.65. Excluding the saturated normally consolidated sample, all samples converge to almost constant normalized vertical stress ratio when reaching 12 mm the cumulative shear displacement. After reaching a total cumulative displacement 20 mm, the shearing continue to 7 mm under static condition. It can be observed the normalized vertical stress significantly increases in the overconsolidated area but cannot converge to the initial condition. For the normally consolidated condition decreases till the end of shearing.

On the other hand, the normalized vertical stress increases for the two-sided cyclic shearing. It can be seen that for both normally consolidated condition and overconsolidated condition, the normalized vertical stress increases rapidly at the beginning of shearing. The increasing of normalized vertical stress might be attributed to effect of cyclic direction amplitude during shearing.

The relationship between the shear displacement and normalized shear stress in the overconsolidated illustrated in Fig. 3.16. There is a significant difference between cyclic one-sided and two-sided shearing. On the cyclic one-sided shearing the test results indicated that the normalized shear stress decreases since the first of cyclic load. This can be attributed to reduction normalized vertical stress during shearing.

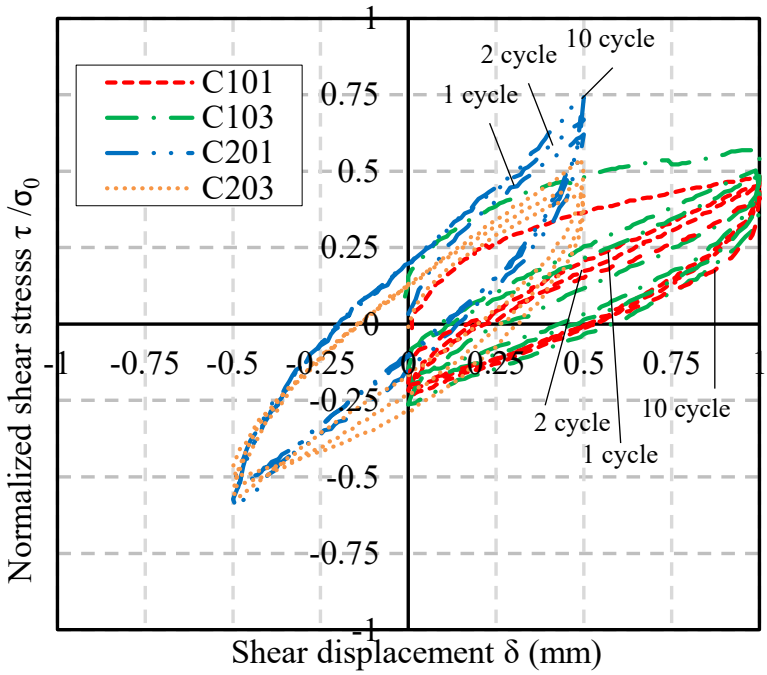

Fig 3.16 Cyclic normalized shear stress - displacement behavior under one-sided and two-sided shearing for the overconsolidated condition

These results are in well agreement with the Takanodai pumice under cyclic loading using direct shear box test (Kasama et al., 2018). On the other hand for the two-sided cyclic shearing test, the normalized shear stress value is higher than the one-sided cyclic shearing test. It can be observed that the normalized shear stress value increases with the increasing number of cyclic till reaching the maximum value at the 10^{th} cycles (final cycles). This might be justified to be a result increasing of frictional resistance of soils. The obtained results also are in good agreement with two-sided cyclic test direct shear box test results obtained by (Cabalar et al., 2013) which reported that increasing of the normalized shear stress with the number of cycles for strain-controlled test. Finally, it can be concluded that the cyclic shearing pattern and direction significantly affect the normalized vertical stress and shear stress of soil.

Furthermore, it can be observed the normalized shear stress of unsaturated

condition, it is significantly larger. The obtained results are in good agreement with the shearing behaviour in the static shearing. This can be related to the suction forces to the total strength of soils.

3.7 Post cyclic behavior

Post cyclic analysis is the one of the methods to evaluate the reduction of soil shear strength due to earthquake load. Fig 3.17 illustrates the schematic of post cyclic test. It can be seen that the post cyclic test was carried out after applying the cyclic loading. In this test, the post cyclic samples were sheared under undrained condition up to 7 mm at a shearing rate of 0.2 mm/min according to the Japanese Geotechnical Society standards. (JGS 0560, 2009). The cyclic one-sided shearing with the displacement 1 mm was adopted.

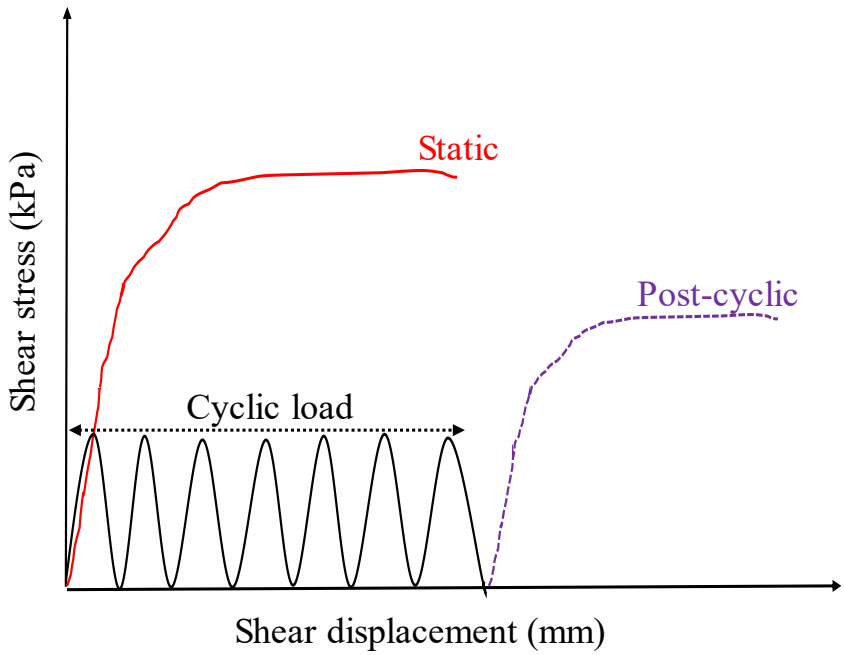

Fig 3.17 Schematic of post cyclic analysis

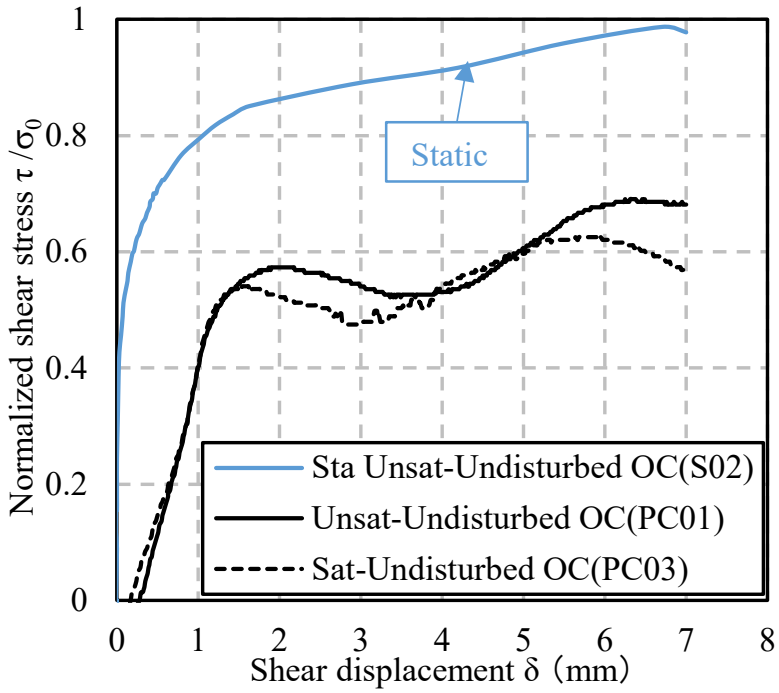

Fig 3.18 Relationship of normalized shear stress and shear displacement of overconsolidated samples (static and post cyclic)

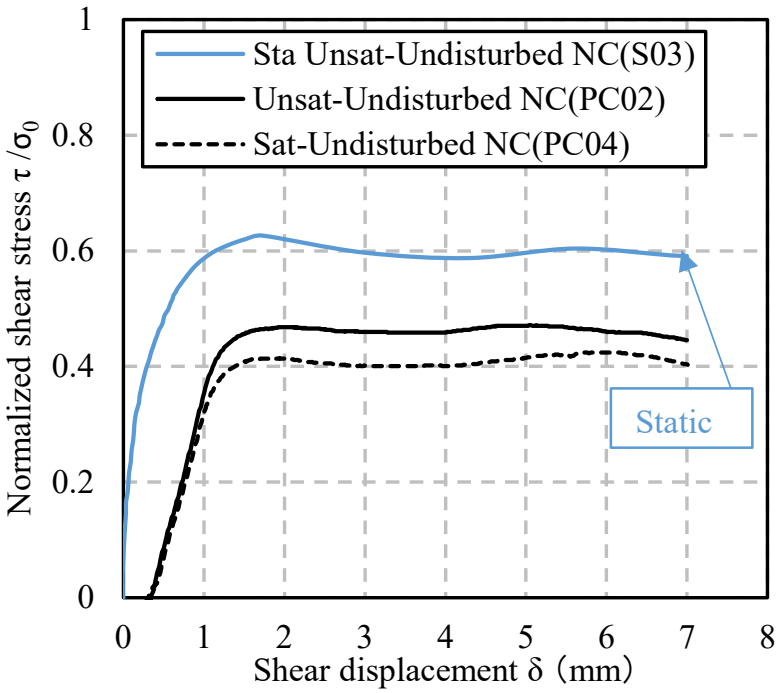

Fig 3.19 Relationship of normalized shear stress and shear displacement of overconsolidated samples (static and post cyclic)

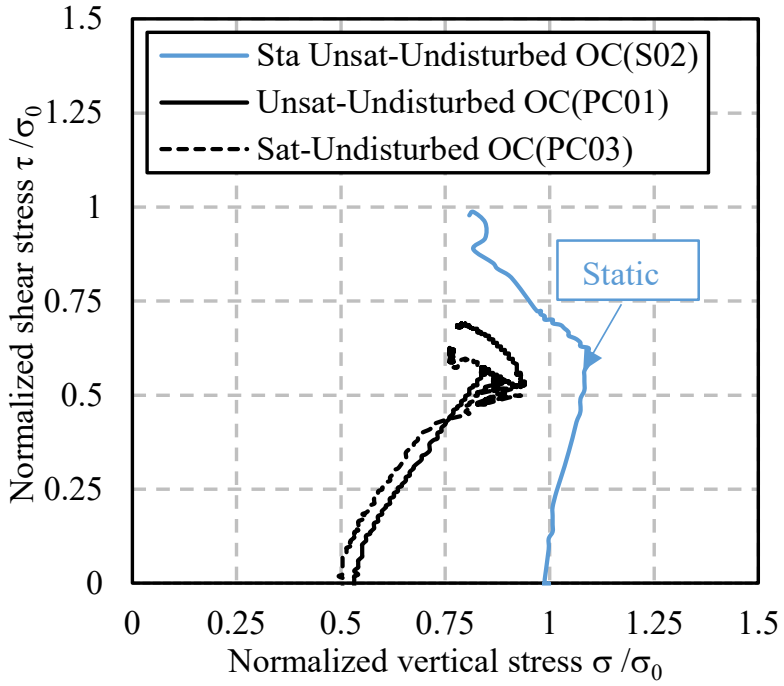

Fig 3.20 Stress path of overconsolidated samples (static and post cyclic)

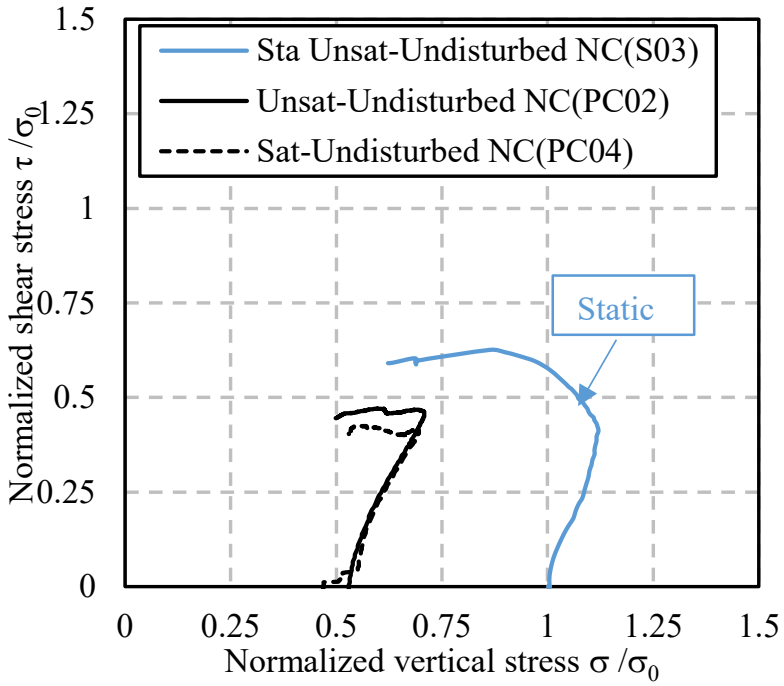

Fig 3.21 Stress path of normally consolidated samples (static and post cyclic)

Fig 3.18 and Fig 3.19 illustrate the relationship of normalized shear stress and shear displacement of overconsolidated and normally consolidated samples under static and post cyclic. It can be seen that the shear stress of the volcanic ash soil decreased significantly after cyclic loading (post cyclic). The shear stress reduction both overconsolidated and normally consolidated samples nearly 30% from static shear stress. It might be attributed to the microstructure of the volcanic ash soil during cyclic loading. On the other hand, the shear stress of unsaturated sample is lower than saturated sample. It can be related to the water content which can be translated to the suction force during shearing.

Furthermore, Fig 3.20 and Fig 3.21 illustrate the stress path of overconsolidated and normally consolidated samples under static and post cyclic. It can be seen that the normalized vertical stress of volcanic ash soil dramatically reduced after cyclic loading. The normalized vertical stress reduction both overconsolidated and normally consolidated samples nearly 50% from static normalized vertical stress. On the other hand, to clearly understand the normalized vertical stress trend, the shear displacement and the normalized vertical stress were plotted as indicated in Fig 3.22 and Fig 3.23. It can be observed that the normalized vertical stress behavior of overconsolidated sample changes to be a heavily overconsolidated behavior. On the other hand, the normalized vertical stress behavior of normally consolidated sample converts to lightly overconsolidated behavior. It might be attributed to the accumulation of pore water generated during cyclic loading both overconsolidated and normally consolidated samples.

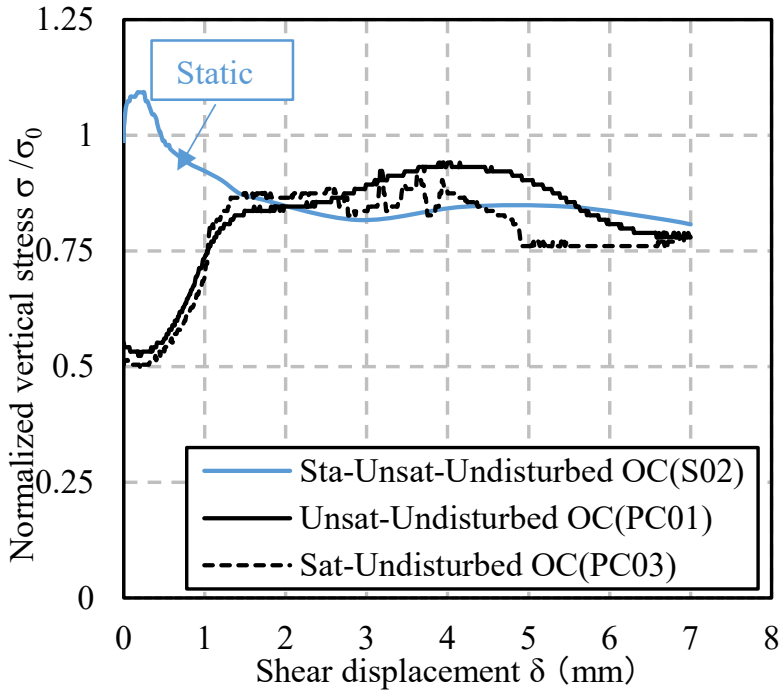

Fig 3.22 Relationship of normalized vertical stress and shear displacement of overconsolidated samples (static and post cyclic)

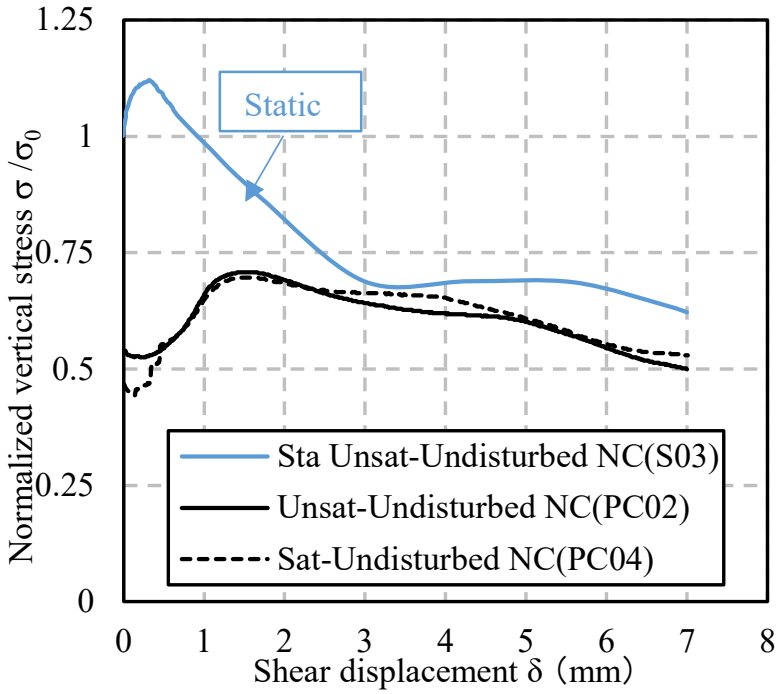

Fig 3.23 Relationship of normalized vertical stress and shear displacement of normally consolidated samples (static and post cyclic)

3.8 Summary

Through this chapter, the mechanical behavior of unsaturated undisturbed volcanic ash soils was investigated using a constant volume direct shear box apparatus. A series of static and cyclic tests were conducted. Also, the post cyclic behavior of the volcanic ash soil was evaluated. The main conclusions are as follows:

1. Under static shearing, unsaturated sample exhibits a higher the apparent cohesion and friction angle in comparison to the saturated sample condition.
2. The normalized vertical stress under one-sided cyclic shearing in both overconsolidated and the normally consolidated samples rapidly reduced at the beginning of shearing.
3. The normalized shear stress of the unsaturated undisturbed sample was found to be larger than that of the saturated sample under both one-sided and two-sided cyclic shearing. This can be attributed to the influence of the matric suction contribution in the total shear strength of soils.
4. In the post cyclic analysis, the normalized shear stress and vertical stress of volcanic ash soil dramatically reduced after cyclic loading.

However, most of the shear strength properties determination considers remolded samples than that of undisturbed samples. Therefore, it is necessary to evaluate the effect of degree of disturbance on the volcanic ash soil which related to the soil structure characteristics through the next chapter.

References

Alowaisy, A., Yasufuku, N., Ishikura, R., Yamamoto, R., Hatakeyama., 2017. Japanese Society Civil Engineers

Atkinson, J. H., Richardson, D., 1987. The effect of local drainage in shear zones on the undrained strength of overconsolidated clay. Geotechnique, 37 (3): 393-403

Cabalar, A. F., Dulundu, K., Tuncay, K., 2013. Strength of various sands in triaxial and cyclic direct shear tests. Journal Engineering Geology, 156: 92-102.

Chiaro, G., Umar, M., Kiyota, T., Massey, C., 2018. The Takanodai landslide, Kumamoto, Japan: insights from post-earthquake field observations, laboratory tests, and numerical analyses. Proc. Geotechnical Earthquake Engineering and Soil Dynamics V, June 10-13, 2018, Austin, Texas: 98-111

Kasama, K., Yamagata, S., Tanaka, H., Furukawa, Z., Yasufuku, N., 2018. Japanese Society Civil Engineers

Kiyota, T., Ikeda, T., Konagai, K., Shiga, M., 2017. Geotechnical damaged caused by the 2016 Kumamoto earthquake, Japan. International of Journal Geoengineering Case Histories, 4 (2): 78-95

Matsuda, H., Hendrawan, A. P., Ishikura, R., Kawahara, S., 2011. Effective stress change and post-earthquake settlement properties of granular materials subjected to multi-directional cyclic simple shear. Soils and Foundations, 51 (5): 873-884

Mayne, P. W., 1984. K0−Cu/συ0 Trends for Overconsolidated Clays. Journal of Geotechnical Engineering, 110 (10): 1511

Miyabuchi, Y., 2016. Landslide disaster triggered by the 2016 earthquake in and around Minamiaso village, western part of Aso caldera, southwestern Japan. Journal of Geography, 125 (3): 421-429

Mukonoki, T., Kasama, K., Murakami, S., Ikemi, H., Ishikura, R., Fujikawa, T., Yasufuku, N., Kitazono, Y., 2016. Reconnaissance report on geotechnical damage caused by an earthquake with JMA seismic intensity 7 twice in 28 h, Kumamoto, Japan. Soils and Foundations, 56 (6): 947-964

Rousseaux, J., and Warkentin, B., 1976. Surface properties and forces holding water in allophane soils. Soil Science of America Journal, 40 (3): 446-451

Wesley, L., 2002. Geotechnical properties of two volcanic soils. University of Auckland.

CHAPTER IV

EFFECT OF SOIL STRUCTURE DISTURBANCE ON THE SHEAR STRENGTH VOLCANIC ASH SOIL

4.1 Introduction

The sample condition gives a great impact to the shear strength of soil to get the reliability of the shear strength properties which in turn directly affects the decisions related to the slope stability analysis, countermeasures, and mitigation in the case of Geo-disasters. Generally, the shear strength properties determination considers remolded samples than that of undisturbed samples. Therefore, it is necessary to evaluate the effect of degree of disturbance on the volcanic ash soil which related to the soil structure characteristics.

Through this chapter, since the volcanic ash soil has unique properties, the chemical composition of the volcanic ash soil was evaluated. On the other hand, the effect of degree of disturbance on the shear strength volcanic ash soil which related to the soil structure characteristics was evaluated. In general, most of the existing studies investigate the soil structure disturbance effect by comparing total shear strength characteristics using a series of cyclic triaxial tests. In addition, the microstructure characteristics are commonly studied using the Scanning Electron Microscope (SEM) (Qinghui et al., 2016; Ding et al., 2019). These methods need special equipment and skill that are generally not available in common Geotechnical laboratories. Through this chapter, the effect of degree of disturbance on the shear strength volcanic ash soil which related to the soil structure characteristics was evaluated using a simple method

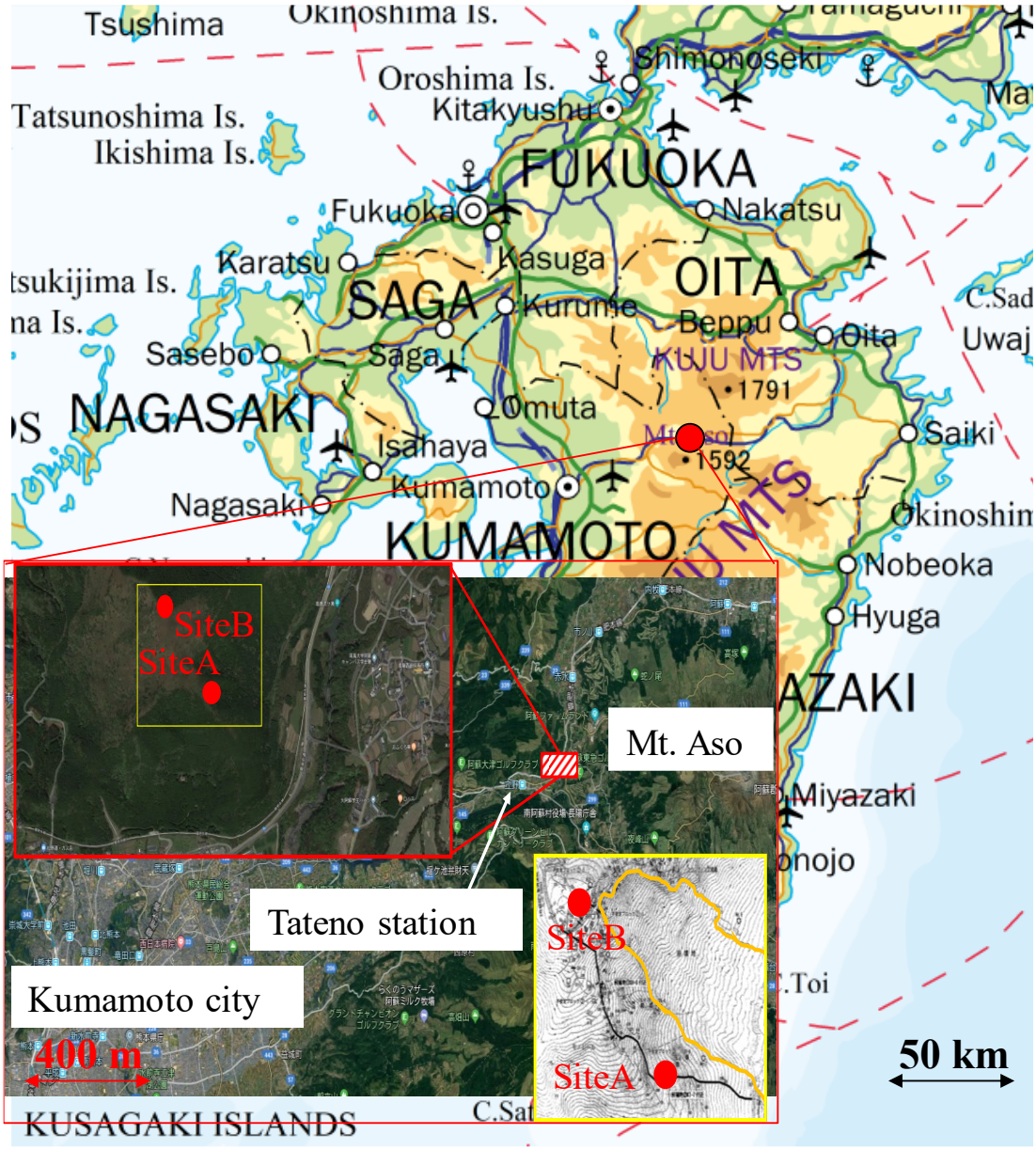

Fig 4.1 Sampling location for undisturbed and disturbed samples

where the disturbance on soil structure was indirectly considered by studying the pore size distribution which was reflected from the soil-water characteristic curve (SWCC) using disturbed and undisturbed samples.

Furthermore, the conventional constant volume direct shear box was used, where several series of static and cyclic tests were carried out. The effect of the precipitation events and the changes in the moisture content was considered by testing and

comparing saturated and unsaturated samples.

4.2 Materials

Tests were conducted using undisturbed and disturbed samples. After Kumamoto earthquake 2016, many slope failures around Aso area occurred. Samples were collected at the middle and the top boundaries of a large slope failure zone as illustrated in Fig 4.1. The sampling points were located 1.5 m below the natural ground surface next to the failure zone boundaries where the cross-section mainly comprised of volcanic ash.

The physical properties of the collected volcanic ash are listed in Table 4.1. The particle size distribution is shown in Fig 4.2. it can be seen that the median grain size D_{50} is approximately 0.012 mm. Consequently, the volcanic ash soil in this research can be classified as volcanic cohesive soil type II (VH2) according to the Japanese Geotechnical Society standards (JGS 0051, 2009).

Table 4.1. Physical properties of the volcanic ash

Physical properties		Volcanic ash
Water content	(%)	111-159
Dry density, ρ_d	(g/cm^3)	0.56-0.58
Bulk density, ρ_t	(g/cm^3)	1.18-1.25
Liquid limit	(%)	154-214
Plastic limit	(%)	112-139
Organic matter	(%)	22.9-28.2
Specific gravity	Gs	2.28-2.34
Coefficient of uniformity	U_c	4.33
D_{50}	mm	0.012
Classification by JGS	Volcanic cohesive soil type II (VH_2)	

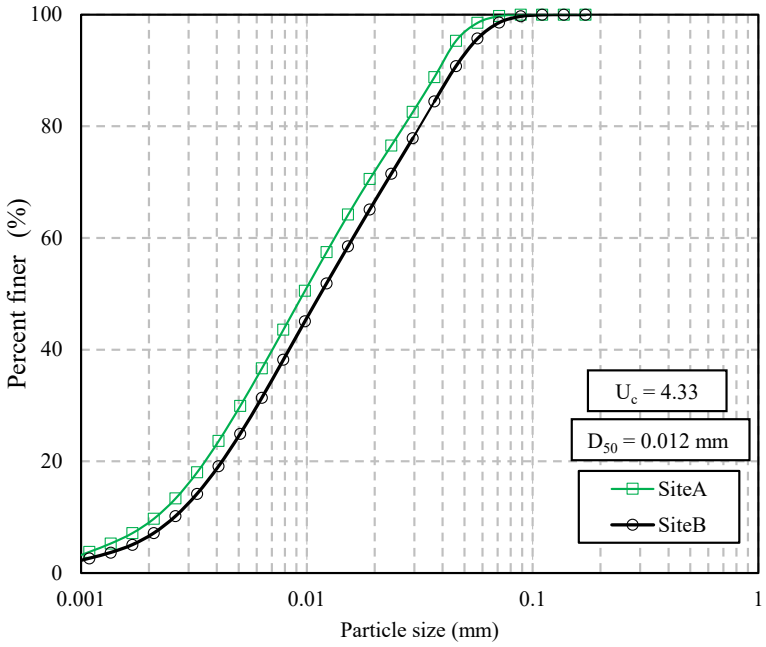

Fig 4.2 Particle size distribution of the volcanic ash soil

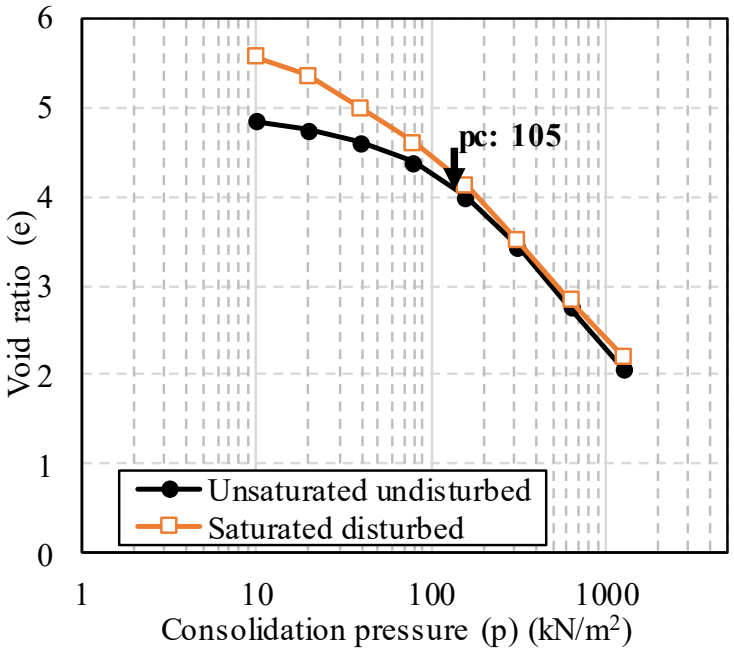

Fig 4.3 Consolidation test result of the volcanic ash soil

The consolidation test results of the saturated and unsaturated volcanic ash are indicated in Fig 4.3. The yield stress corresponding to the unsaturated undisturbed sample was 105 kN/m^2 on average. Based on the consolidation test results, the collected volcanic ash in this research is considered as over-consolidated soil, where the sampling depth was around 1.5 m, therefore the soil was subjected to an overburden pressure less than 105 kPa.

4.3 Methodology

4.3.1 Chemical content analysis

In order to investigate the chemical content, an experiment was performed using X-ray diffraction (MutiFlex 50kv. 50mA) and an energy dispersive X-ray fluorescence analyzer (Shimadzu EDX-7000 50kv. 1000μA). Furthermore, the sample that has been sieved through a 2 mm sieve was prepared for the chemical content test. Similar with the organic matter content test, the sample will dry with 110 ° C oven dryer for 24 hours.

4.3.2 Shearing tests

The shear strength characteristics of the volcanic ash soil were evaluated using the direct shear box (constant volume) tests considering both undisturbed and disturbed samples. In the constant volume test, the volume of the samples is maintained constant. Fig 4.4 shows a schematic diagram of the used direct shear box apparatus. A circular sample with 2 cm in height and 6 cm in diameter was adopted for testing. Both static and cyclic tests were carried out. In the static tests for the over-consolidated (OC) samples, 10 and 50 kPa vertical stress was applied.

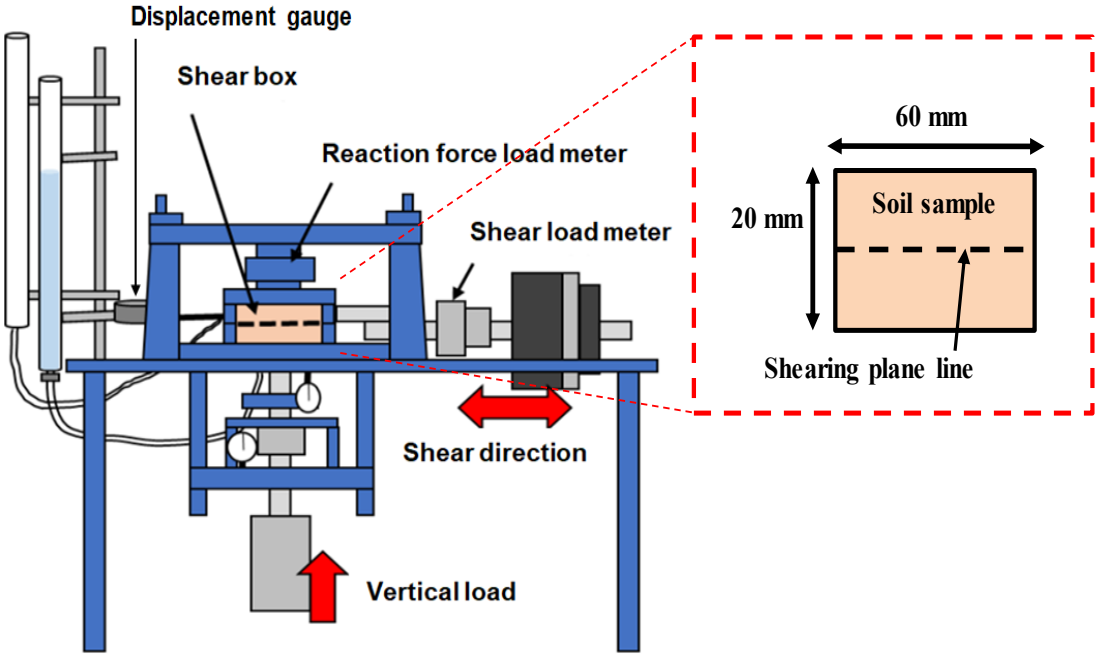

Fig 4.4 Schematic diagram of conventional direct shear box apparatus

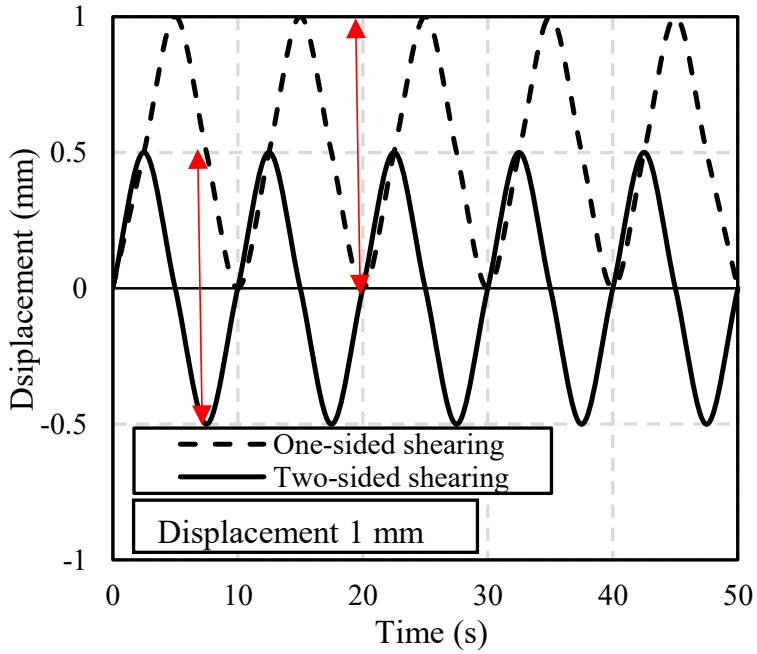

Fig 4.5 Schematic of (one-sided and two-sided) cyclic loading

On the other hand, for the normally consolidated (NC) samples, 200 kPa vertical stress was applied. Prior to shearing, specimens were consolidated under the designated vertical stress for 1 hour. Then, samples were sheared under undrained condition (constant water content) up to 7 mm at a shearing rate of 0.2 mm/min according to the Japanese Geotechnical Society standards. (JGS 0560, 2009)

The cyclic tests were carried out to evaluate the shear strength behavior under the earthquake load. 50 kPa vertical stress was applied for the (OC) samples. While 200 kPa vertical stress for the (NC) sample was applied. Two shearing patterns with a shearing displacement of 1 mm were adopted. The first pattern is one-sided cyclic shearing, while two-sided cyclic shearing corresponds to the second pattern. A schematic diagram illustrating the adopted shearing patterns is shown in Fig 4.5. In the one-sided cyclic shearing pattern, the 1 mm positive displacement was used. While, for the two-sided cyclic pattern, 0.5 mm positive displacement followed by 0.5 mm negative displacement was adopted. For both patterns, the cumulative displacement for each cycle is 2 mm. A total number of 10 cycles was adopted for each pattern. Table 4.2 illustrates the testing program and conditions.

4.4 Chemical composition

In order to elaborate the chemical composition of the volcanic ash soil, X-ray fluorescence analysis (XRF) was carried out. Fig 4.6 shows the chemical composition of the volcanic ash. It was found that the volcanic ash is comprised mainly of SiO_2, Al_2O_3, Fe_2O_3 accounting for as high as about 94%. Those three are the main components formulating a substance called allophane. The individual particles of allophane are much smaller than other clay minerals and are extremely porous.

Table 4.2. Testing program for static and cyclic loading

Test ID	Sample Condition	Sr_0 (%)	Void ratio (e_0)	Vertical stress (kN/m^2)
Static test				
S01	Unsat-Undisturbed	65.5	4.70	10
S02	Unsat-Undisturbed	68.0	5.16	50
S03	Unsat-Undisturbed	72.5	4.95	200
S04	Sat-Undisturbed	99.7	4.60	10
S05	Sat-Undisturbed	99.3	4.77	50
S06	Sat-Undisturbed	100	4.72	200
SD01	Sat-Disturbed	100	5.10	10
SD02	Sat-Disturbed	100	4.82	50
SD03	Sat-Disturbed	100	5.12	200
One-sided cyclic				
C101	Unsat-Undisturbed	67.8	4.03	50
C102	Unsat-Undisturbed	69.5	4.01	200
C103	Sat-Undisturbed	99.5	4.41	50
C104	Sat-Undisturbed	96.8	4.45	200
CD101	Unsat-Disturbed	80.7	4.82	50
CD102	Unsat-Disturbed	79.4	4.61	200
CD103	Sat-Disturbed	100	4.96	50
CD104	Sat-Disturbed	100	4.90	200
Two-sided cyclic				
C201	Unsat-Undisturbed	74.1	4.73	50
C202	Unsat-Undisturbed	82.9	4.96	200
C203	Sat-Undisturbed	100	4.43	50
C204	Sat-Undisturbed	100	4.77	200
CD201	Unsat-Disturbed	81.6	4.54	50
CD202	Unsat-Disturbed	82.2	4.64	200
CD203	Sat-Disturbed	100	4.49	50
CD204	Sat-Disturbed	100	4.23	200

Allophane is a product of the weathering process of volcanic ash,where the ash is formed by the rapid cooling of the material generating from volcanic eruptions. The rapid cooling is too fast and prevents the formation of crystalline structure. For the ash to transfer into allophane, it was found that the material from which the ash is originally reported must be non-crystalline and that it must remain well-drained during cooling (Wesley, 2002). Several researchers have shown that the allophane molecule is effective at retaining water (Parfitt, 1990; Rousseaux and Warkentin, 1976)

The ‘rule of thumb’ that ‘allophanic soils always have a high water content’ has been investigated by (So, 1995 and Wesley, 2002). Their combined findings using some allophane soils from New Zealand (NZ) and Indonesia (INA) are illustrated in Fig. 4.7, where an obvious correlation between the allophane content and water content can be observed.

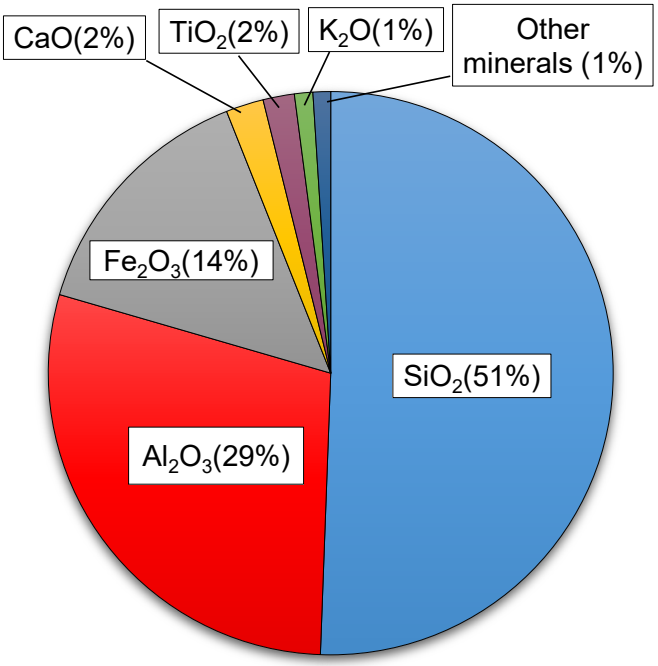

Fig 4.6 Chemical composition of the volcanic ash soil

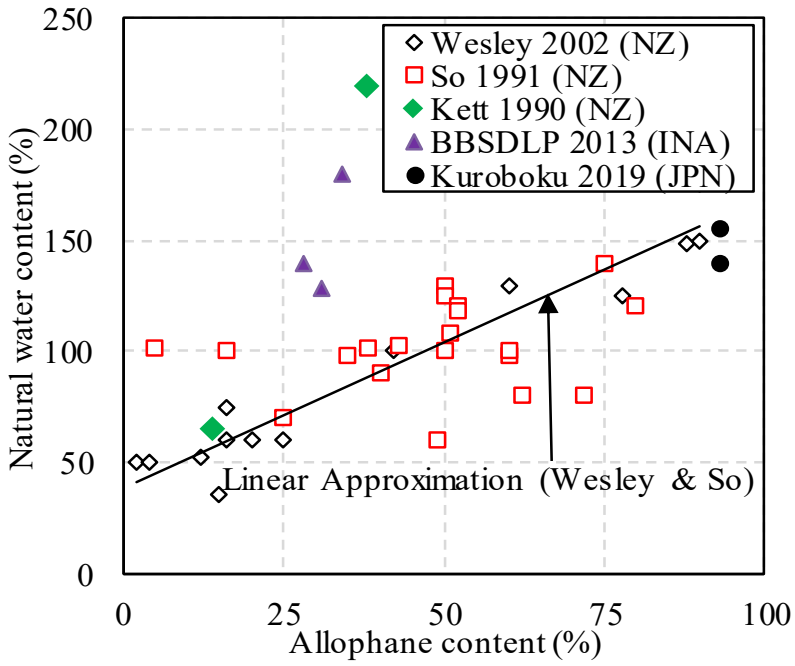

Fig 4.7 Natural water content of allophanic soils in some areas compared to their allophane content

Furthermore, allophane behavior in response to the external loads (such as compaction and earthquake shakes) is generally different from that of other clay types. Wesley, 2009 reported that the external load destroys the chemical structure of the allophane, consequently transforming the mineral into an amorphous mass with low strength. In addition, the breakdown of the chemical structure releases large amounts of adsorbed water that is held within that structure, causing further strength reduction.

4.5 Pore size distribution

Soil mass is a collection of soil particles of various sizes and shapes with pores filled with air and water. The pore-size distribution (PSD) is critical in understanding the physical, mechanical, and hydraulic behavior of soil (Simms et al., 2001; Saranya et al., 2016; and Niu et al., 2019). Mercury Intrusion Porosimetry (MIP) is a commonly

used technique for evaluating the pore size distribution (PSD) for porous media, such as soil and rock. In this technique, mercury at an increasing pressuring step is injected into the porous material, and the volume of the injected mercury is recorded. (Wang et al., 2016) has developed a simple technique to determine the pore size distribution based on the soil-water characteristic curve (SWCC). The obtained results compare well to the MIP test results with an excellent correlation. However, the determination of the PSD using the SWCC based technique may be valid only for the drying phase.

Based on that, in this paper, the pore size distribution for volcanic ash soil was evaluated using SWCC for the drying phase. Different suction pressures correspond to the penetration of air in different pore sizes, which can be determined using the Washburn equation (Nimmo, 2014) as follows:

$$d = 4Ts\cos\alpha/P \quad (4.1)$$

where d is the soil pore diameter; Ts is the surface tension; α is the contact angle between the soil particles and the fluid, and P is the applied pressure or the capillary/suction pressure.

The SWCC corresponding to the undisturbed and disturbed samples of volcanic ash soil was reported by (Alowaisy et al., 2019) as illustrated in Fig 4.8. It can be observed that the SWCC of the undisturbed sample differs from that of the disturbed sample. Furthermore, the disturbed sample has a larger air entry value in comparison to the disturbed sample.

Fig 4.9 illustrates the pore size distribution of the volcanic ash soil. It can be seen that there is a significant difference between the undisturbed and disturbed samples, where the cumulative pore volume corresponding to the undisturbed samples was found to be larger than that of the disturbed sample. The dominant pore diameter of

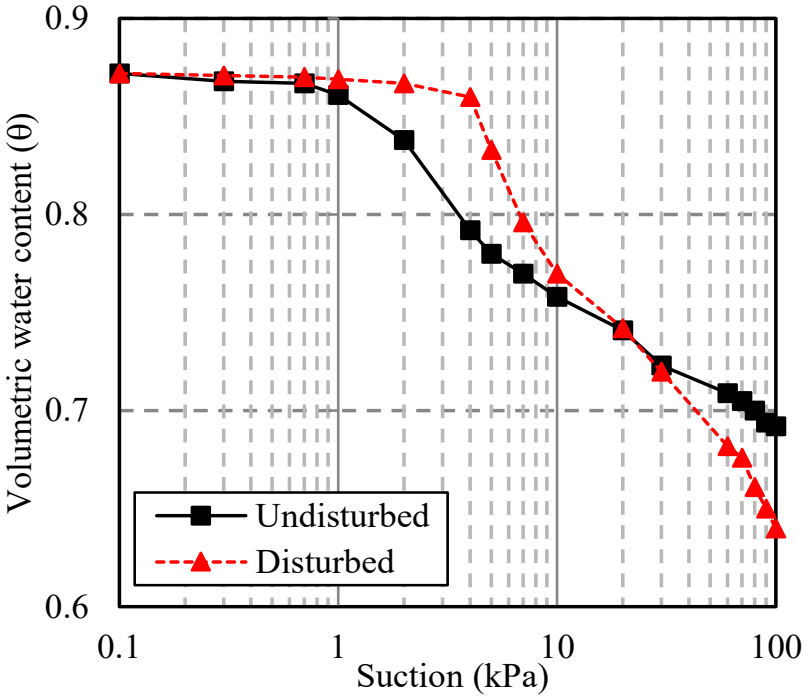

Fig 4.8 The SWCC of the volcanic ash soil

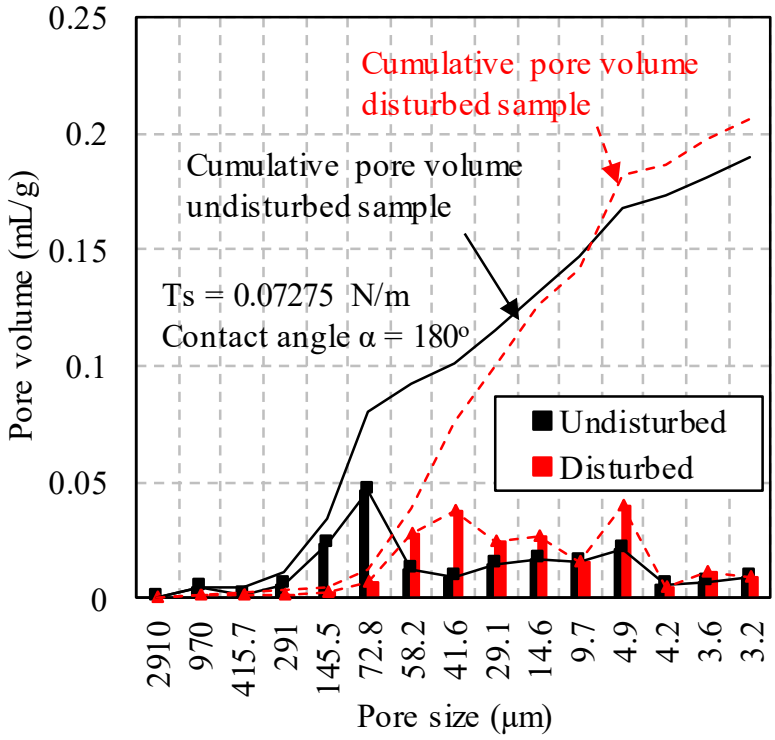

Fig 4.9 The pore size distribution of the volcanic ash soil

the undisturbed sample is observed with an average diameter of 72.8 μm (one peak). While for the disturbed sample, two dominant pore diameters (two peaks) were obtained with diameters of 41.6 and 4.9 μm, respectively. That behavior can be attributed to the pore structure disturbance, where the undisturbed sample exhibits a unimodal pore structure, while the disturbed sample exhibits a bimodal pore structure. It must be noted that unimodal distribution indicates the existence of inter pore water only. While a bimodal distribution reflects both an inter pore and intra pore morphology. The inter pore represents the water molecules bounded between soil aggregates whereas the intra pore represents the water molecules bounded within the soil aggregates and on the clay particles surface. Consequently, it can be concluded that the pore structure of the disturbed sample is relatively unstable.

4.6 Static shearing characteristic

Fig 4.10 illustrates the relationship of shear stress and shear displacement. It can be seen the shear stress of disturbed sample is lower than undisturbed sample. On the other hand, Fig 4.11 illustrates the stress path of undisturbed and disturbed samples. For the undisturbed sample, the apparent cohesion decreases from 24.6 kN/m^2 under the unsaturated condition to 13 kN/m^2 for saturated conditions. In addition, the apparent friction angle slightly reduced from 35.5° under the unsaturated condition to 35.1° for the saturated condition. Furthermore, the apparent cohesion decreases dramatically more than 50 % for the saturated disturbed sample condition, while the apparent friction angle slightly reduced to 34.08° in comparison to the undisturbed conditions. This behavior can be related to the effect of soil structure disturbance in the volcanic ash soil which was elaborated in the pore size distribution characteristics.

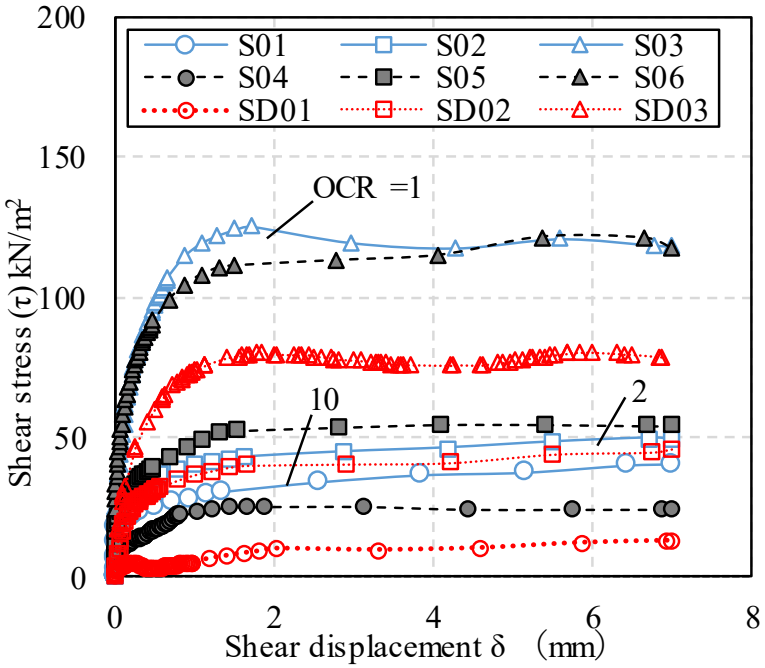

Fig 4.10 Relationship of shear stress and shear displacement

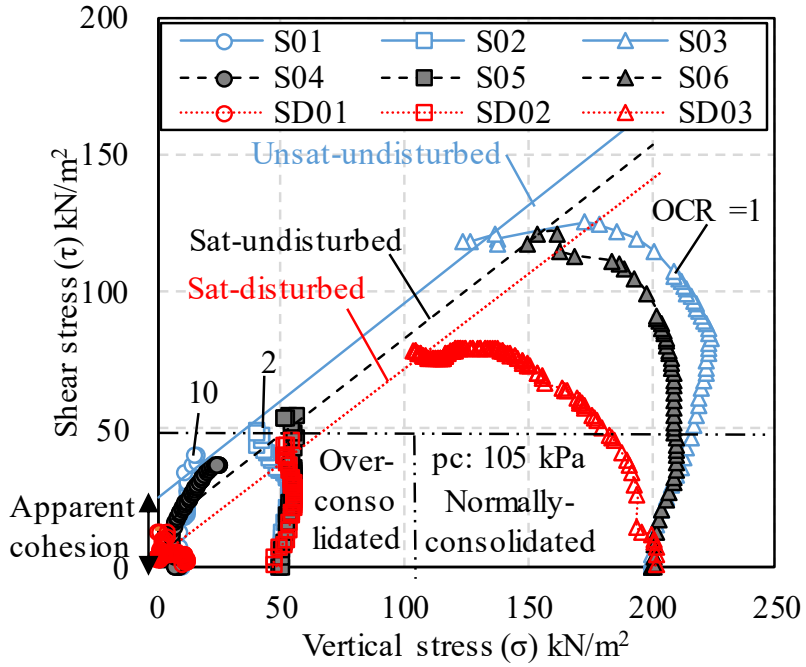

Fig 4.11 Stress path of undisturbed and disturbed samples

Finally, it can be concluded that the shear strength strongly depends on the soil structure and water content which is translated into suction force that contributes significantly to the total shear strength of the soil.

4.7 Cyclic shearing behavior

For the cyclic strain-controlled mode, the normalized vertical stress degradation with the number of cycles (N) can be quantified using the degradation index (δ). Where S_1 and S_N are the initial normalized vertical stress and the normalized vertical stress after N cycles at constant shear strain amplitude.

$$\delta = \left(1 - \frac{\sigma_{SN}/\sigma_0}{\sigma_{S1}/\sigma_0}\right) = \left(1 - \frac{\sigma_{SN}}{\sigma_{S1}}\right) \quad (4.2)$$

In general, for the one-sided cyclic shearing, the normalized vertical stress reduces by increasing the number of cycles. Consequently, the reduction in the normalized vertical stress leads to a reduction in the total shear strength of the soil (Matsuda et al., 2011). The reduction of the normalized vertical stress might be associated with an increase of the pore water pressure during the shearing test.

The relationship between the degradation index of the cyclic normalized vertical stress and the number of cycles for the over-consolidated and normally consolidated samples are illustrated in Fig 4.12 and Fig 4.13 respectively. A significant difference between the undisturbed and disturbed samples can be observed. The degradation index value corresponding to the disturbed sample is 20 % higher than that of the undisturbed sample, where for both conditions the degradation index increases by increasing the number cycles. In other words, the cyclic normalized vertical stress of disturbed samples degrades faster than that of the undisturbed samples under cyclic

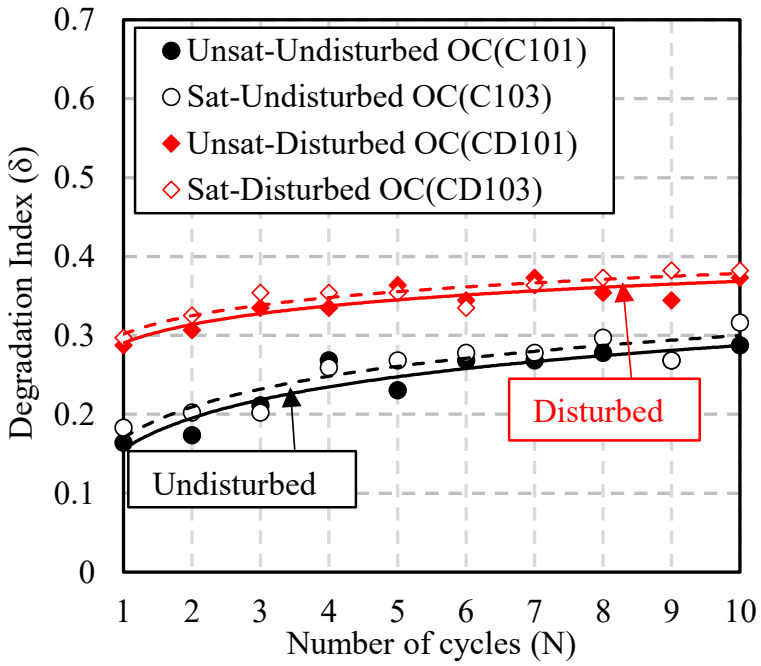

Fig 4.12 Degradation index (δ) over-consolidated sample

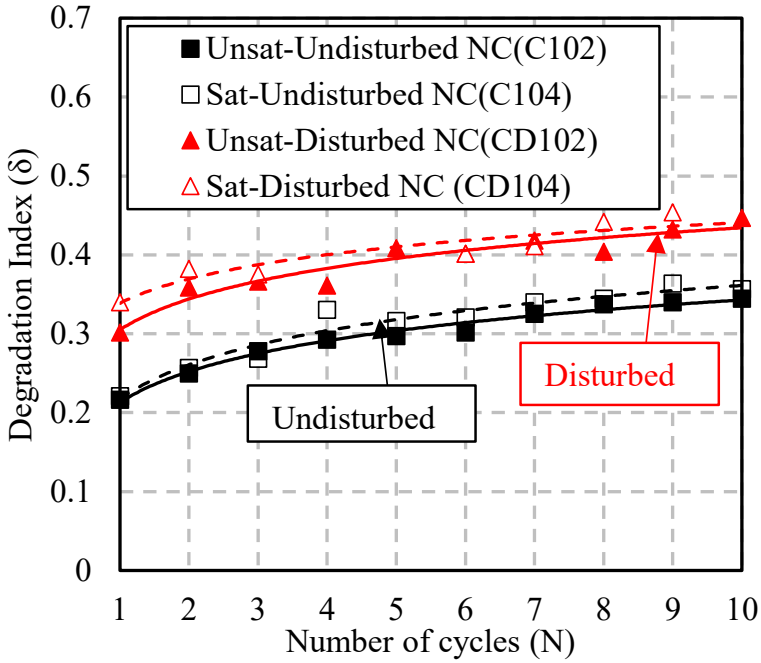

Fig 4.13 Degradation index (δ) normally consolidated sample

loading. It must be noted that for both over-consolidated and normally consolidated samples, the normalized vertical stress shows a similar reduction tendency. The normalized vertical stress decreases immediately at the beginning of the shearing. It can be concluded that the effect of soil structure disturbance can be observed in the cyclic normalized vertical stress degradation, where the degradation index of the cyclic normalized vertical stress is higher for the disturbed samples which can be attributed to the unstable micro-pore structure of the disturbed samples.

On the other hand, the degradation index of the cyclic normalized vertical stress in the normally consolidated samples was found to be larger than that of the over-consolidated samples. This trend can be attributed to the increase in the pore water pressure during shearing, where, the generated pore water pressure is lower for over-consolidated samples in comparison to the normally consolidated samples.

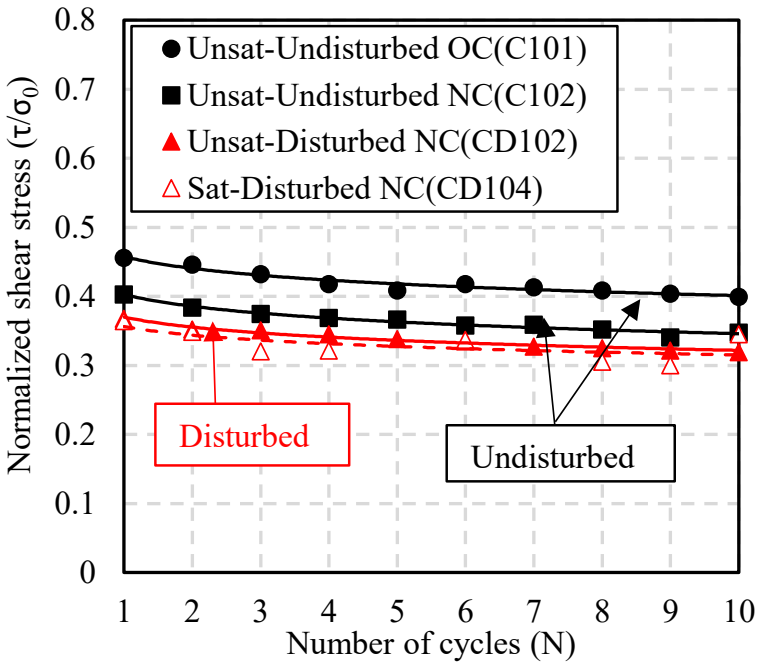

Fig 4.14 Normalized shear stress for one-sided shearing

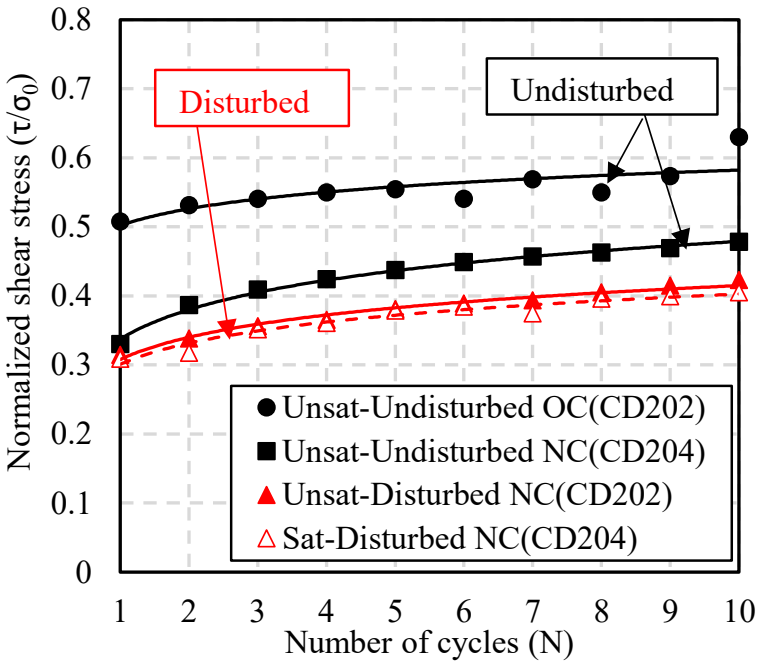

Fig 4.15 Normalized shear stress for two-sided shearing

Furthermore, the degradation index tends to be lower for the unsaturated condition than that of the saturated conditions for both over-consolidated and normally consolidated samples. It can be said that the total shear strength of the soil strongly depends on the water content, which can be translated into the suction force which contributes to the total shear strength.

The relationship between the normalized shear stress and the number of cycles for the normally consolidated samples under one-sided and two-sided shearing patterns are shown in Fig 4.14 and Fig 4.15, respectively. The normalized shear stress corresponding to the undisturbed samples is 10% higher than that of the disturbed samples. On the other hand, a significant difference in the shear stress development pattern was observed. For the one-sided cyclic shearing, the test results showed that the normalized shear stress reduces starting from the first cycle for both disturbed and undisturbed samples. While significantly higher normalized shear stress value was

obtained under the two-sided cyclic shearing test in comparison to the one-sided cyclic shearing test. It can be seen that the increasing number of cycles leads to a monotonical increase in the normalized shear stress value till achieving the maximum value after 10 cycles (last cycles). This can be attributed to the increase in the frictional resistance of the soil due to the shear displacement direction. The results also compare well to two-sided cyclic shearing direct shear box test results reported by (Putra et al., 2019). It was reported that increasing the number of cycles results in increasing the normalized shear stress for the strain-controlled test. Finally, it can be concluded that the cyclic shearing pattern and direction significantly influence the total shear strength of the soil.

Also, it can be recognized that the normalized shear stress of unsaturated conditions is slightly larger than that of the saturated conditions. It can be related to the suction forces' contribution to the total strength of the soil, where the interparticle forces due to the suction in the unsaturated condition is higher than that of saturated condition.

4.8 Correlation of the average degradation index and the peak shear stress ratio

In order to evaluate the correlation of the degradation index and the static shear stress ratio, the degradation index (δ_{avg}) from the first cycle till the final cycles is plotted against the peak static shear stress ratio (τ_p/σ_0) for the whole soil samples as illustrated in Fig. 4.16. It can be observed that a lower static shear stress ratio (τ_p/σ_0) imposes a higher average degradation. Thus, the normalized vertical stress reduction during the cyclic loading strongly depends on the average degradation index.

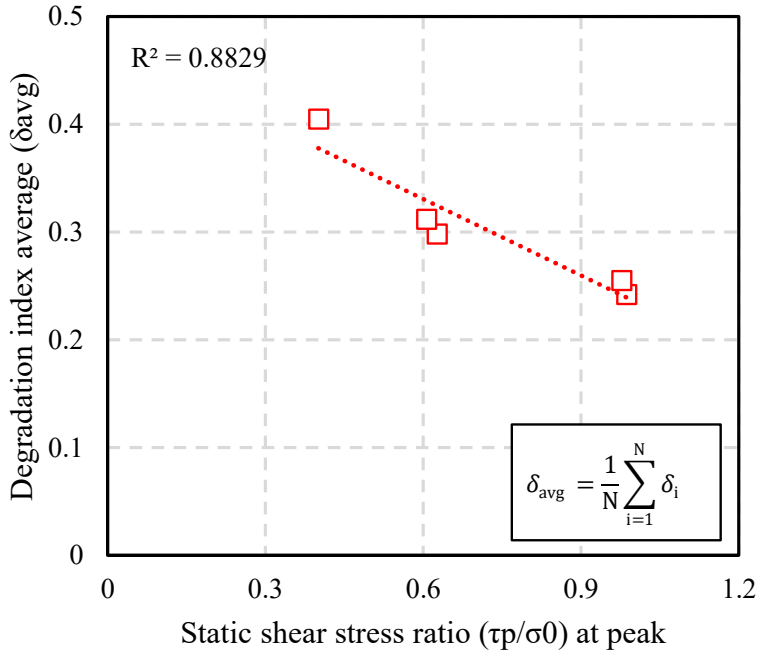

Fig 4.16 Relationship between average degradation index and peak static shear stress ratio

4.9 Summary

Through this chapter, the chemical content of the volcanic ash soil was evaluated. On the other hand, the pore size distribution reflected from the soil-water characteristic curve (SWCC) has been discussed. The shear strength characteristic of the volcanic ash soil was investigated using a constant volume direct shear box apparatus under static and cyclic loading tests. The main conclusions are as follows:

1. It was found that the chemical composition of volcanic ash soil is comprised mainly from SiO_2, Al_2O_3, Fe_2O_3 which accounts for as high as about 94%. It is known that these three substances are the main components of substances called allophane.
2. The undisturbed samples exhibit a unimodal pore structure and the disturbed

samples exhibit a bimodal pore structure. Since the pore structure of the disturbed sample is unstable, the static shear strength tends to be lower, and the degradation index value is around 20 % higher than that of the undisturbed sample. In other words, the cyclic normalized vertical stress of disturbed samples degrades faster under cyclic loading. It can be said that the disturbed sample do not properly represent the field conditions with significant discrepancies that should be carefully considered when conducting the slope stability analysis.

3. The degradation index value in the normally consolidated samples was found to be larger than that of the over-consolidated samples. It might be associated with the increase in the pore water pressure during shearing, where the pore water pressure reduction in the over-consolidated sample is lower than that of the normally consolidated samples.
4. The normalized vertical stress and shear stress of the unsaturated samples under static and cyclic loading is larger than that of saturated sample. This can be related to the influence of the matric suction which contributes to the total shear strength of the soil.
5. A good correlation between the average degradation index (δ_{avg}) and the static shear stress ratio (τ_p/σ_0) was obtained. A lower static shear stress ratio (τ_p/σ_0) imposes a higher average degradation index.

It was mentioned that the conventional direct shear box apparatus considers only the initial condition for the unsaturated testing. In order to get more reliable and accurate results for unsaturated shear strength, the suction-controlled testing method is needed. Where, the designated suction value can be maintained during shearing.

References

Alowaisy, A., Yasufuku, N., Ishikura, R., Hatakeyama, M., Kyono, S., 2019. Novel rapid measurement system of undisturbed soils water characteristics curve utilizing the continuous pressurization method. Proc. 7th International Symposium on Deformation Characteristics of Geomaterials (IS-Glasgow 2019), June 26-28, 2019, Glasgow: 92

Ding, Z., Kong, B., Wei, X., Zhang, M., Xu, B., Zhao, F., 2019. Laboratory testing to research the microstructure and dynamic characteristics of frozen-thawed marine soft soil. Journal of Marine Science and Engineering, 7 (85): 1-19

Nimmo, J. R., 2004. Porosity and Pore Size Distribution. Elsevier, 3: 295-303

Niu, G., Sun, D., Shao, L., Zeng, L., 2019. The water retention behaviours and pore size distributions of undisturbed and remoulded complete-intense weathering mudstone. European Journal of Environmental and Civil Engineering, 1-17

Matsuda, H., Hendrawan, A. P., Ishikura, R., Kawahara, S., 2011. Effective stress change and post-earthquake settlement properties of granular materials subjected to multi-directional cyclic simple shear. Soils and Foundations, 51 (5): 873-884

Putra, O. A., Yasufuku, N., Ishikura, R., Alowaisy, A., Kawaguchi, Y., 2019. Mechanical behaviour of unsaturated undisturbed volcanic ash soil under static and cyclic loading. Proc. 7th International Symposium on Deformation Characteristics of Geomaterials (IS-Glasgow 2019), June 26-28, 2019, Glasgow: 92

Qinghui, L., Jiajia, Y., Jian, Z., Zhigang, C., 2016. Microstructure study on intact clay behavior subjected to cyclic principal stress rotation. Proc. International Conference on Transportation Geotechnics, September 4-7, 2016, Portugal: 991-998

Saranya, N., and Arnepalli, D. N., 2016. Effect of pore size distribution on unconfined compressive shear strength. Proc. Indian Geotechnical Conferences, December 15-17, 2016, India

Simms, P. H., and Yanful, E. K., 2001. Measurement and estimation of pore shrinkage and pore distribution in a clayey till during soil water characteristic curve tests. Canadian Geotechnical Journal, 38: 741-754

So, E., 1995. Influence of allophane content on the reactivity and pore size distribution of lime stabilized volcanic soil. Journal of the Society of Materials Science Japan, 44 (503), 1007-1010.

Wang, M., Pande, G. N., Kong, L. W., Feng, Y. T., 2016. Comparison of pore-size

distribution of soils obtained by different methods. International Journal of Geomechanics, Technical Note 06016012

Wesley, L., 2002. Geotechnical properties of two volcanic soils. University of Auckland.

Wesley, L., 2009. Behaviour and geotechnical properties of residual soils and allophane clays. Obras y Proyectos, (6): 5-10

CHAPTER V

NEW SUCTION CONTROLLED UNSATURATED DIRECT SHEAR BOX APPARATUS AND TESTING PROCEDURE DEVELOPMENT

5.1 Introduction

Regardless of the adopted technique, the main challenges facing the experimental determination of the shear strength of unsaturated soil are large number of tests required to explain of the shear strength with the matric suction, and the long testing time needed to achieve suction equilibrium in soil samples before they can be sheared. Methods for testing unsaturated shear are generally more complex, time consuming and more expensive when compared to the conventional testing methods for saturated soil. Although the interest in evaluating unsaturated soil characteristics has significantly increased, more studies are required to generalize and validate methods. Further studies considering the practical testing methods that can reduce the cost and time associated with shear strength testing of unsaturated soils are needed (Fredlund et al., 1977, 1978, 1996; Nam et al., 2011).

In general, the shear strength of unsaturated soil can be determined using both laboratory tests and empirical models. The ultimate goal of these experimental methods is to establish the shear strength characteristics of unsaturated soils in terms of net normal stress and matric suction. The matric suction is an important parameter that affects the shear strength of the unsaturated soils and is considered to be a component of the cohesion in unsaturated soil shear strength (Kim et al., 2010, 2013).

Most of the existing studies mainly focus on the unsaturated triaxial testing results. Some experimental methods were conducted using a modified triaxial equipment that allows the control or measurement of the pore air pressure (u_a) and the pore water pressure (u_w) (Gan et al., 1988; Gens et al., 2006; Chai et al., 2010). However, it takes at least several weeks (long time consuming) to conduct one experiment using the triaxial tests for unsaturated soil, and in some cases this process may become an obstacle in solving the in situ problem that should be treated within a short period of time. Based on that, for overcoming these time-consuming problems, the laboratory testing for unsaturated soil has been carried out applying the axis translation technique where the pore air and pore water pressure can be controlled independently using the direct shear box apparatus. The advantages include: shorter drainage distance, testing time, and simple testing operation compared with that of the triaxial test (Vanapalli et al., 1996, 1999).

In this chapter, a new suction controlled direct shear box apparatus for unsaturated soil testing and testing procedure was developed. A series of static constant volume and constant stress direct shear box tests were carried out under unsaturated and saturated conditions using the standard soil (Toyoura sand) and the volcanic ash soil.

5.2 Suction controlled necessity on unsaturated soil test

It was mentioned that the limitation of conventional direct shear box apparatus considers only the initial condition for the unsaturated testing. During shearing, the suction value will be changed. In order to get more reliable and accurate results for unsaturated shear strength, the suction-controlled testing method is needed. Where, the

designated suction value can be maintained during shearing.

Suction controlled tests can be controlled using the axis-translation technique. The suction is usually kept constant during the application of shear stresses. Suction controlled tests are more commonly performed on undrained and drained tests.

The basic principle of the axis-translation technique is to elevate the total stress, the pore air pressure and the pore water pressure by an equal amount so that the pore water pressure is raised to a positive value (relative to atmospheric pressure) and can then be controlled or measured.

The axis translation technique is by far the most common method used in geotechnical engineering for applying controlled value of suction to a soil sample. In order to keep a constant matric suction, the axis-translation technique can be applied in different ways: increase the air pressure u_a while the pore water pressure u_w is kept constant or lower the pore water pressure while keeping the air pressure constant. Lowering the pore water pressure is limited, since the cavitation effect will appear when the pore water pressure approaches –1 atm (i.e. –101.3 kPa). So, it is easier to impose suction by rising the air pressure with respect to the pore water pressure. This method is usually called the imposed air pressure method.

5.3 New suction controlled direct shear box apparatus

A new suction controlled direct shear box apparatus has been developed in Geotechnical Engineering Laboratory of Kyushu University. The pedestal part is equipped with the high air entry value ceramic disk, here various stress conditions for unsaturated sample test conditions can be performed. The axis translation technique was adopted to control both pore air and pore water pressure in order to maintain matric

suction within the specimen. Furthermore, the direct shear box apparatus is used in this study to obtain the mechanical properties of a cylindrical soil specimen by performing a Constant Volume Direct Shear Test according to JGS 0560-2000. Fig. 5.1 and Fig. 5.2 show a photograph and completed schematic layout diagram of the unsaturated direct shear box apparatus. This apparatus consists of top and bottom shear boxes in which soil sample is contained for testing. All the data including (consolidation stress, vertical displacement, shear stress, shear displacement and suction pressure) are recorded using the data logger and then transmitted to the PC (main computer).

The unsaturated direct shear box apparatus consists of the main system comprised of several components. From the schematic layout, it can be seen that the main components are: (a) The shear boxes (upper and lower box) with 60 mm in diameter and 20 mm in height sample inside. The lower box is made from stainless steel while the upper box is made from acrylic material. (b) The vertical stress load cell with a maximum capacity of 100 kPa. When the maximum vertical stress is achieved, the test is automatically stopped. This apparatus is low-stress type unsaturated direct shear box test apparatus. (c) 7 mm ceramic disk in thickness with an air entry value of 100 kPa equipped with a metal porous disk attached to the pedestal part as shown in Fig. 5.3. The metal porous disk was used to saturate the sample with the water supplied from the burette tube. While for the water drainage from the saturated sample to reach the unsaturated state, the ceramic disk was used. Both the ceramic disk and the metal porous line were controlled using the control box. (d) Air pressure chamber was installed in the upper and lower apparatus to cover the shear box and keep the designated pore air pressure at a specific value. During testing, the

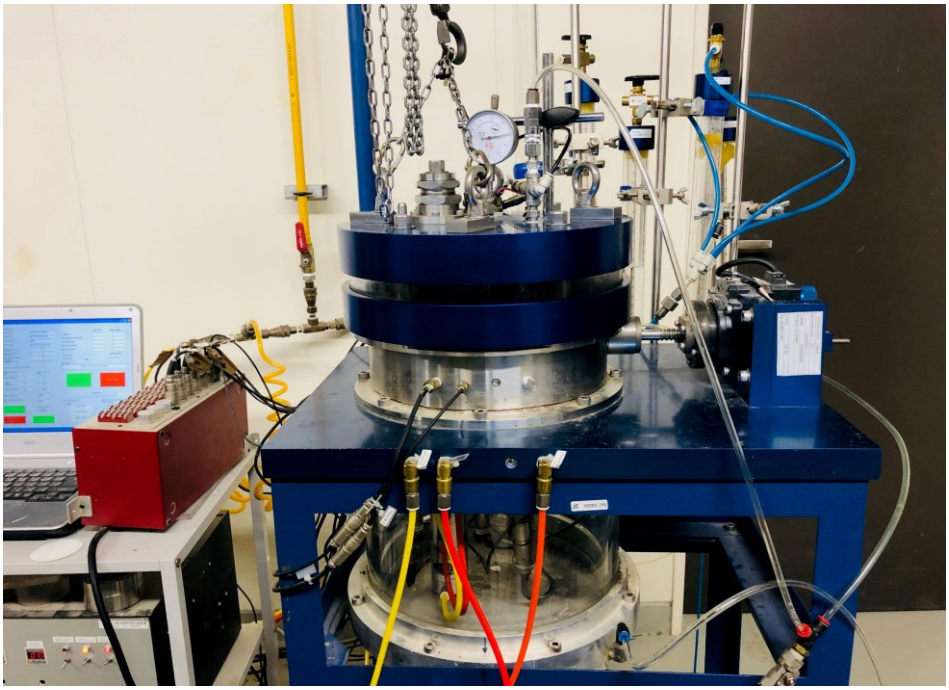

Fig 5.1 Photograph of unsaturated direct shear box test.

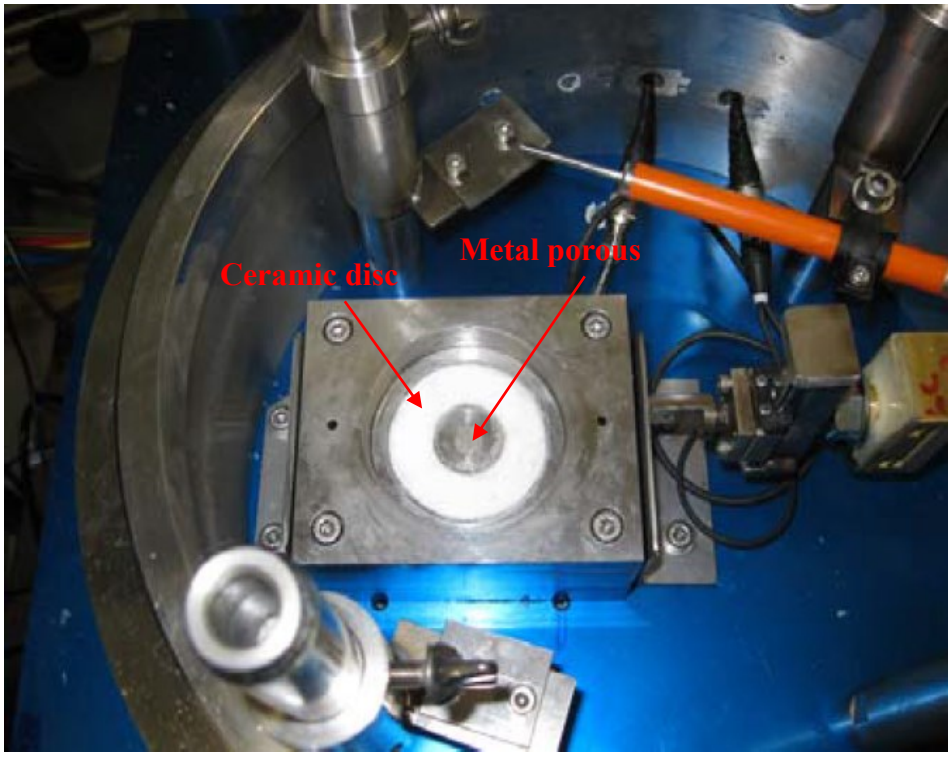

Fig 5.3 Photograph of ceramic disk and metal porous.

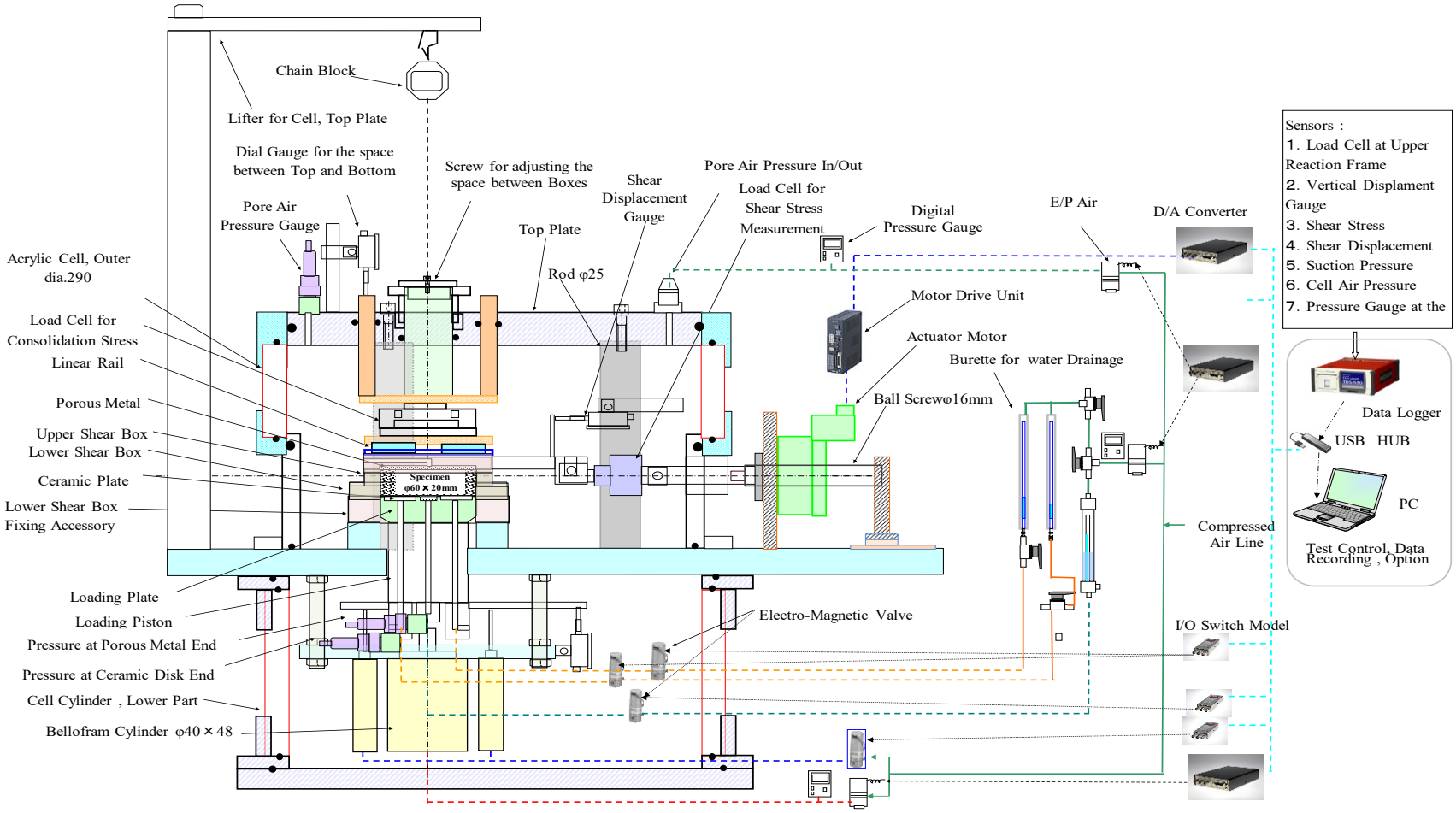

Fig 5.2 Schematic layout diagram of unsaturated direct shear box test.

pressure between the upper and lower chamber is equal. (e) Shear loading motor part to apply the horizontal displacement for the upper shear box at a constant rate with the digital control using the PC. The shear loading part can apply a shearing rate between 0.0001 – 6 mm/min. (f) Shear box adjustment screw and nut on the top of air pressure chamber to keep the gap between the upper and lower shear box. In addition, the dial gauge was equipped to monitor the gap value. (g) Burette tubes serving as water supply to saturate the sample and monitoring the equilibrium condition after applying the air pressure.

5.4 Materials

In this chapter, two types of soils were using for testing. For the first step, tests were conducted using standard silica sand (Toyoura sand) compacted to 1.560 g/cm^3. 2 cm in height and 6 cm diameter circular sample were prepared for the test. The initial water content for each sample was about 10.0% with a relative density of about 70.0%.

On the other hand, for the next step, tests were conducted using volcanic ash soil with density 1.107 g/cm^3. Same as before, 2 cm in height and 6 cm diameter circular sample were prepared for the test. The initial sample was saturated for 24 hours before testing.

5.5 Methodology

5.5.1 Equilibrium condition

Matric suction in an unsaturated soil specimen is defined as the difference between the pore-air pressure, u_a, and the pore-water pressure, u_w. Typically, in an

unsaturated soil, pore-air pressure is atmospheric (i.e., ua = 0) and pore water pressure is negative with respect to the atmospheric pressure. The axis-translation technique is conventionally used to determine or apply matric suction to soil specimens. The axis-translation technique allows the pore water pressure, u_w, in an unsaturated soil to be measured (or controlled) using a ceramic disk with fine pores (i.e., referred to as the high air-entry disk).

The saturated soil specimen is placed in the sample box on top of the high-air entry disk, which is previously saturated. A good contact should be assured between the soil and the high-air entry disk. As soon as the air pressure will increase and water drainage from the specimen through the ceramic disk pores will be allowed. The drainage continues until the water content of the specimen reaches equilibrium conditions with the applied matric suction, which is recorded as the difference from the water level on the burette tube. A condition of equilibrium is attained when water in the specimen does not go into burette tube as illustrated in Fig. 5.4.

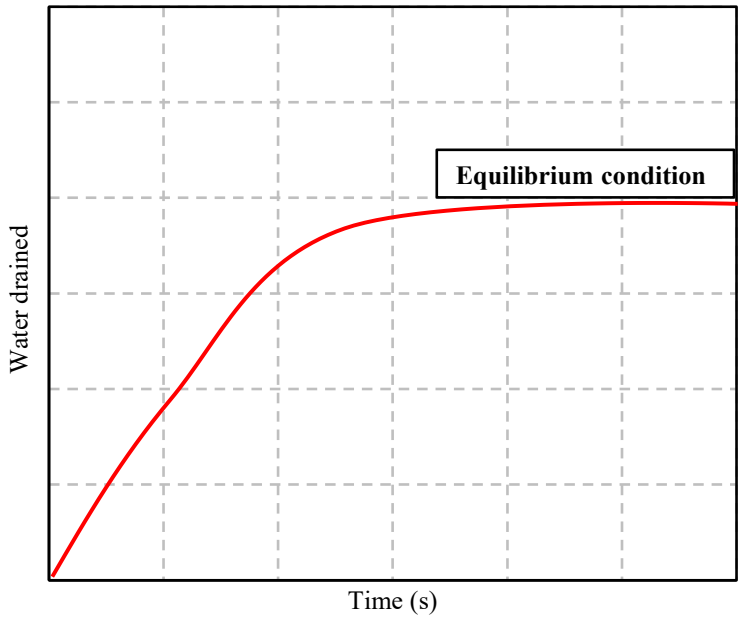

Fig 5.4 Illustration of equilibrium condition.

The equilibration time is dependent of the type of soil, size of specimen and air-entry value of the disk. In many cases, the equilibration occurs in 3 to 6 hours in 20 mm thick compacted specimens (Vanapalli et al. 1999; Fredlund and Vanapalli 2002). The applied pore-air pressure, u_a, is the matric suction when the pore-water pressure, u_w, is set to zero.

5.5.2 Type of unsaturated testing

5.5.2.1 Undrained tests

For the first step as a validation, tests were conducted using standard silica sand (Toyoura sand) under undrained condition. In the direct shear test under undrained condition, the water drained is not allowed from the sample. This test also called as constant volume condition. The volume of the specimen is kept constant during shearing. The vertical stress is controlled to correspond with the dilatancy during the shear process. Because the variation of the vertical stress also corresponds to that of the excess pore water pressure under the consolidated undrained (CU) condition, the constant volume test provides the results on the notion of effective stress. The testing procedure of constant volume test is as follows: The initial conditions of the specimen made by the static compaction method are summarized in Table 5.1.

Table 5.1. Test program for undrained test.

Test ID	Sample condition	Air pressure (kPa)	Void ratio (e_0)	Vertical Stress (kPa)
CVS1	Saturated	0	0.693	30
CVS2	Saturated	0	0.693	50
CVU1	Unsaturated	50	0.693	30
CVU2	Unsaturated	50	0.693	50

The consolidation process was carried out for 1 hour. Accordingly, the shear process for unsaturated and saturated samples were conducted at the fixed speed of 0.2 mm/minutes.

5.5.2.2 Drained tests

The next step is the drained tests using volcanic ash soil. The direct shear test under drained condition is a test method where the water is allowed drained form the sample. The vertical stress is kept constant on the shear plane. The excessive pore water pressure is not induced under the consolidated drained (CD) condition during the shear process.

In general, the unsaturated direct shear box apparatus has the possibility water drainage through ceramic disc line, metal porous line and gap between the shear box. Fig 5.5 shows possibility water drainage in the unsaturated direct shear box apparatus.

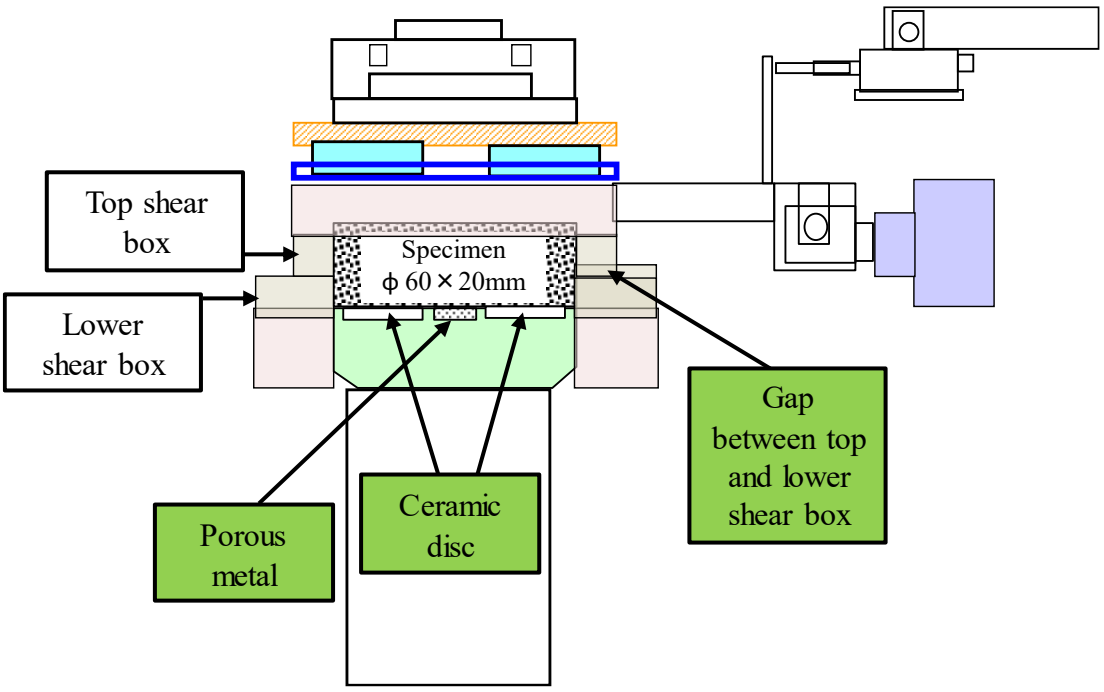

Fig 5.5 Possibility water drainage in the unsaturated direct shear box apparatus.

According to testing procedure, the valve in the porous metal line will be closed during testing. On the other hand, to confirm the sensor measurement in the ceramic disc line, open valve and close valve the ceramic disc line during testing were adopted. The testing program for drained test illustrated in Table 5.2. In addition, according to Japanese Geotechnical Society standards a shearing rate 0.2 mm/min was adopted

Table 5.2 The testing program for drained

Test ID	Air pressure (u_a) (kPa)	Vertical stress (σ_v) (kPa)	Valve condition
CDOV1	0	20	Open
CDOV2	30	20	Open
CDOV3	60	20	Open
CDOV4	80	20	Open
CDOV5	0	40	Open
CDOV6	30	40	Open
CDOV7	60	40	Open
CDOV8	80	40	Open
CDOV9	0	60	Open
CDOV10	30	60	Open
CDOV11	60	60	Open
CDOV12	80	60	Open
CDCV1	0	20	Close
CDCV2	30	20	Close
CDCV3	60	20	Close
CDCV4	80	20	Close
CDCV5	0	40	Close
CDCV6	30	40	Close
CDCV7	60	40	Close
CDCV8	80	40	Close
CDCV9	0	60	Close
CDCV10	30	60	Close
CDCV11	60	60	Close
CDCV12	80	60	Close

For the drained tests, the volcanic ash sample will be saturated outside. Fig 5.6 shows the saturation process of the volcanic ash sample. The volcanic ash soil compacted to 1.037 g/cm^3. Samples with a diameter of 6 cm and a height of 2 cm is prepared and installed directly into the acrylic cylinder with compaction into three layers. The compaction was carried out using the steel plate which has the same diameter as the sample. After that bottom part of this sample were sandwiched between filter paper and porous stone, and both sides were flooded. Finally, the saturated sample was prepared by soaking in the water for 24 hours.

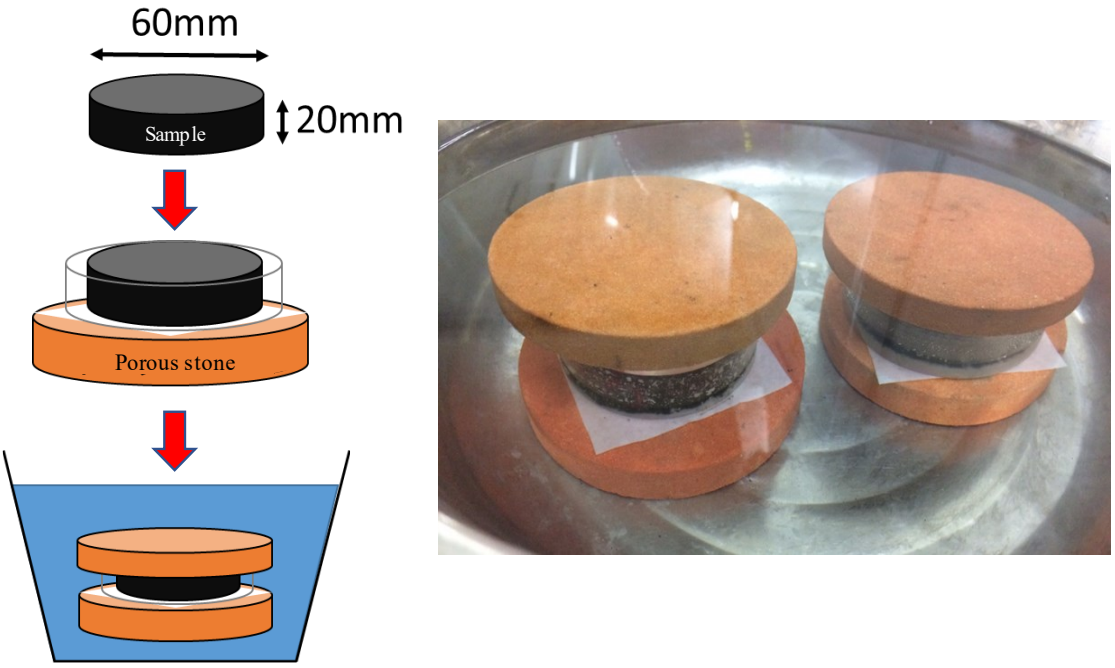

Fig 5.6 Saturation process of the volcanic ash sample.

5.6 Optimizing of testing procedure

The flow diagram for using the new unsaturated direct shear box test apparatus starting from preparation, equilibrium condition and till removal the specimen has been developed and illustrates in Fig 5.7.

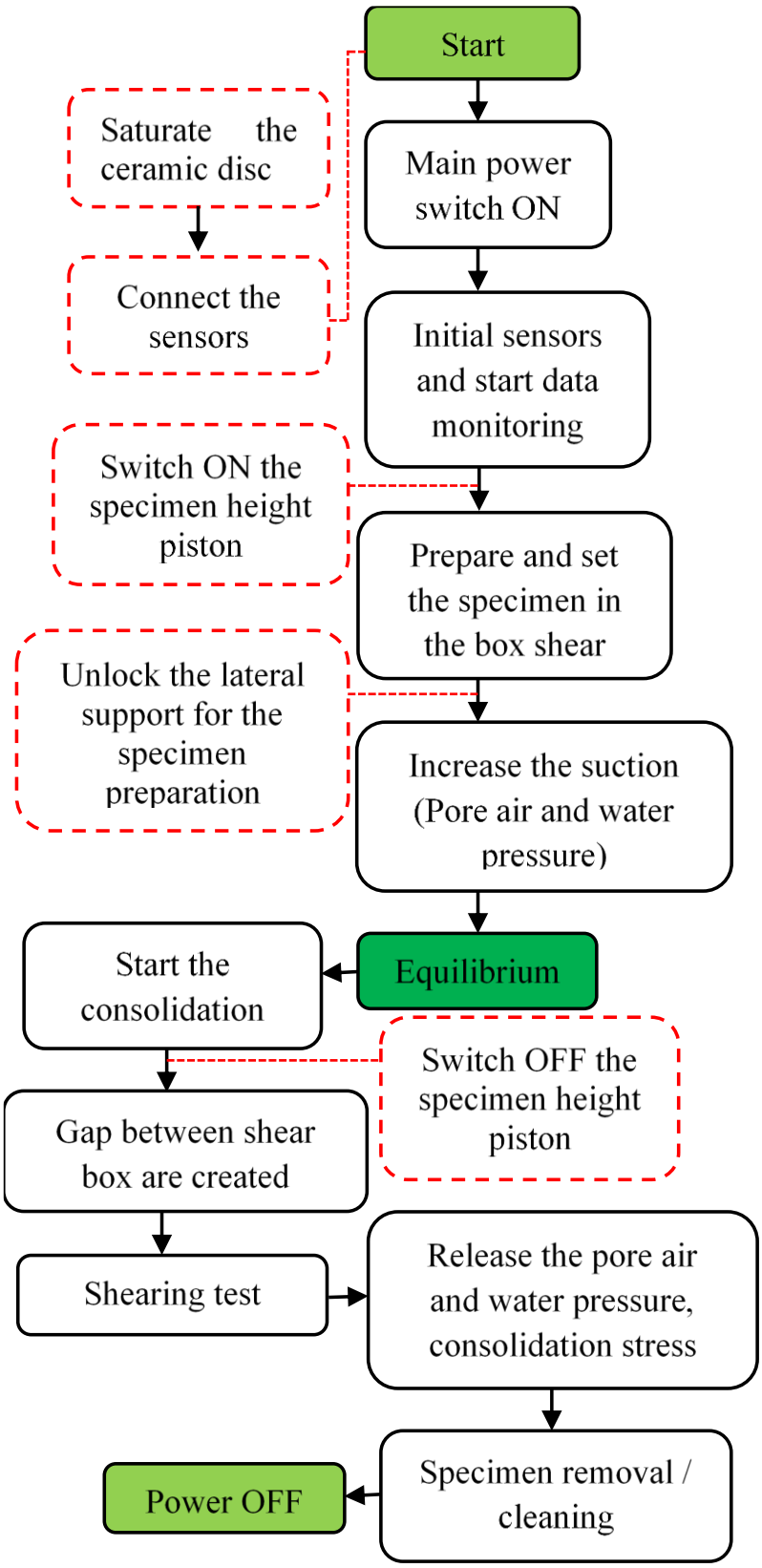

Fig 5.7 Testing flow diagram of unsaturated direct shear box test

The laboratory testing for unsaturated soil has been carried out applying the axis translation technique and controlling the pore air and the pore water pressure independently. The axis-translation technique allows the pore water pressure, u_w, in an unsaturated soil to be measured (or controlled) using a ceramic disk with fine pores (i.e., referred to as the high air-entry disk). The saturated soil specimen is placed in the sample box on top of the high-air entry disk, which is previously saturated. A good contact should be assured between the soil and the high-air entry disk.

In general, the unsaturated direct shear box apparatus consists of three parts of sensors to determine the equilibrium step. The first sensor is the pore air pressure sensor, which will measure the applied air pressure in the chamber. Furthermore, the pore water pressure 1 through the ceramic disk and the pore water pressure 2 in the porous metal are measured. The development of pressure until reaching the equilibrium state in the unsaturated direct shear box test apparatus is illustrated in Fig 5.8.

After applying the air pressure, the top and bottom chamber are filled with the designated air pressure. Increasing the air pressure can be seen in the graph represented by the black line. The air pressure increases slowly and remains constant after achieving the designated value. On the other hand, during increasing the pore air pressure, the pore water pressure sensor 2 in the metal porous measures the pore water pressure directly. The value and shape of the pore water pressure graph represented with a red line are in good agreement with the pore air pressure. Furthermore, the pore water pressure sensor 1 through the ceramic disk also measures the pore water pressure value. The pore water pressure development with time is illustrated with a blue dash line. The pore water pressure increases slower than that of the pore water pressure in

metal porous and keeps constant after achieving the designated pore air pressure value. After reaching a constant value, the water drainage from the specimen through the ceramic disk pores was allowed. The valve in the burette tube which connecting to the ceramic disk line is opened. The drainage of the water can be monitored with the change of water level in the burette tube. Due to drainage of the water, the pore water pressure 1 value in the metal porous slightly decreases. On the other hand, the pore water pressure 2 value in the ceramic disk dramatically decreases. The drainage continued until the water content of the specimen reached the equilibrium condition. A condition of equilibrium was attained when the water drainage from the specimen into the burette tube stops. The valve in the burette tube is closed and the pore water pressure 2 value in the metal porous value increases until achieving the initial value. Finally, in this condition the applied pore air pressure, Ua equals the matric suction value.

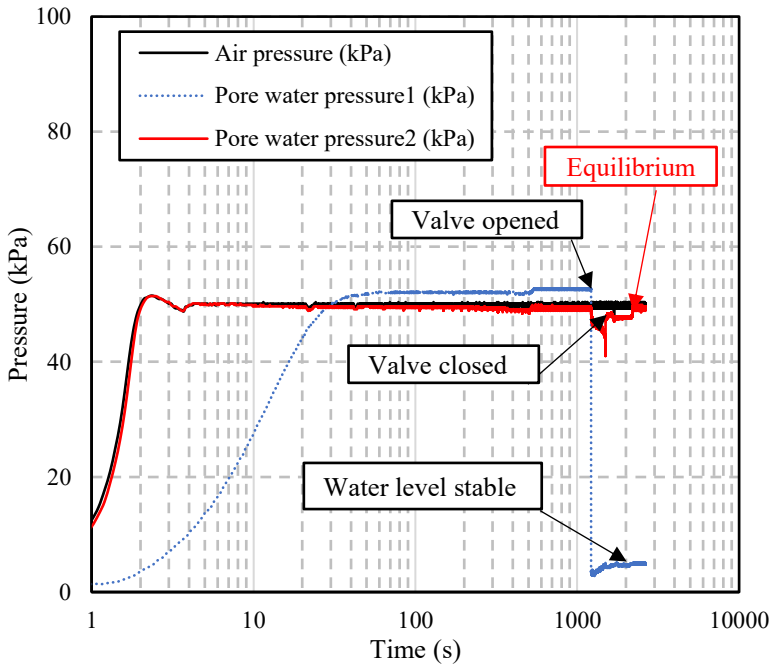

Fig. 5.8 Equilibrium condition of sample

5.7 Confirmation of the suction-controlled system

A series of constant volume tests for Toyoura sand was performed using the new suction controlled direct shear box apparatus considering both unsaturated and saturated conditions as a validation. The tests were carried out using two types of consolidation stresses 30 and 50 kPa. On the other hand, for the unsaturated case, the air pressure was set to 50 kPa.

Fig. 5.9 presents the relationship between shear stress and shear displacement. It can be seen that the shear stress was increased dramatically both unsaturated and saturated samples. The shear stress of the unsaturated sample was found to be larger than that of the saturated sample. It can be observed that the shear stress of the unsaturated sample reached 60 kPa on the consolidation stress 50 kPa. While in the saturated sample with the same consolidation stress, the vertical stress was 40 kPa.

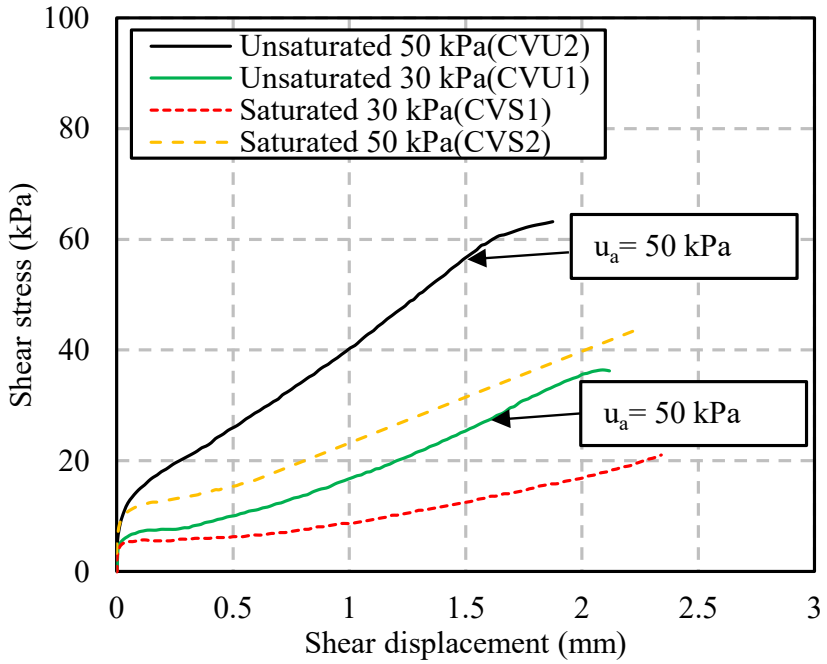

Fig. 5.9 Relationship between shear stress and shear displacement

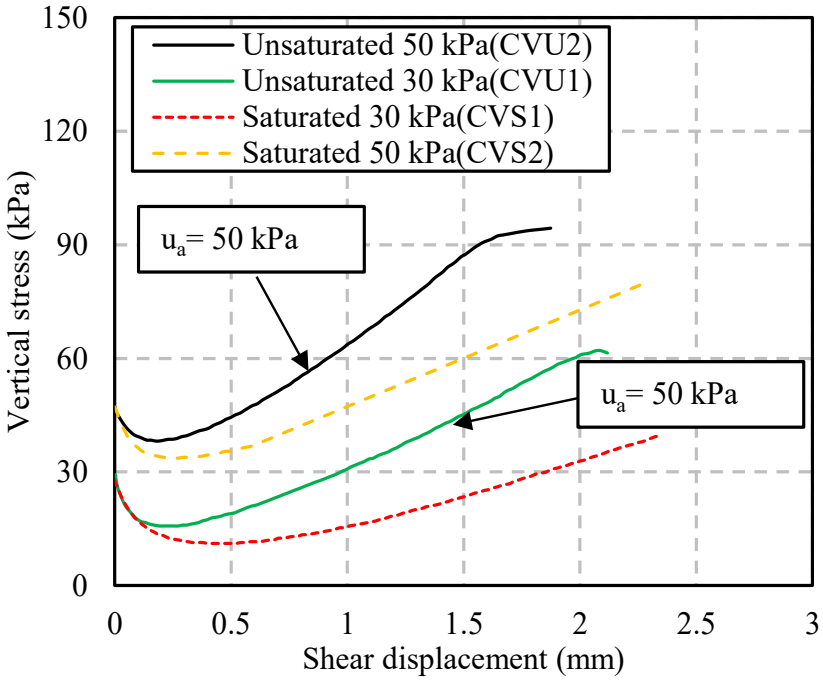

Fig. 5.10 Relationship between vertical stress and shear displacement

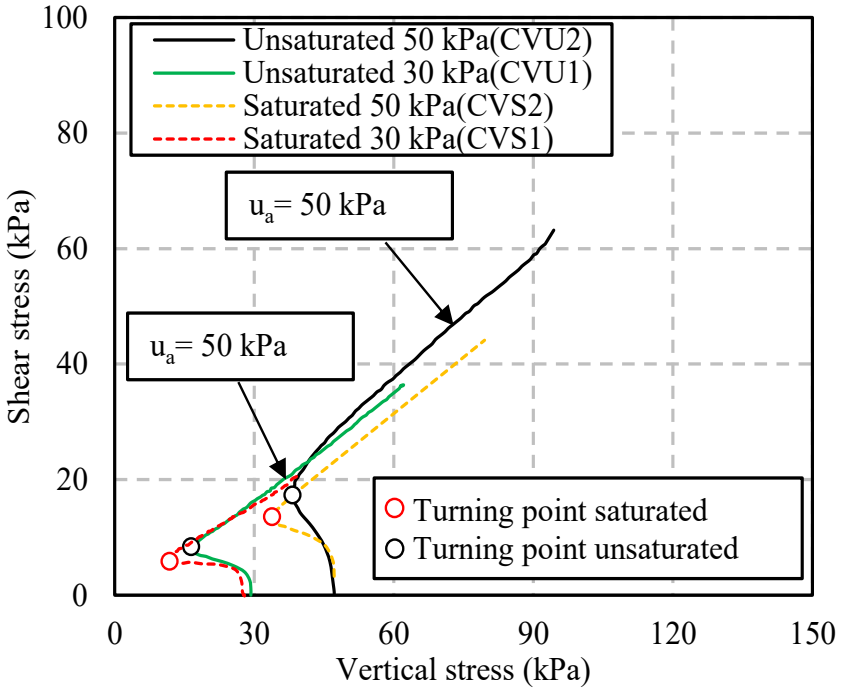

Fig. 5.11 Stress path for Toyoura sand

On the other hand, the relationship between vertical stress and shear displacement is illustrated in Fig 5.10. Due to the constant volume test, the vertical

stress corresponds to that of the excess pore water pressure under the consolidated undrained (CU) condition and provides the results of effective stress. It can be seen that the reduction of vertical stress for saturated sample both 30 and 50 kPa consolidation stress are higher than that of unsaturated sample. It can be concluded that increasing of pore water pressure during shearing in the unsaturated sample is significantly lower than that of the saturated sample. Furthermore, the relationship between the vertical stress and shear stress for the unsaturated and saturated samples is shown in Fig 5.11. The unsaturated sample represented with a black circle plots and red circle plots for the saturated sample. The obtained results show that the turning point of the unsaturated sample both 30 and 50 kPa consolidation stress is significantly larger than the saturated sample. Finally, it can be concluded that the total shear strength of the soil strongly depends on the suction force which can be observed with the new suction-controlled apparatus.

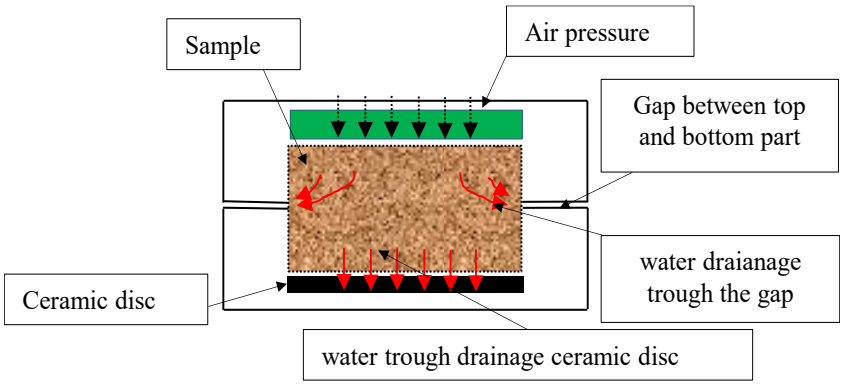

	Sample Ua = 50 kPa		Water content
	σ=50 kPa	σ=30 kPa	
Top part	1.16	1.18	(%)
Middle part	1.17	1.21	
Bottom part	1.25	1.28	

Fig. 5.12 Distribution of water drainage

The distribution of water within the sample during testing using this apparatus (between top and bottom part shear box) is illustrated in Fig 5.12. In order to investigate the water redistribution under unsaturated conditions, the water content of unsaturated samples after the test was checked into three levels (top, middle, and bottom). The obtained results show that the water content is not significantly different. It can be concluded that the distribution of water is uniform.

5.8 Unsaturated shear strength of behavior of volcanic ash soil

Before the evaluation of volcanic ash soil in the new unsaturated direct shear box apparatus, the validation with comparison results from the conventional direct shear box apparatus with the same sample under saturated conditions is needed. Fig 5.13 and Fig 5.14 show the comparison result of new unsaturated and conventional direct shear box apparatus.

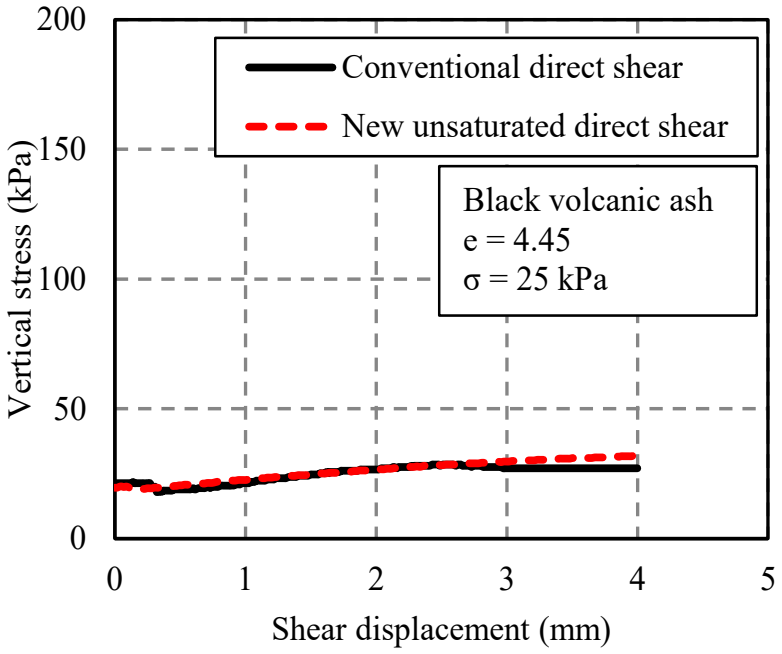

Fig. 5.13 Comparison result of vertical stress

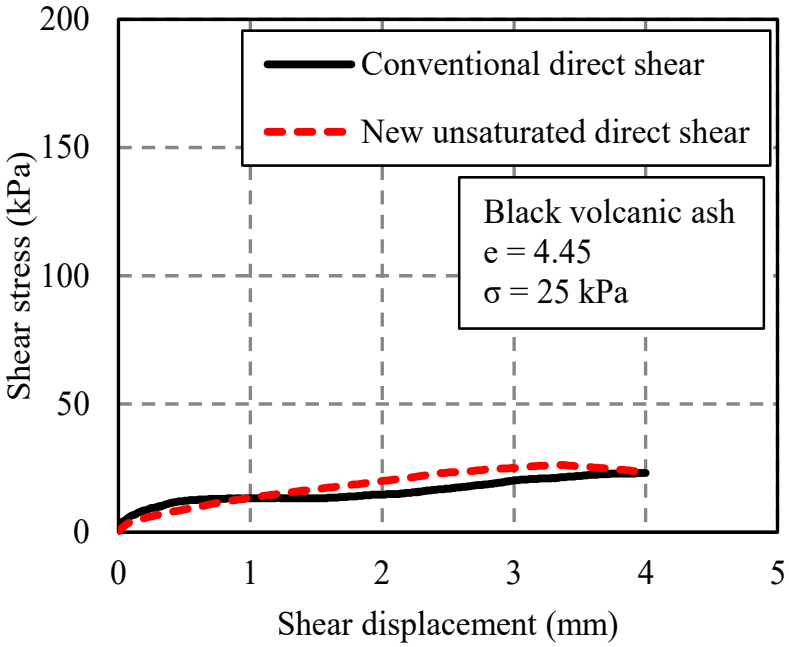

Fig. 5.14 Comparison result of shear stress

It can be observed that the good correlation of vertical stress and shear stress volcanic ash soil was obtained under saturated condition using new unsaturated and conventional direct shear box test apparatus for saturated sample. It can be concluded that the new unsaturated direct shear box apparatus can be used to evaluate of unsaturated shear strength volcanic ash soil.

5.8.1 Undrained water through ceramic disc line test (close valve)

5.8.1.1 Effects of net normal stress on shear strength and volume change behaviors of soil

Fig 5.15 and Fig 5.16 show the effects of the net normal stress ($\sigma_n - u_a$) on shear stress–shear displacement and volume change behaviors of the volcanic ash soil with constant suction ($u_a - u_w$) 60 kPa which was achieved by following a drying process. It can be observed that the shear strength and the initial stiffness of unsaturated soils

increase with increasing net normal stress ($\sigma_n - u_a$). Further, the volume of unsaturated soils becomes contractive as the net normal stress increases.

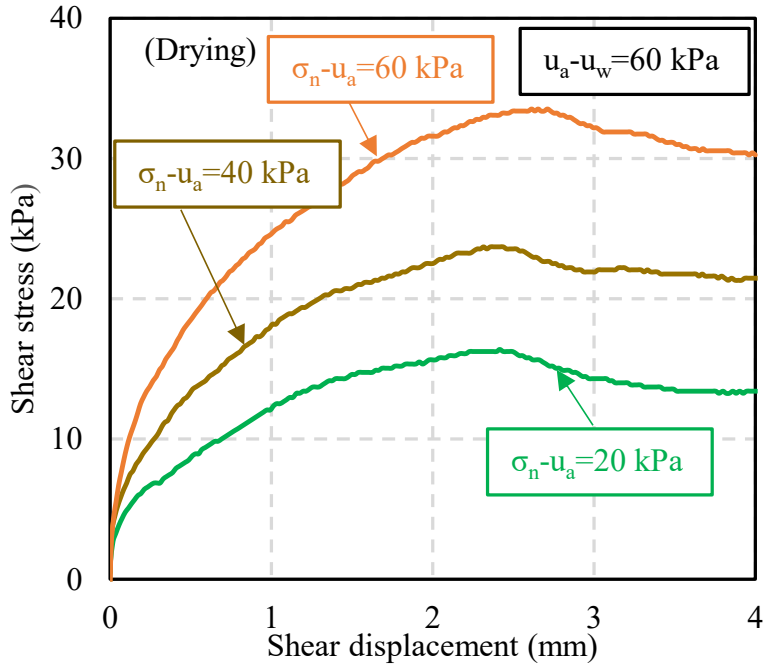

Fig. 5.15 Relationship of shear stress and shear displacement (suction 60 kPa)

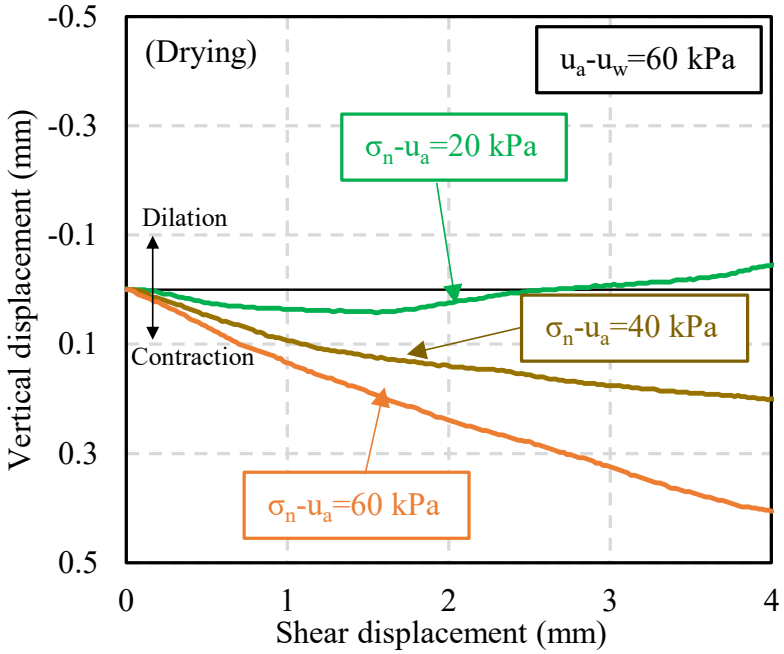

Fig. 5.16 Relationship of vertical stress and shear displacement (suction 60 kPa)

These behaviors are independent of the degree of saturation, the method of suction achievement (drying or wetting), and soil type.

The frictional resistance increases with increasing the normal stress acting on the plane according to Newton's friction law. The same concept is applied to the shear plane when a direct shear test is conducted on soil. In a direct shear test, the applied vertical stress is normal to the shear plane and therefore when the vertical stress (net normal stress) is increased, the shear strength (the failure shear stress) of soil increases. The greater vertical stress induces a higher confinement to the direct shear sample. As a result, the shear stiffness (the initial slope of the shear stress–shear displacement curve) of soil increases with the vertical net normal stress. Therefore, when these samples are sheared, the net normal stress may force soil particles into a close-packed arrangement (volume contraction) during shearing. As a result, samples become more contractive as the net normal stress increases. It can be concluded that under constant suction, the increase in vertical stress causes a progressive sample volume change from dilatancy to compression.

5.8.1.2 Effects of suction on shear strength and volume change behaviors of soil

Fig 5.17, Fig 5.18 and Fig 5.19 show the shear stress–shear displacement and the volumetric behaviors, respectively, of four tests conducted on volcanic ash soil samples under net normal stress of 20 kPa, 40 kPa, 60 kPa and different suction values (0, 30, 60, and 80 kPa). Under close valve condition, the obtained results show that the shear strength and stiffness of the soil increase with the increase in soil suction. The soil exhibits more dilative volumetric behavior as suction is increased. Similar results were observed for every group of three tests net normal stress (20 kPa, 40 kPa, and 60 kPa) with the four different suction values (0, 30, 60, and 80 kPa).

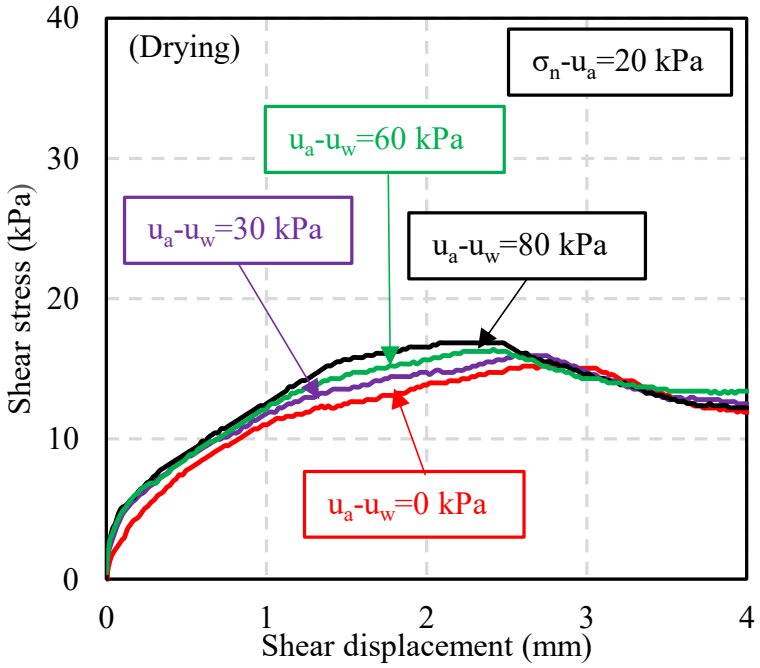

(a)

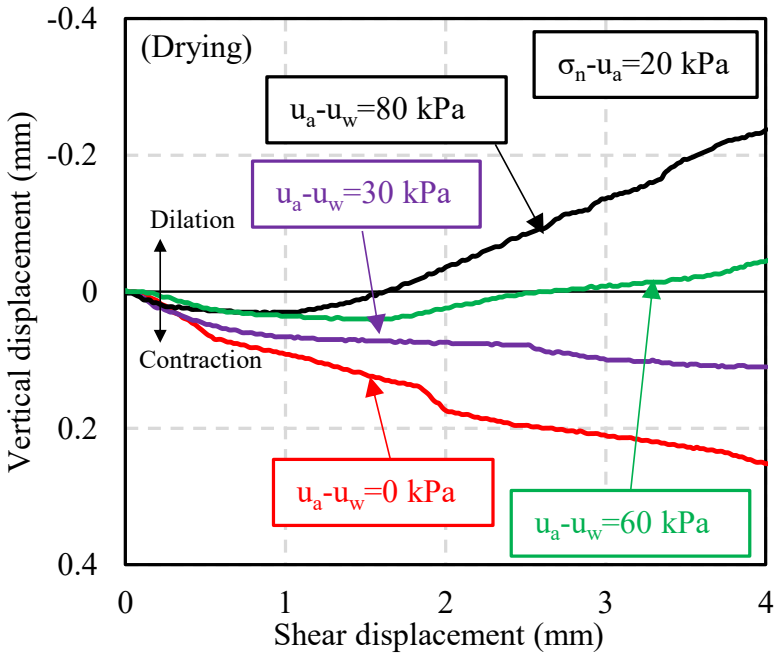

(b)

Fig. 5.17 Effects of the suction on (a) shear stress–shear displacement behavior; (b) volumetric behavior (net normal stress 20 kPa)

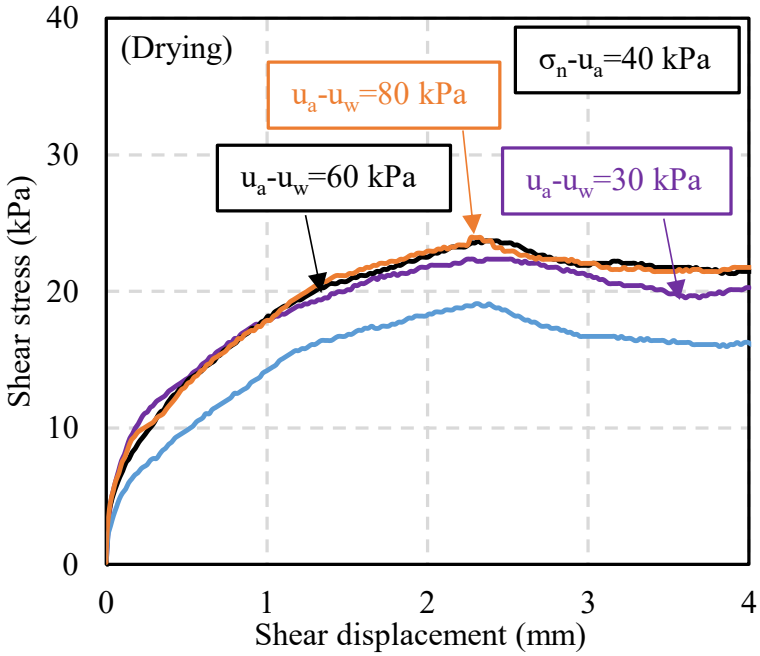

(a)

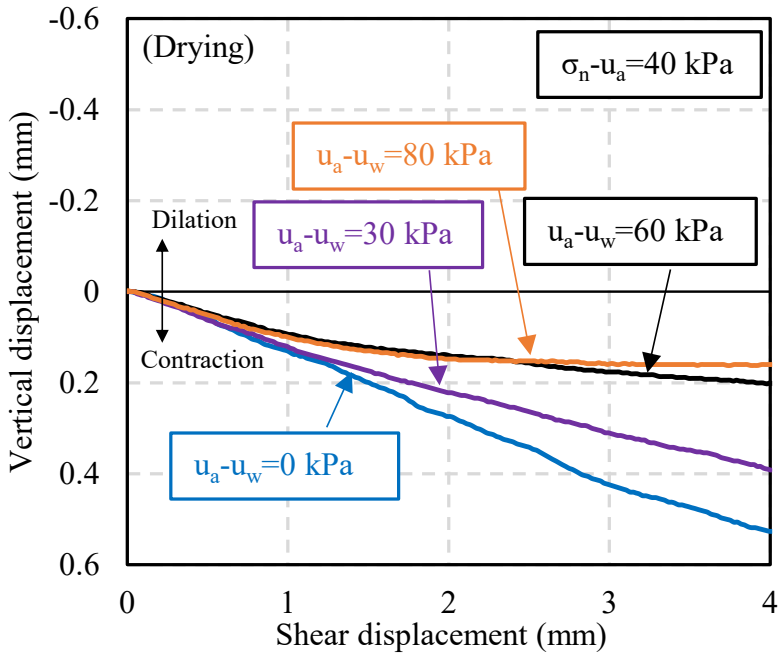

(b)

Fig. 5.18 Effects of the suction on (a) shear stress–shear displacement behavior; (b) volumetric behavior (net normal stress 40 kPa)

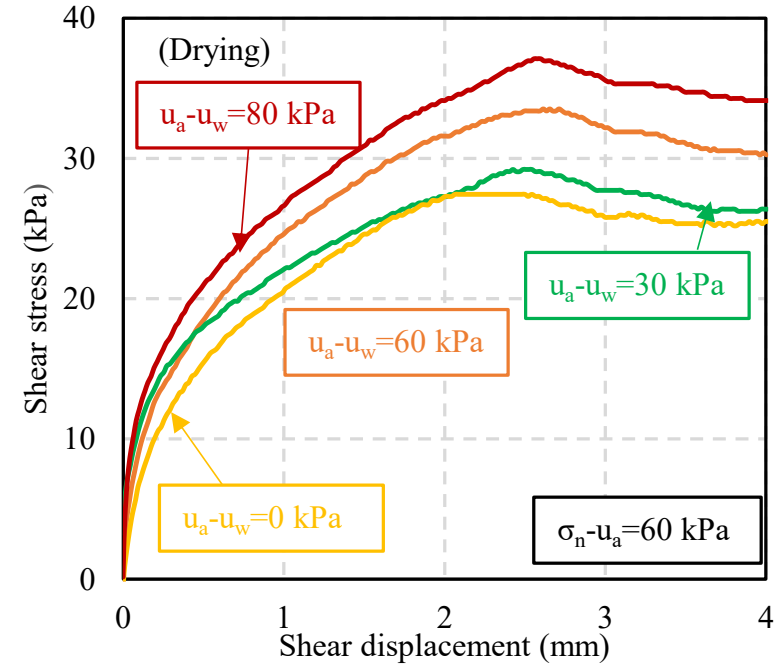

(a)

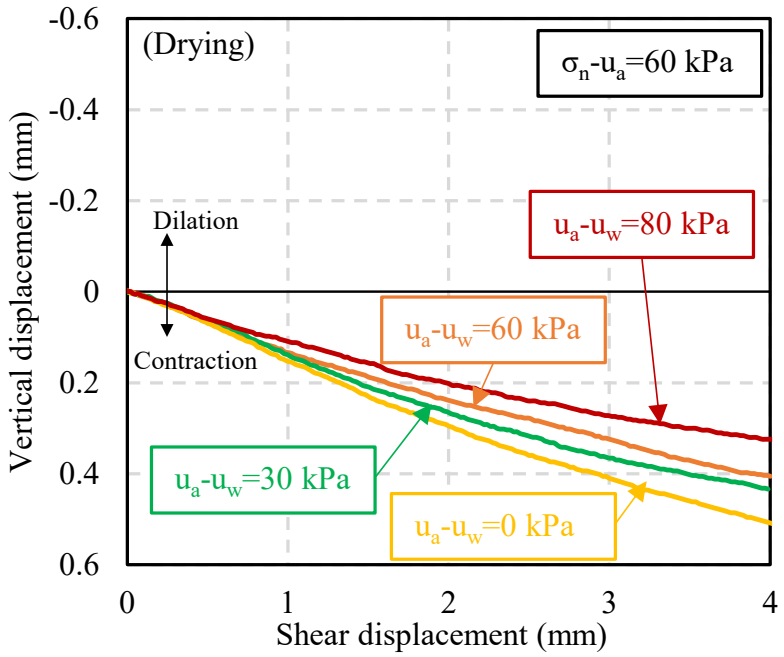

(b)

Fig. 5.19 Effects of the suction on (a) shear stress–shear displacement behavior; (b) volumetric behavior (net normal stress 60 kPa)

The test results strongly demonstrate that suction has influence on the shear characteristic of unsaturated soil. The shear resistance and stiffness of soils increase, and the specimens exhibit more dilative behaviors as suction increases. These phenomena are consistent with the fact that interparticle forces in soils increase as suction increases. It can be seen clearly for the four different suction values (0, 30, 60, and 80 kPa) in the 20 kPa net normal stress, the volumetric behavior become dilative with increasing of suction value. The vertical displacement of 60 kPa and 80 kPa move from contractive condition to dilative condition and the vertical displacement samples was -0.05 and -0.23 mm at the end of shearing. Furthermore, the shear strength versus matric suction with different net normal stress was plotted in the Fig 5.20. It can be observed that the shear strength of volcanic ash soils increases with increasing of matric suction. Similar results were observed for every group of three tests net normal stress with the four different suction values (0, 30, 60, and 80 kPa)

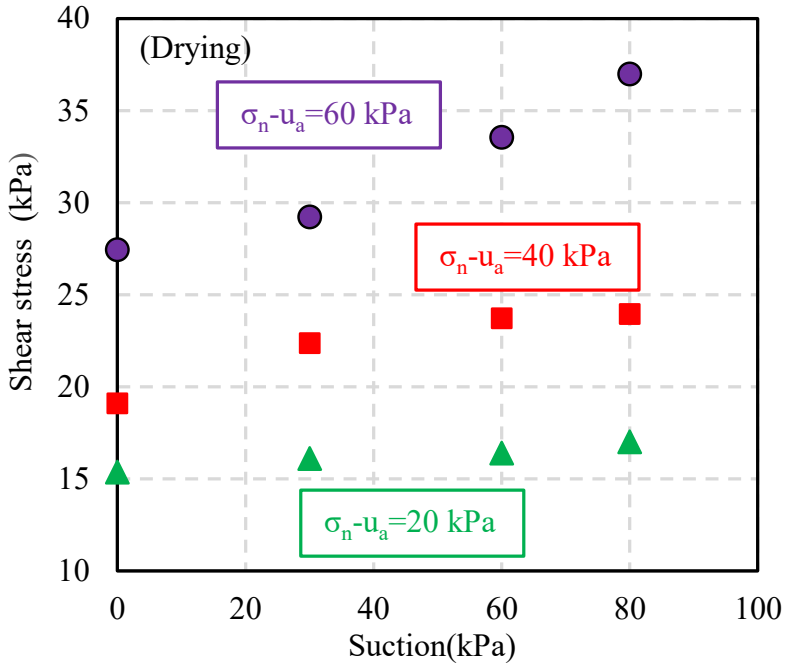

Fig. 5.20 Shear strength versus matric suction with different net normal stress

5.8.2 Drained water through ceramic disc line test (open valve)

5.8.2.1 Effects of net normal stress on shear strength and volume change behaviors of soil

Fig 5.21 and Fig 5.22 illustrate the effects of the net normal stress ($\sigma_n - u_a$) on shear stress–shear displacement and volume change behaviors of the volcanic ash soil with constant suction ($u_a - u_w$) 80 kPa which was achieved by following a drying process under open valve condition on the ceramic disc line. It can be seen that the shear strength and the initial stiffness of unsaturated soils increase with increasing net normal stress ($\sigma_n - u_a$). This behavior is similar in comparison with close valve condition on the ceramic disc line. From the obtained results, the peak shear stress value of 60 kPa net normal stress around 39 kPa, for 40 kPa net normal stress is 30 kPa, and 19 kPa for net normal stress 20 kPa.

Furthermore, the volume of unsaturated soils becomes contractive as the net normal stress increases. It can be seen clearly the vertical displacement of 20 kPa net normal stress is in dilative condition from 1 mm till the end of shearing. On the other hand, with the increasing of net normal stress to 40 kPa, the vertical displacement is in contraction condition from beginning till the end of shearing. Furthermore, the vertical displacement of 60 kPa net normal stress become more contractive with the vertical displacement 0.3 mm at the end of shearing.

The greater vertical stress induces a higher confinement to the direct shear sample. Therefore, when these samples are sheared, the net normal stress may force soil particles into a close-packed arrangement (volume contraction) during shearing. As a result, samples become more contractive as the net normal stress increases.

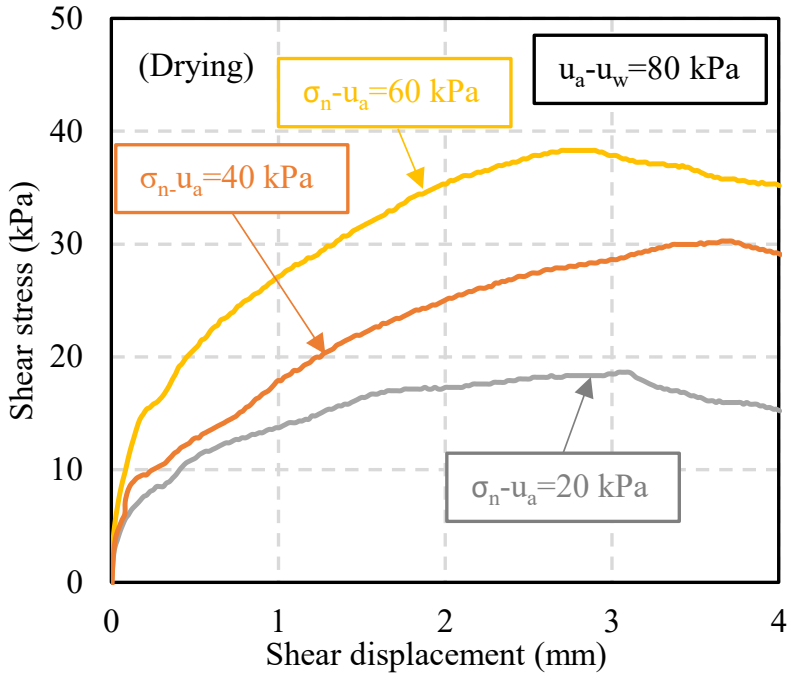

Fig. 5.21 Relationship of shear stress and shear displacement (suction 80 kPa)

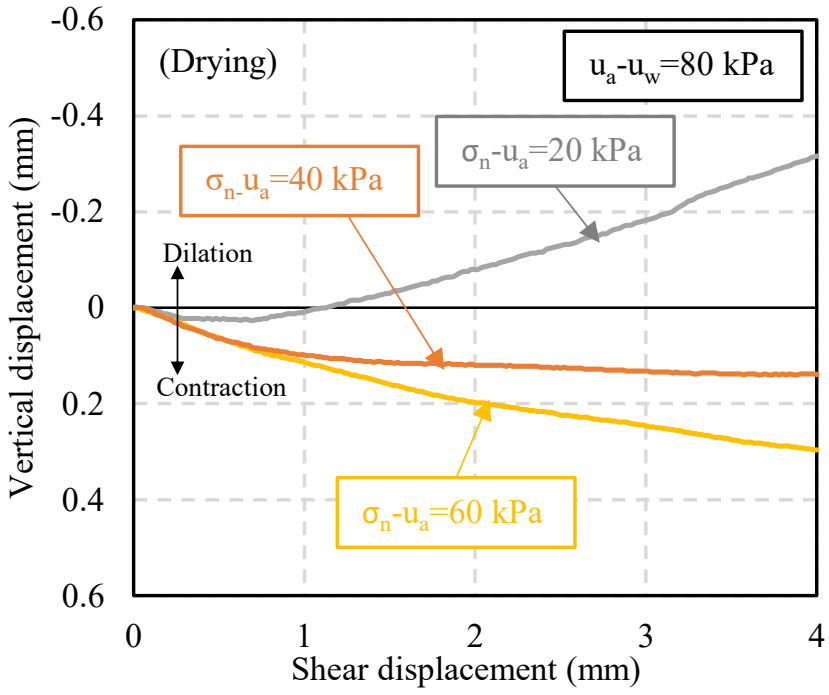

Fig. 5.22 Relationship of vertical stress and shear displacement (suction 80 kPa)

5.8.2.2 Effects of suction on shear strength and volume change behaviors of soil

Fig 5.23, Fig 5.24 and Fig 5.25 show the shear stress–shear displacement and the volumetric behaviors, respectively, of four tests conducted on volcanic ash soil samples under net normal stress of 20 kPa, 40 kPa, 60 kPa and different suction values (0, 30, 60, and 80 kPa) under open valve condition on the ceramic disc line. The obtained results behavior is similar with the close valve condition where the shear strength and stiffness of the soil increase with the increase in soil suction. The soil exhibits more dilative volumetric behavior as suction is increased. Similar results were observed for every group of three tests net normal stress (20 kPa, 40 kPa, and 60 kPa) with the four different suction values (0, 30, 60, and 80 kPa). It can be seen clearly for the four the suction values (60, and 80 kPa) in the 20 kPa net normal stress, the volumetric behavior is in dilative condition from beginning till the end of shearing.

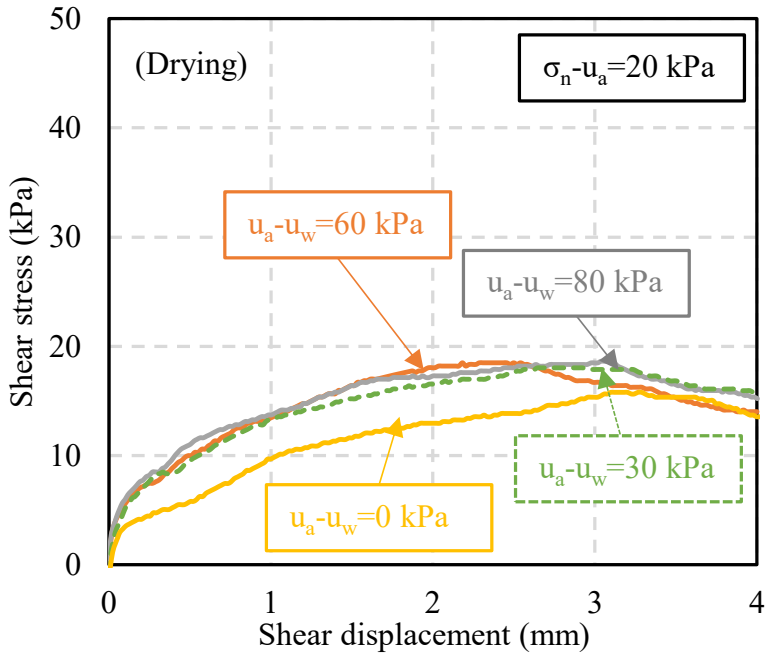

(a)

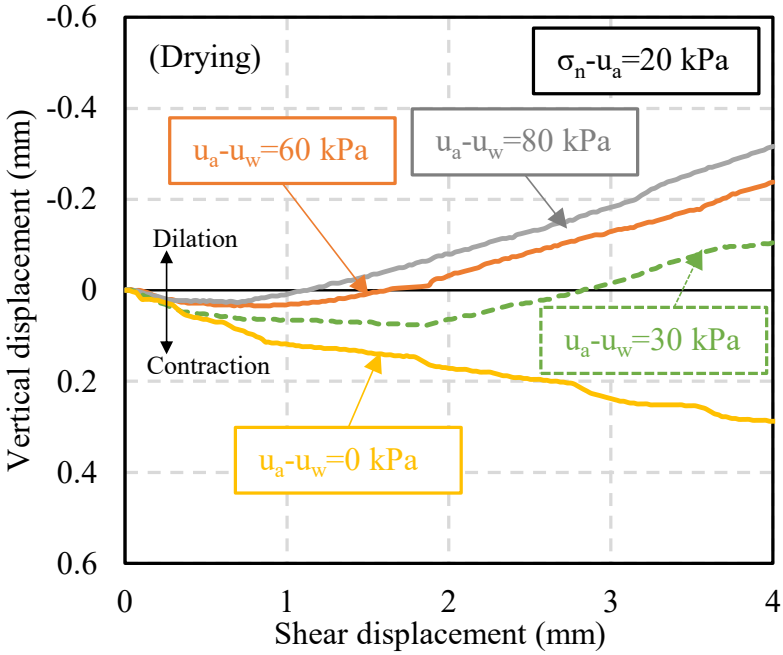

(b)

Fig. 5.23 Effects of the suction on (a) shear stress–shear displacement behavior; (b) volumetric behavior (net normal stress 20 kPa)

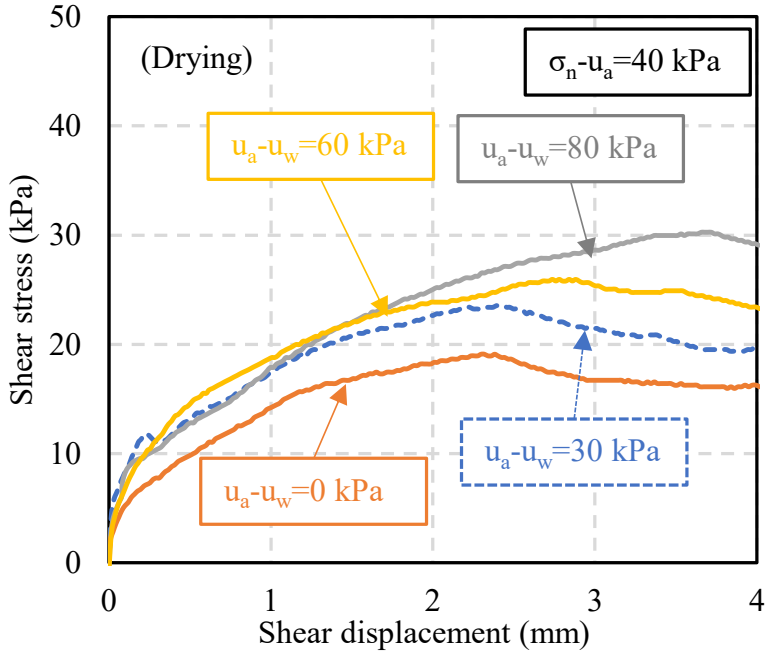

(a)

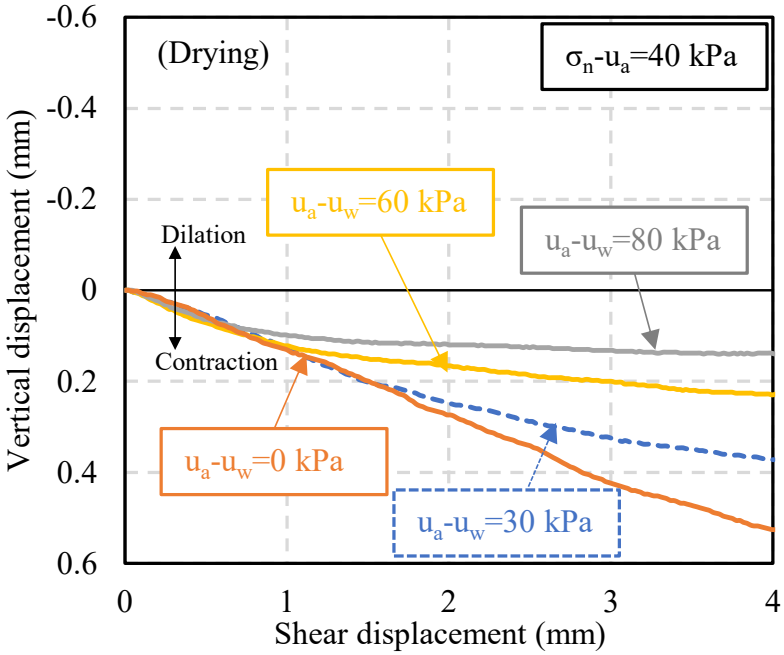

(b)

Fig. 5.24 Effects of the suction on (a) shear stress–shear displacement behavior; (b) volumetric behavior (net normal stress 40 kPa)

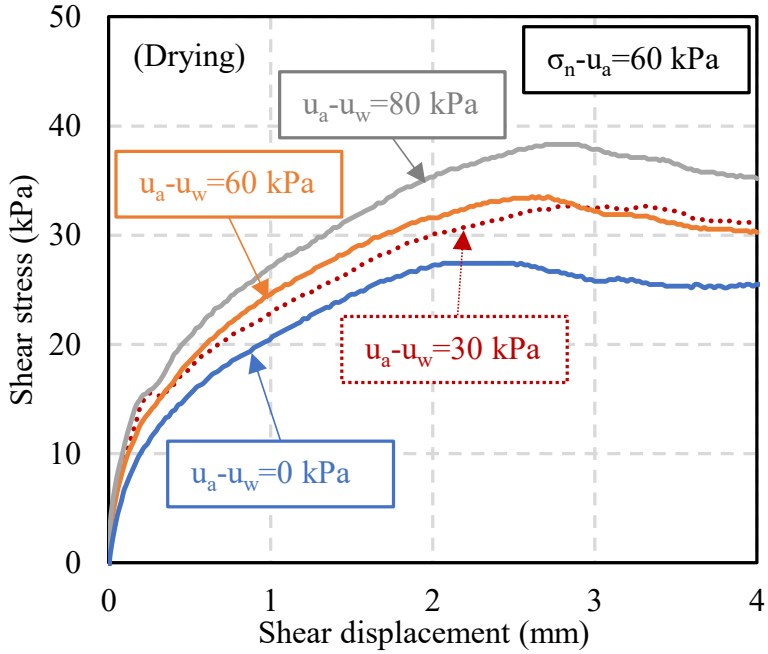

(a)

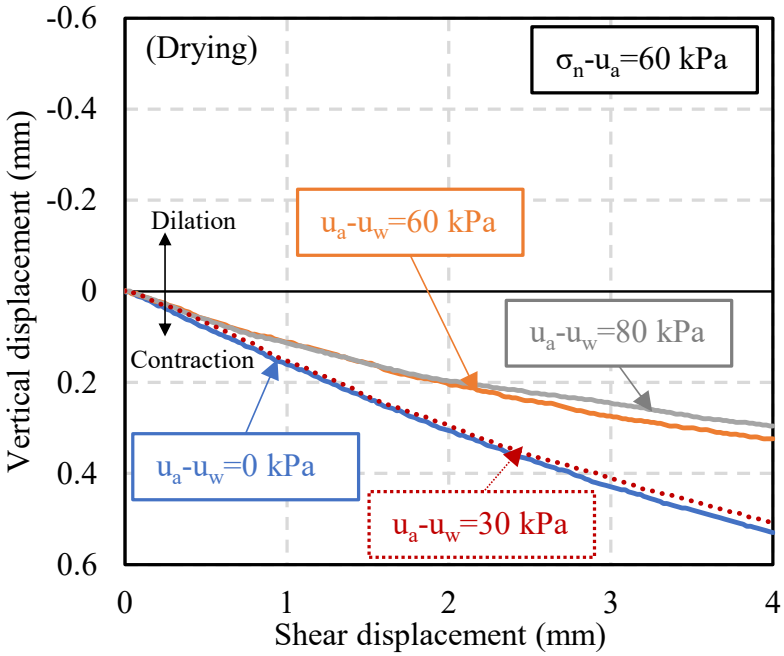

(b)

Fig. 5.25 Effects of the suction on (a) shear stress–shear displacement behavior; (b) volumetric behavior (net normal stress 60 kPa)

To clarify the physics of unsaturated particulate media, two spherical particles of radius R in contact are considered. The water meniscus between them is bound by the two particles and by an imaginary torus. The small radius of this doughnut-shaped torus is r_1 and the distance from the center to the inside wall of the torus is r_2. Therefore, the local contact force, F, which the meniscus imposes on the particles, contributed by the pressure of the fluid acting on the cross-sectional area of the meniscus and the surface tension (*Ts*) acting along the perimeter of the meniscus, can be expressed as (Cho and Santamarina 2001) in Equation 5.1 and the details in illustrated in the Fig 5.26.

$$F = (u_a - u_w)(\pi r_{2^2}) + Ts(2\pi r_2) \quad (5.1)$$

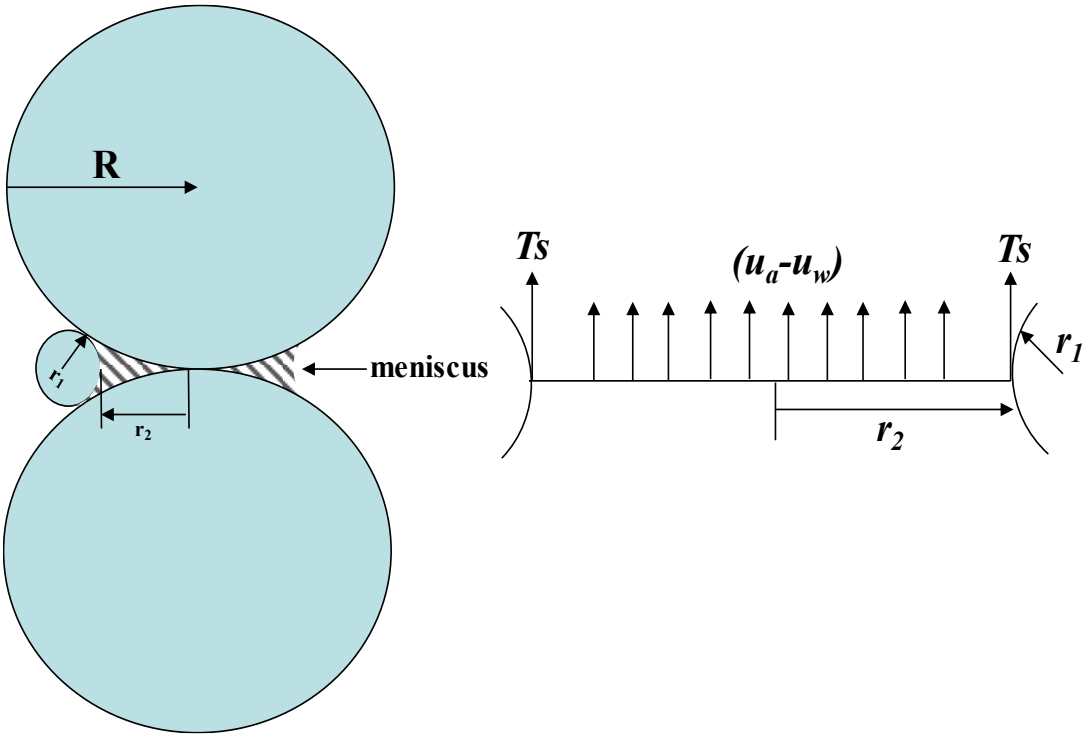

Fig. 5.26 Schematic representation of spherical particles and forces involved

This force is the only one arising from meniscus water and increases as suction increases. Therefore, the effects of matric suction result in a greater normal force holding the particles together (Sawangsuriya 2006). As a result, the stiffness and the strength of unsaturated soils increase with increasing matric suction.

Another effect of suction on the unsaturated soil behavior can be clearly seen in the volumetric deformation during shearing. As shown in these figures, the soil is more contractive at zero suction and becomes less contractive with the increasing value of suction prior to shear, regardless of the value of the net confining pressure. As soil structures become stronger and less deformable with an increase in suction, it is expected that they will exhibit dilative (less contractive) behavior with an increase in suction.

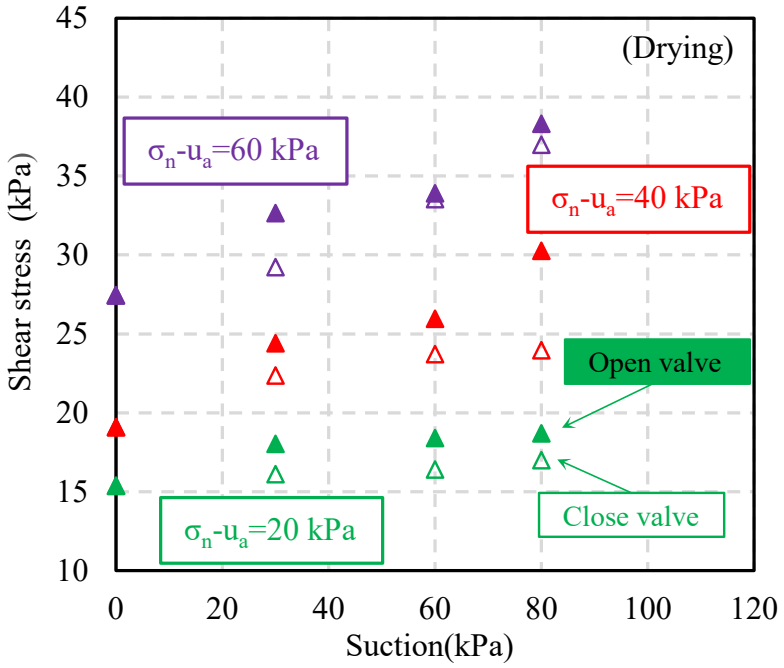

Fig. 5.27 Shear strength versus matric suction with different net normal stress

Fig 5.27 shows the relationship of shear strength versus matric suction with different net normal stress. It can be observed that the shear strength of volcanic ash soils increases with increasing of matric suction. However, in the open valve condition in the ceramic disc line, the shear stress is higher for every net normal stress in comparison with close valve condition. It can be attributed to amount of water drainage during shearing process. Where, in the open valve condition is higher in comparison to the close valve condition. In theoretical of unsaturated testing, the open valve condition more reasonable. Thus, for determine the unsaturated shear strength of volcanic ash soil, open valve condition was adopted.

To obtain the shear strength parameters [the apparent cohesion (c) and the internal friction angle (ϕ)] corresponding to a particular suction value, samples subjected to the different suction and three different net normal stresses (i.e., 20, 40, and 60 kPa) were sheared. Implying the mentioned failure criterion, the failure shear

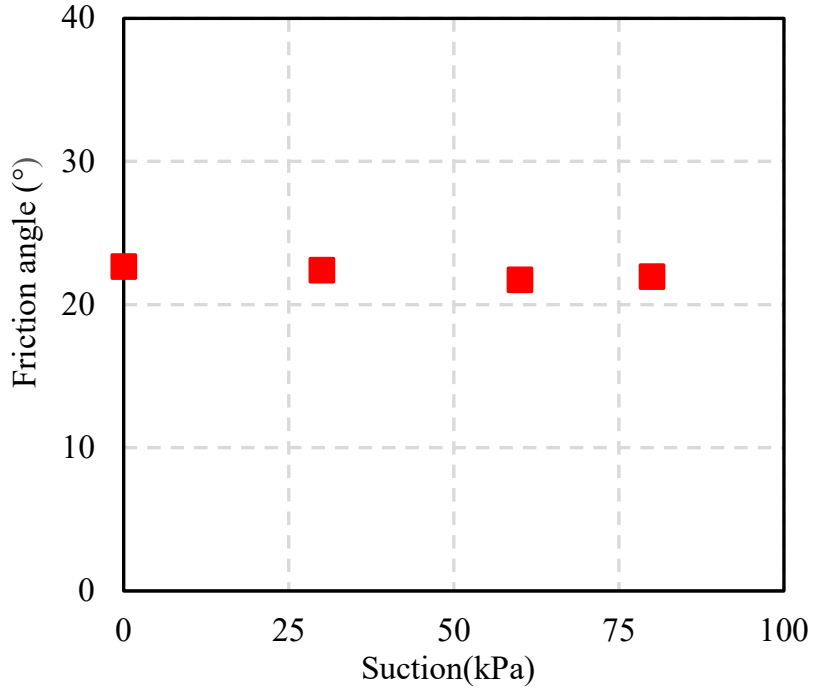

Fig. 5.28 Internal friction angle with different suction

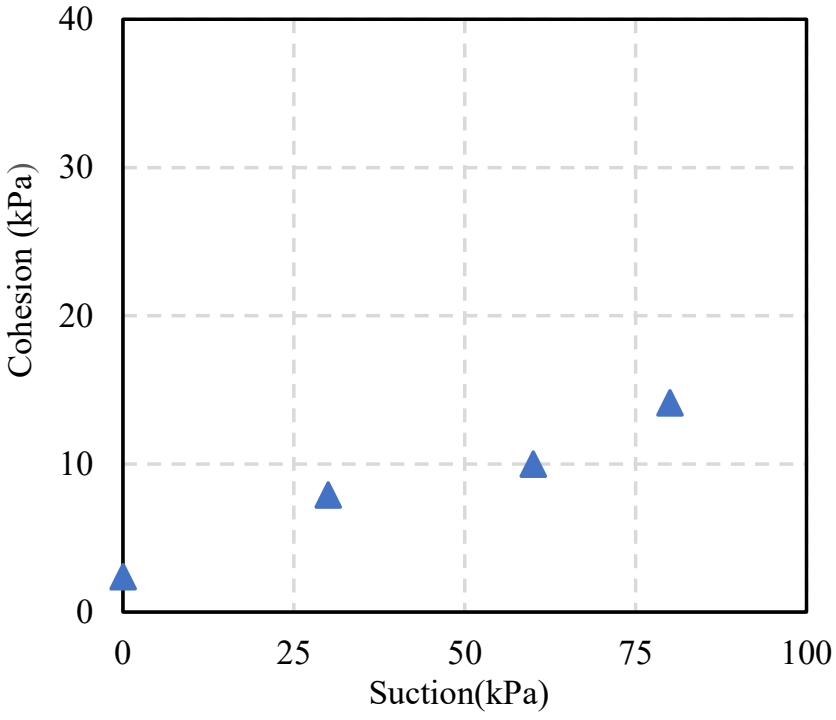

Fig. 5.29 Cohesion with different suction

stress for each test was then obtained. Plotting these failure shear stresses with the corresponding net normal stress and performing a best linear fit on the plotted data, the apparent cohesion (c) and the internal friction angle (ϕ) corresponding to the particular suction value were obtained.

It can be seen from Fig. 5.28 that ϕ is relatively independent of the increase in suction, and the ϕ of unsaturated condition values are quite consistent with the internal friction angle of the saturated soil. It can be observed that the friction angle of saturated soil makes the same contribution to the shear strength of unsaturated soil.

Fig. 5.29 shows that the apparent cohesion (c) increases with increasing the suction value. A number of researchers found a linear increase of c with suction until the air-entry value of soil. The air-entry values of soils used in this study are relatively small, 8 kPa. The increase in suction may increase the interparticle bonding force that can contribute to the apparent cohesive force between particles.

5.9 Summary

Through this chapter, a new suction controlled direct shear box apparatus was developed. In order to evaluate this apparatus, a series of static undrained and drained tests were carried out using the standard soil (Toyoura sand) and volcanic ash soils. The main conclusions are as follows:

1. The test for Toyoura sand as a confirmation was successfully performed in the new suction controlled direct shear box apparatus.
2. The total shear strength of Toyoura sand strongly depends on the suction which can be observed with the new suction controlled direct shear box apparatus.

3. Distribution of water drainage in the new suction controlled direct shear box apparatus is uniform. It can be seen in the water content of unsaturated samples after the test.
4. In the volcanic ash soil results, the shear strength and stiffness of the soil increase with the increase in soil suction. The soil exhibits more dilative volumetric behavior as suction is increased. Similar results were observed under open valve and close valve condition for every group of three tests net normal stress (20 kPa, 40 kPa, and 60 kPa) with the four different suction values (0, 30, 60, and 80 kPa).
5. In the open valve condition in the ceramic disc line, the shear strength is higher for every net normal stress in comparison with close valve condition. It might be attributed to the amount of water drainage during shearing process.
6. The internal friction angle (ϕ) of volcanic ash soil is relatively independent of the increase in suction, and the apparent cohesion (c) increases with increasing the suction value.

References

Barbour, S.L., 1996. The relationship of the unsaturated soil shear strength to the soil–water characteristic curve. Canadian Geotechnical Journal, 33 (3): 440–448.

Chae, J.G., Kim, B.S., Park, S.W., Kato, S., 2010. Effect of suction on unconfined compressive strength in partly saturated soils. KSCE Journal of Civil Engineering, 14 (3): 281–290.

Cho, G. C., and Santamarina, J. C., 2001. Unsaturated particulate materials: Particle-level studies. Journal of Geotechnical and Geoenvironmental Engineering, 1(84): 84–96.

Fredlund, D.G., Morgenstern, N.R., 1977. Stress state variables for unsaturated soils. American Society of Civil Engineers. Journal of the Geotechnical Engineering Division ,103 (5): 447–466.

Fredlund, D.G., Morgenstern, N.R., Widger, R.A., 1978. Shear strength of unsaturated soils. Canadian Geotechnical Journal, 15 (3): 313–321.

Fredlund, D.G., Xing, A., Fredlund, M.D., Barbour, S.L., 1996. The relationship of the unsaturated soil shear strength to the soil–water characteristic curve. Canadian Geotechnical Journal, 33 (3): 440–448.

Gan, J.K.M., Fredlund, D.G., Rahardjo, H., 1988. Determination of the shear strength parameters of an unsaturated soil using the direct shear test. Canadian Geotechnical Journal, 25 (3): 500–510.

Gens, A., Sanchez, M., Sheng, D., 2006. On constitutive modeling of unsaturated soils. Acta Geotechnica, 1(3): 137–147.

Kim, B.S., Shibuya, S., Park, S.W., Kato, S., 2010. Application of suction stress for estimating unsaturated shear strength of soils using direct shear testing under low confining pressure. Canadian Geotechnical Journal, 47 (9): 955–970.

Kim, B.S., Shibuya, S., Park, S.W., Kato, S., 2013. Suction stress and its application on unsaturated direct shear test under constant volume condition. Journal of Engineering Geology, 155: 10–18.

Nam, S., Gutierrez, M., Diplas, P., Petrie, J., 2011. Determination of the shear strength of unsaturated soils using the multistage direct shear test. Journal of Engineering Geology, 122: 272–280.

Sawangsuriya, A., 2006. Stiffness-suction-moisture relationship for compacted soils. Ph.D. thesis, Univ. of Wisconsin, Madison, Wisconsin.

Vanapalli, S.K., Fredlund, D.G., Pufahl, M.D., Clifton, A.W., 1996. Model for prediction of shear strength with respect to soil suction. Canadian Geotechnical Journal, 33 (3): 379–392.

Vanapalli, S.K., Fredlund, D.G., Pufahl, D.E., 1999. The influence of soil structure and stress history on the soil–water characteristics of a compacted till. Geotechnique, 49 (2): 143–159.

CHAPTER VI

EVALUATION OF UNSATURATED VOLCANIC ASH SOIL SLOPE STABILITY

6.1 Introduction

A key step in the soil slope stability analysis is measuring or estimating the strengths of the soils. Reliable analysis can only be performed if the provided shear strength properties are appropriate for the considered soil and representative for the investigated location.

Through this chapter, for the application of the experimental results, the slope stability analysis considering the Kumamoto slope properties was studied. The infinite slope and circular slope stability were presented under static and earthquake load. Furthermore, the unsaturated shear strength results experimentally obtained using the conventional and the newly developed direct shear box apparatus were used to analyze. Finally, the effect of the rainfall infiltration on the slope stability using HYDRUS FEM software analysis is presented.

6.2 Theory (Slope Stability Analysis)

6.2.1 Infinite slip surface

6.2.1.1 Static load

In the infinite slope procedure, the slope is assumed to be infinite in extent, and sliding is assumed to occur along a plane parallel to the face of the slope. Consider a

straight slope with infinite length and uniform soil thickness. The safety factor is defined as the ratio of the shear resistance force on the slip surface to the force acting on the slip surface to cause sliding. The surface slip model for a slope without seepage flow is shown:

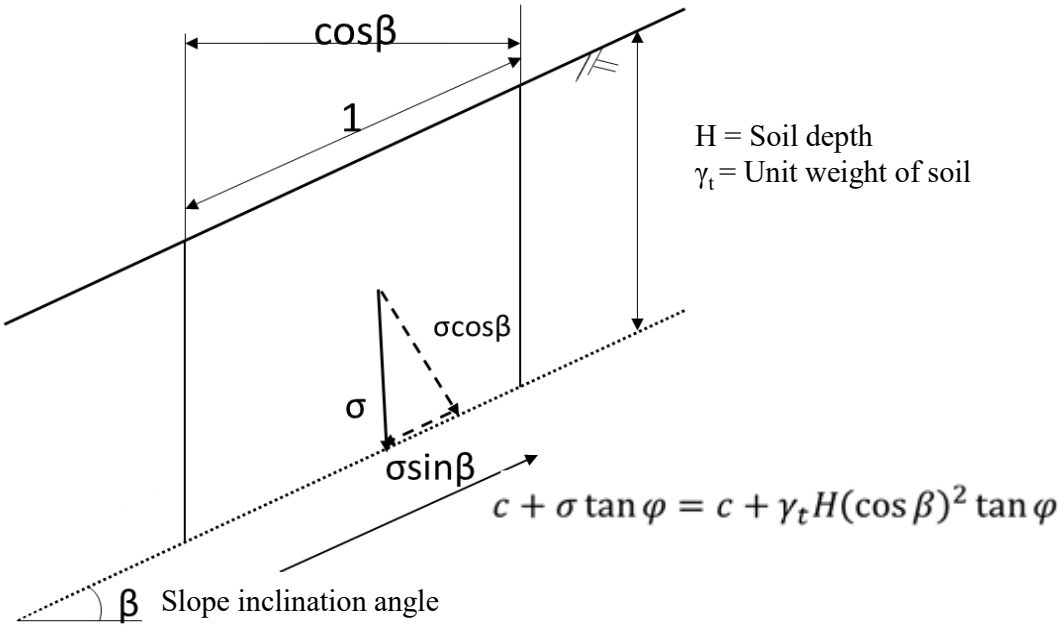

Fig 6.1 Infinite slip surface model.

Where c is the cohesion of soil, φ is the internal friction angle, γ_t is the unit weight of soil, H is the soil thickness, and β is the slope inclination angle. Based on the Fig 6.1, the safety factor of the slope can be determined as:

$$F_s = \frac{c + \gamma_t H(\cos\beta)^2 \tan\varphi}{\gamma_t H \cos\beta \sin\beta} \tag{6.1}$$

Then, the equation 6.1 can be simplified as follows:

$$F_s = \frac{c}{\gamma_t H \cos\beta \sin\beta} + \frac{\tan\varphi}{\tan\beta} \tag{6.2}$$

6.2.1.2 Seismic load (Pseudostatic)

Furthermore, in order to evaluate the slope stability considering of earthquake load, the basic equation of infinite slope stability can be modified considering the acceleration of earthquake load as illustrated in Fig.6.2

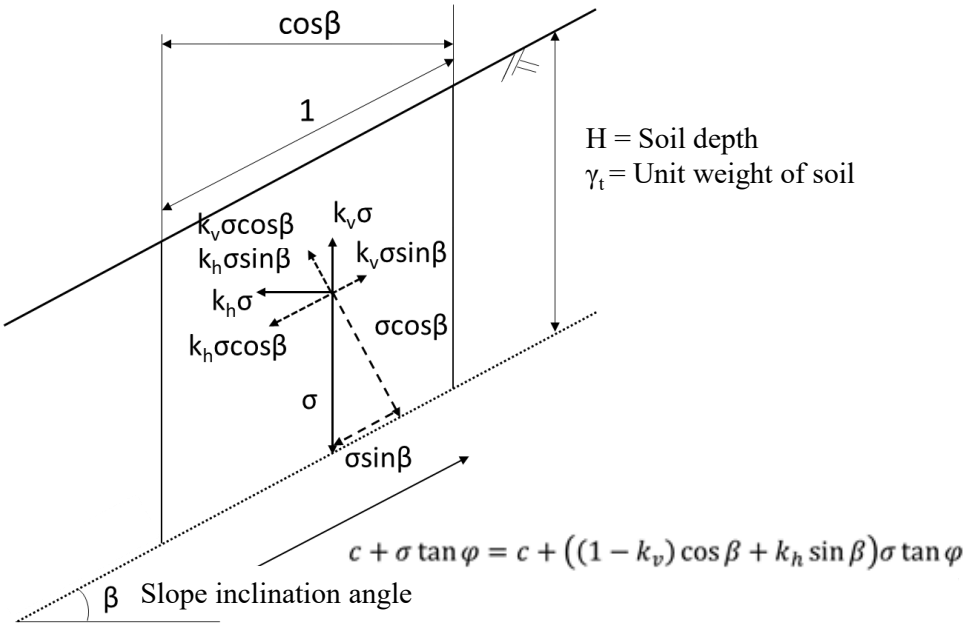

$$c + \sigma \tan\varphi = c + \big((1 - k_v)\cos\beta + k_h \sin\beta\big)\sigma \tan\varphi$$

Fig 6.2 Infinite slip surface model considering the earthquake load

From Fig. 6.2, the safety factor for slip surface is considered as follows based on the relationship of force balance:

$$F_s = \frac{\sigma\{(1 - k_v)\cos\beta - k_h \sin\beta\}\tan\varphi + \sigma k_v \sin\beta + c}{\sigma(k_h \cos\beta + \sin\beta)} \tag{6.3}$$

Where c is the cohesion of soil, γ_t is the unit weight of soil, H is the soil thickness, β is the slope inclination angle, k_h is the horizontal seismic intensity, and k_v is the vertical seismic intensity. Then, the formula 6.3 can be simplified as follows:

$$F_s = \frac{\tan\varphi\,(1 - k_v - k_h \tan\beta) + k_v \tan\beta + c/\gamma H(\cos\beta)^2}{k_h + \tan\beta} \tag{6.4}$$

In the analysis, most of the researchers considering k_h (the horizontal seismic intensity) only. Thus, in the safety factor calculation in this research, the vertical seismic intensity is neglected ($k_v = 0$). The design of horizontal seismic intensity is expressed as follows according to the Road Bridge Specification of Japan:

$$k_h = c\, k_{h0} \tag{6.5}$$

Where k_h is the design horizontal seismic intensity, c is the correction coefficient for each region, and k_{h0} is the standard value of the design horizontal seismic intensity on the ground surface for each level of ground motion. The regional correction coefficient c is determined by each region in Japan, as shown in Figure 6.3. From the figure, the Aso area indicated in the B2 area.

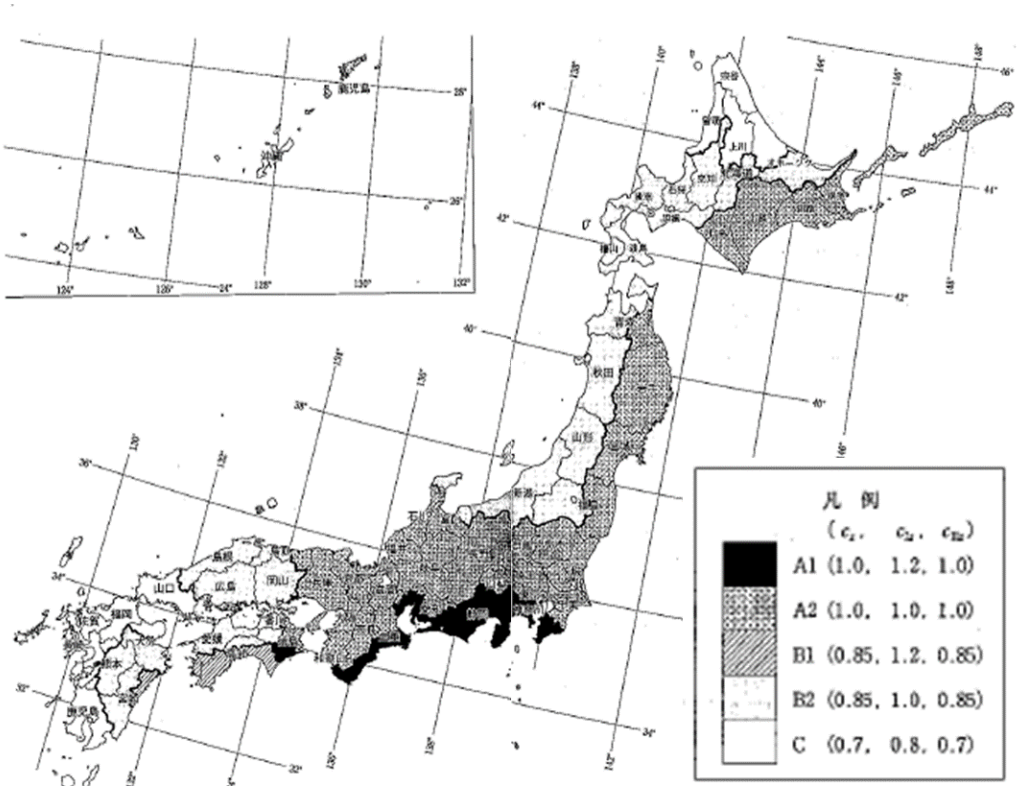

Fig 6.3 The regional correction coefficient for each area in Japan.

The standard value k_{h0} of the design horizontal seismic intensity on the ground surface for each level of ground motion varies depending on the ground type. According to Kawaguchi, 2019 the value of the design horizontal seismic intensity in the Aso area is 0.6. Thus, with following the design of horizontal seismic intensity according to the Road Bridge Specification of Japan and the maximum standard value of the design horizontal seismic intensity on the ground surface, The k_h (the design horizontal seismic intensity) was decided 0.6 in this research.

6.2.1.3 Newmark method

The Newmark sliding method was proposed by Newmark,1965 which considers that the slide will begin to slip when the seismic acceleration exceeds the critical acceleration, and the final displacement of the slide can be obtained by double integral over the time of the difference between the seismic acceleration and the critical acceleration, which is called permanent displacement.

The important parameter in this method is the yield seismic intensity. The yield seismic intensity is the horizontal seismic intensity when the safety factor Fs=1 and represented by k_{hy}. In the field condition of Aso Ohashi area, since the seepage flow is not in the Kuroboku layer, the yield seismic intensity k_{hy} without considering the seepage flow is as follows.

$$k_{hy} = \frac{(1 - k_v)(\tan\varphi - \tan\beta) + c/\gamma H(\cos\beta)^2}{1 + \tan\varphi \tan\beta} \tag{6.6}$$

Furthermore, according to Kasama et al., 2018, the yield seismic intensity considering the reduction rate R of vertical stress due to cyclic shear test is considered as follows.

$$k_{hy} = \frac{(1 - k_v)(\mathrm{R} \times \tan\varphi - \tan\beta) + c/\gamma H(\cos\beta)^2}{1 + \tan\varphi \tan\beta} \tag{6.7}$$

Furthermore, in this calculation, the reduction of vertical stress (R) under cyclic load will be represented with the average degradation index (δ_{avg}) from the experimental results.

The permanent displacement is obtained by multiplying the difference between the horizontal seismic intensity and the yield seismic intensity obtained above by the gravitational acceleration, and then double integration it. Furthermore, η' is as follows.

$$l = \eta' \iint (k_h - k_{hy}) g \cdot dt \tag{6.8}$$

$$\eta' = \cos\beta + \tan\varphi \sin\beta \tag{6.9}$$

The slope of the Aso Ohashi collapse site is around 33 degrees at the top. In addition, the main shock that occurred at 01:25 on April 16, 2016 was used in this calculation (Kasama et al., 2018)

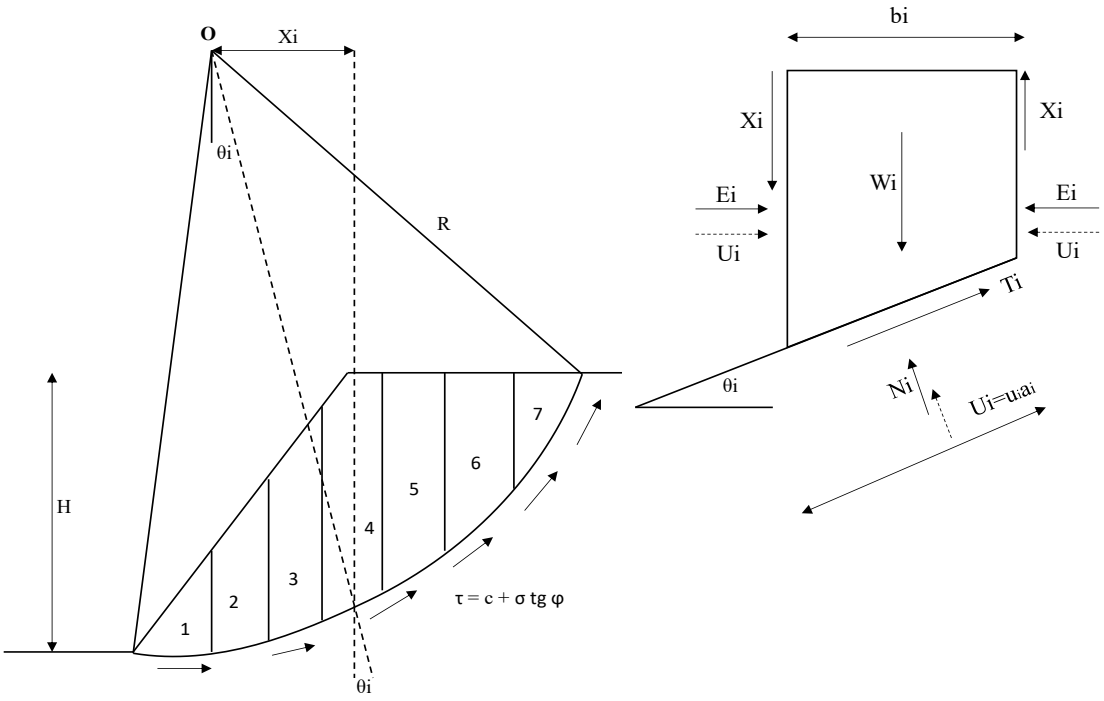

Fig 6.4 The circular slope stability analysis

6.2.2 Circular slip surface

Fig 6.4 shows the circular slope stability analysis. In the circular slope stability considers the forces acting on the right and left sides of any slice to have a resultant of 0 on the perpendicular plane of the landslide. With this assumption, the balance of the vertical direction and the forces acting with respect to pore water pressure is:

$$N_i + U_i = W_i \cos\theta_i \tag{6.10}$$

The safety factor of slope can be defined as the ratio of the moment resistance force on the slip surface to the moment acting on the slip surface to cause sliding.

$$SF = \frac{Resisting\ moment}{Overturning\ moment} = \frac{\Sigma M_r}{\Sigma M_d} \tag{6.11}$$

Where the resisting moment and overturning can be determined:

$$\sum M_d = R \sum_{i=1}^{i=n} W_i \sin\theta_i \tag{6.12}$$

$$\sum M_r = R \sum_{i=1}^{i=n} ca_i + N_i\, tg\, \varphi \tag{6.13}$$

Finally, the safety factor of slope can be simplified as follows.

$$F = \frac{\sum_{i=1}^{i=n}(ca_i + N_i\, tg\, \varphi)}{\sum_{i=1}^{i=n} W_i \sin\theta_i} \tag{6.14}$$

Furthermore, in order to evaluate the slope stability considering of earthquake load, the basic formula of circular slope stability formula can be modified considering the acceleration of earthquake load as illustrated in Fig.6.5 and Equation 6.15.

$$F = \frac{\sum_{i=1}^{i=n}(ca_i + N_i\, tg\, \varphi)}{\sum_{i=1}^{i=n} W_i \sin\theta_i + k_h W_i\,(\frac{L_i}{R})} \tag{6.15}$$

In the Pseudostatic analysis, most of the researchers considering k_h (the horizontal seismic intensity) only. Thus, in the safety factor calculation in this research, the vertical seismic intensity is neglected ($k_v = 0$).

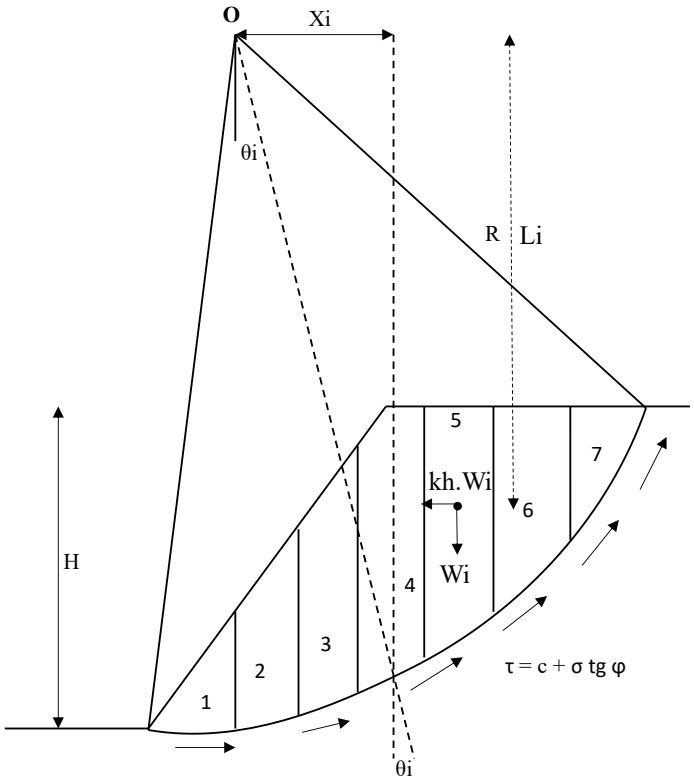

Fig 6.5 The circular slope stability analysis with the seismic intensity.

6.3 Effect of soil structure disturbance on the safety factor of slope

In the chapter 4 has been shown that the discrepancies of the soil shear strength between undisturbed and disturbed samples which related to the soil structure characteristics. Furthermore, for the application of the effect of soil structure disturbance, the safety factor of the slope was analyzed. The Kumamoto slope

Table 6.1. Soil shear strength properties for the slope stability analysis

Properties	Case I	Case II	Case III	Case IV
	Undisturbed saturated	Disturbed saturated	Undisturbed unsaturated	Disturbed unsaturated
β = Inclination angle of slope = 33°				
c (kN/m^2)	13	4.7	24.6	11.75
φ	35.1	34.08	35.5	35.0
γ_t (kN/m^2) = 11.21				

properties were adopted for the slope stability analysis. The infinite slope and circular slope stability were presented under static and earthquake load with various depth layers. Properties of the soil shear strength from the experimental was used in this analysis as shown in Table 6.1.

6.3.1 Infinite slip surface

The factor of safety is defined as the ratio of the forces resisting movement to those driving movement. In general, if the factor of safety of a slope is within the interval between 0 and 1.0, the slope is unstable. The value over 1.0 indicates that the slope is considered stable. Fig 6.6 shows the safety factor of slope under various conditions. It can be observed that the discrepancies of the soil shear strength between undisturbed and disturbed samples which related to the soil structure characteristics give a huge impact on the safety factor of slope. For the undisturbed sample both unsaturated and saturated conditions, the safety factor is significantly larger. Where in the 1 m depth layer, the undisturbed sample both unsaturated and saturated conditions have a safety factor 5.9 and 3.8 respectively. On the other hand, the disturbed sample both unsaturated and saturated conditions have a safety factor 3.4 and 2.0, respectively.

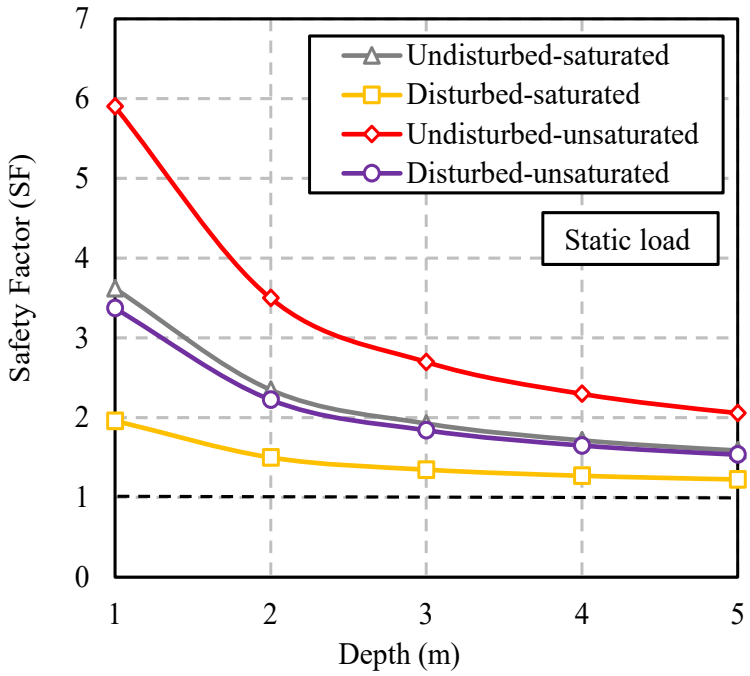

Fig 6.6 The safety factor of slope under static load.

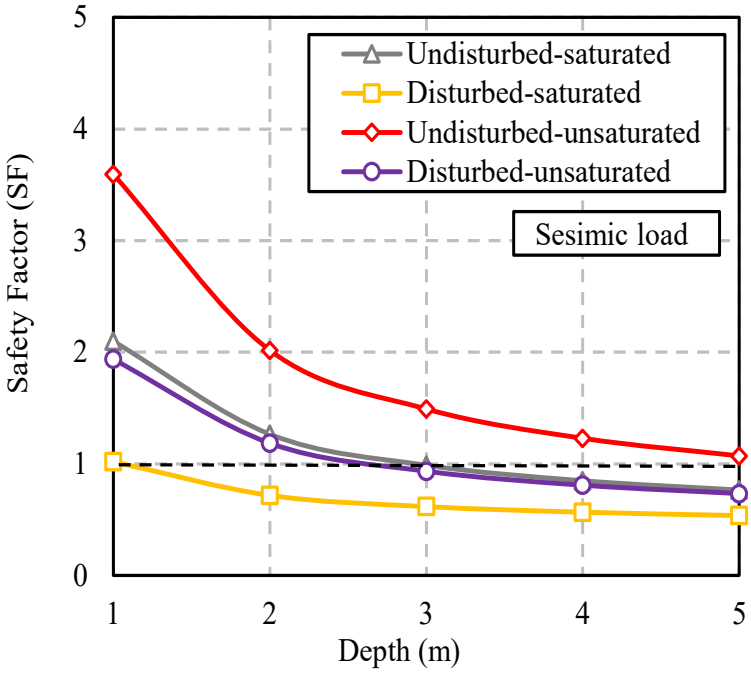

Fig 6.7 The safety factor of slope under seismic load.

Thus, it can be said that the disturbed samples do not properly represent the field conditions with significant discrepancies that should be carefully considered when conducting the slope stability analysis.

Furthermore, the effect of soil thickness can be observed for the condition of each sample. It can be seen that with the increase of soil thickness, the safety factor of slope dramatically reduces.

Fig 6.7 shows the safety factor of slope under seismic load. It can be observed that the seismic load gives a huge impact on the safety factor of slope. For the undisturbed sample both unsaturated and saturated conditions, the safety factor is significantly larger. However, only unsaturated undisturbed sample is still stable until 5 m depth. It can be observed that the saturated undisturbed sample becomes unstable condition from 3 m depth. On the other hand, the saturated disturbed sample condition becomes unstable condition after 1 m depth. Thus, it can be said that the disturbed samples do not properly represent the field conditions with significant discrepancies not only in under static load but also seismic load condition.

Fig 6.8 shows the acceleration of the main shock Kumamoto earthquake at 01:25 on April 16, 2016 and the yield seismic intensity. It can be observed that the yield seismic intensity of disturbed samples both unsaturated and saturated condition is significantly lower than that of undisturbed samples. Where the disturbed sample under saturated condition has a yield seismic intensity 0.1 in average. On the other hand, the undisturbed sample under unsaturated condition indicate a yield seismic intensity 0.35 in average.

Furthermore, Fig 6.9 illustrates the permanent displacement of the volcanic ash soil under various condition. Since the disturbed sample has a lower yield seismic

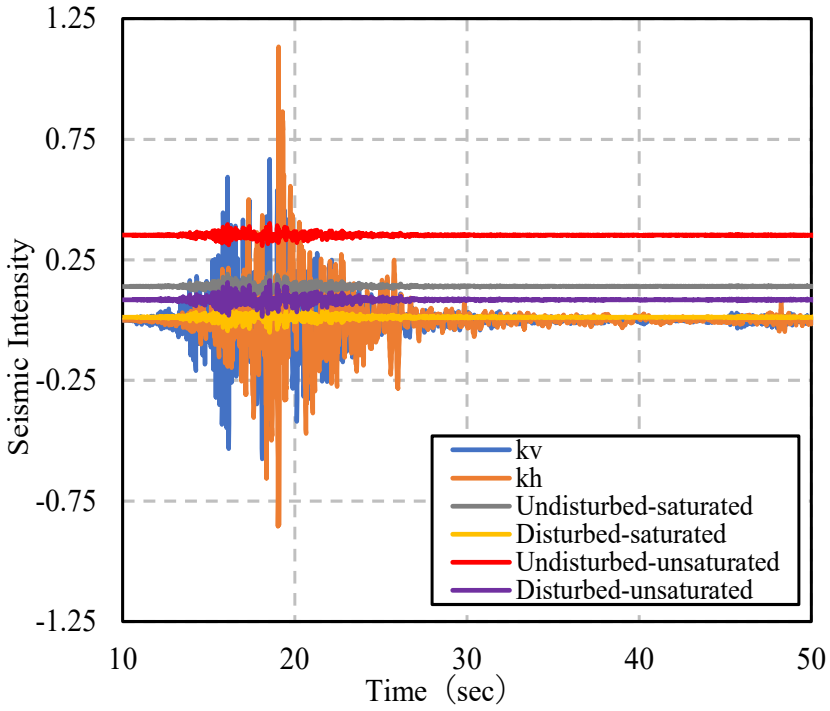

Fig 6.8 The main shock of Kumamoto earthquake at 01:25 on April 16, 2016 and the yield seismic intensity (Japan Meteorology Agency, 2016)

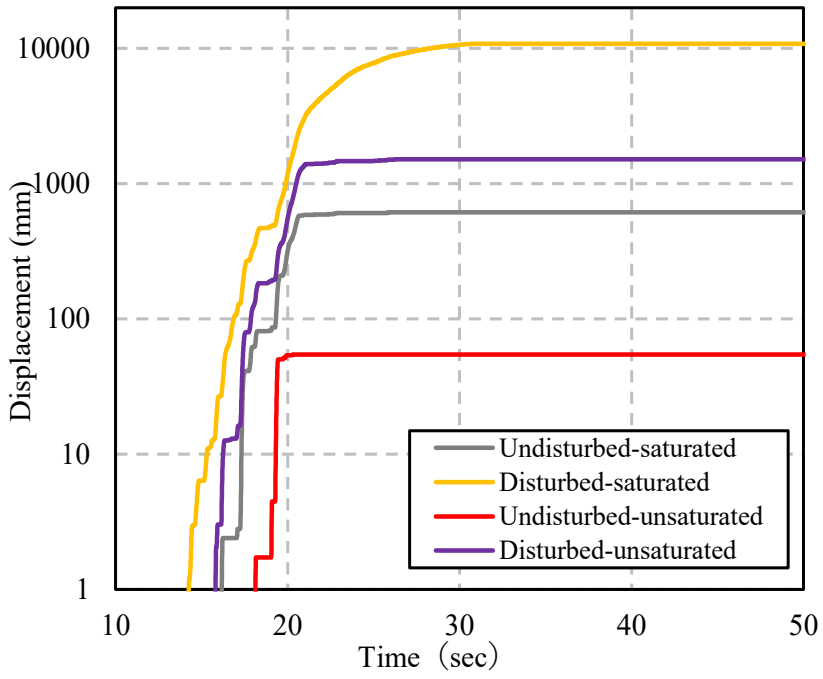

Fig 6.9 The permanent displacement of the volcanic ash soil

intensity, the permanent displacement will be higher. It can be observed that the disturbed sample under saturated condition indicates around 10000 mm permanent displacement. On the other hand, the undisturbed sample under unsaturated and saturated condition show 80 mm and 700 mm, respectively. Thus, it can be concluded that the effect of soil structure disturbance clearly observed in the permanent displacement of the volcanic ash soil under seismic load.

6.3.2 Circular slip surface

Fig 6.10 and 6.11 show the safety factor of circular slip surface slope under static and seismic load. It can be observed that the discrepancies of the soil shear strength between undisturbed and disturbed samples affected the safety factor of slope. For the undisturbed sample both unsaturated and saturated conditions, the safety factor is significantly larger. Where in the 5 m depth layer, the undisturbed sample both unsaturated and saturated conditions indicate a safety factor 2.9 and 2.1, respectively. On the other hand, the disturbed sample both unsaturated and saturated conditions have a safety factor 2.0 and 1.5, respectively. Furthermore, it can be observed that the safety factor of slope reduces under seismic load. For the disturbed sample both unsaturated and saturated conditions, the safety factor is significantly lower. The saturated disturbed sample condition becomes unstable condition after 1 m depth. However, for the other condition the safety factor of slope is stable until 5 m depth. Thus, it can be clearly observed that the disturbed samples do not properly represent the field conditions with significant discrepancies not only in under static load but also seismic load condition.

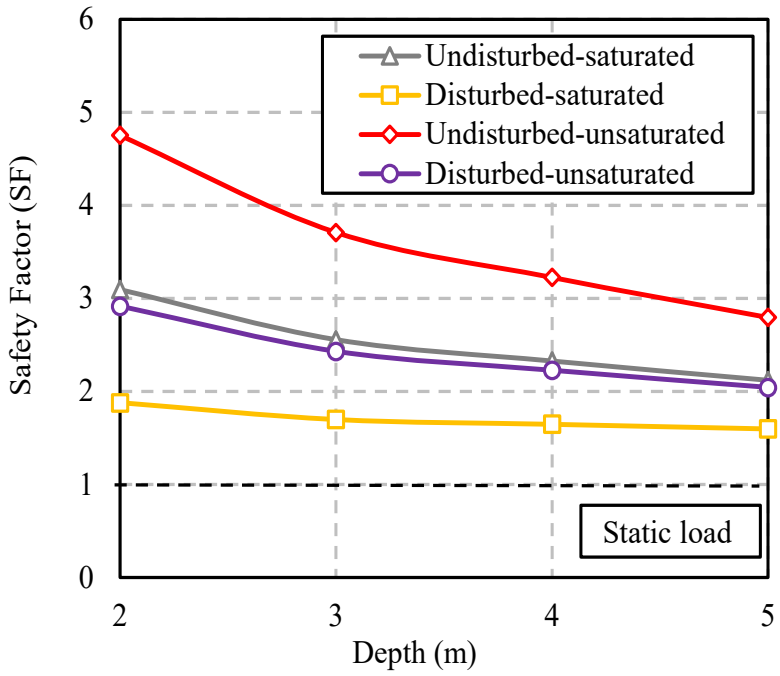

Fig 6.10 The safety factor of slope under static load

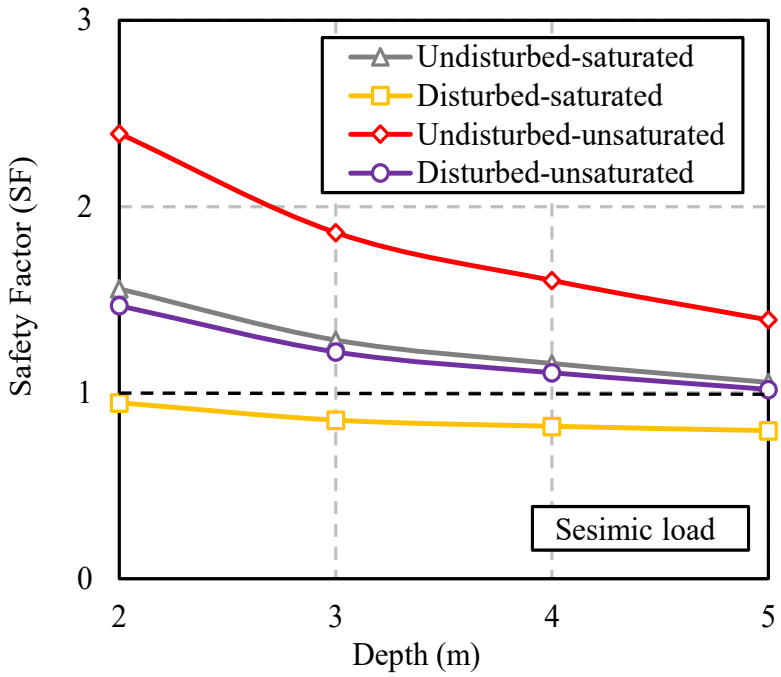

Fig 6.11 The safety factor of slope under seismic load

6.4 Effect of precipitation events on the slope stability behavior

Numerical simulations are used to evaluate the Kumamoto slope stability behavior during precipitation event. The numerical simulations apply the field condition and properties to get the reliable results.

To investigate the slope stability of Kumamoto slope during precipitation event, Hydrus 2-D Slope Cube commercial software was used. The focusing point in the simulation is the safety factor of slope characteristics under various condition. Currently, several common research approaches are used to better understand and predict such geologic hazards, namely statistically or/and physically based analyses. In Hydrus 2-D Slope Cube, a physically based hydro-mechanical framework focusing on assessment and prediction of the initiation and locations of slope failure occurrences under rainfall conditions. Slope Cube couples variably saturated flow and stress fields to simulate transient hillslope hydrologic and mechanical responses to rainfall events. Three recent advancements are implemented in Slope Cube that are beyond the traditional physically based slope failure models. The first is the utilization of the suction stress-based effective stress to unify the description of effective stress distribution in hillslopes under variably-saturated conditions. The second is calculation of deformations due to changes in suction stress-based effective stress. The third is to employ a recently established concept of the local factor of safety to capture evolution of stress paths toward the failure state in hillslopes.

6.4.1 Slope stability characteristics with various thickness of volcanic ash

In the Kumamoto slope properties, the volcanic ash soil covers the top layer. In order to evaluate the behavior of the volcanic ash slope under precipitation event, 3

various depth layers of volcanic ash soil were adopted in this analysis. Fig 6.12 shows the stratigraphy of the Kumamoto slope which the main slope indicates 33° of inclination angle (Hung et al., 2017). Furthermore, the observation points for the analysis were set in the middle of the main slope. Fig 6.13 and Table 6.2 illustrate the observation points and the variety of depth layers.

On the other hand, the soil shear strength properties from the experimental results were used. Where the cohesion (c) is 24.6 kN/m^2, internal friction angle (ϕ) is 35.5°, and the bulk density is 11.21 kN/m^3. Furthermore, the initial volumetric water content (θ) is 0.72 according to the natural condition. To simulate the precipitation, the heavy rainfall intensity 0.07 mm/h (Monjo,2016) was applied. Then, the SWCC properties for volcanic ash soil was adopted from Alowaisy et al., 2019 as illustrated in Fig. 6.14.

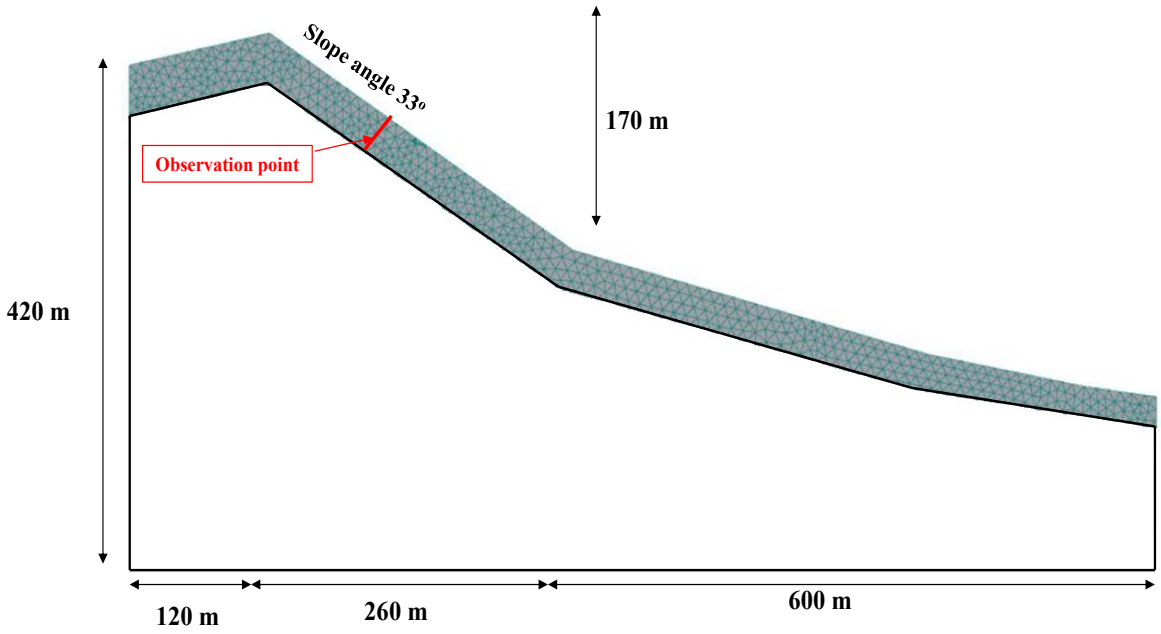

Fig 6.12 Stratigraphy of Kumamoto slope

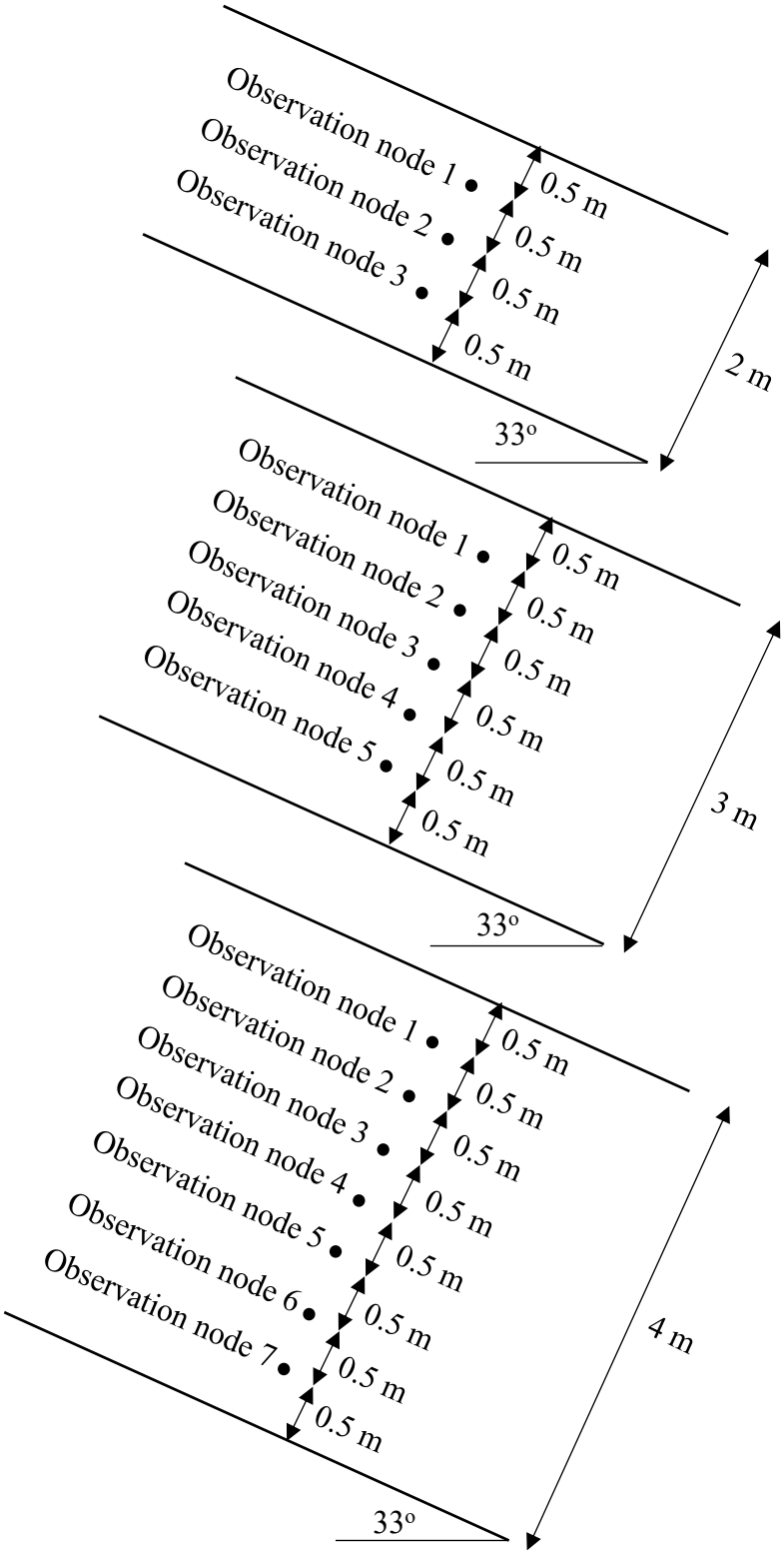

Fig 6.13 The observation points and the variety of depth layers

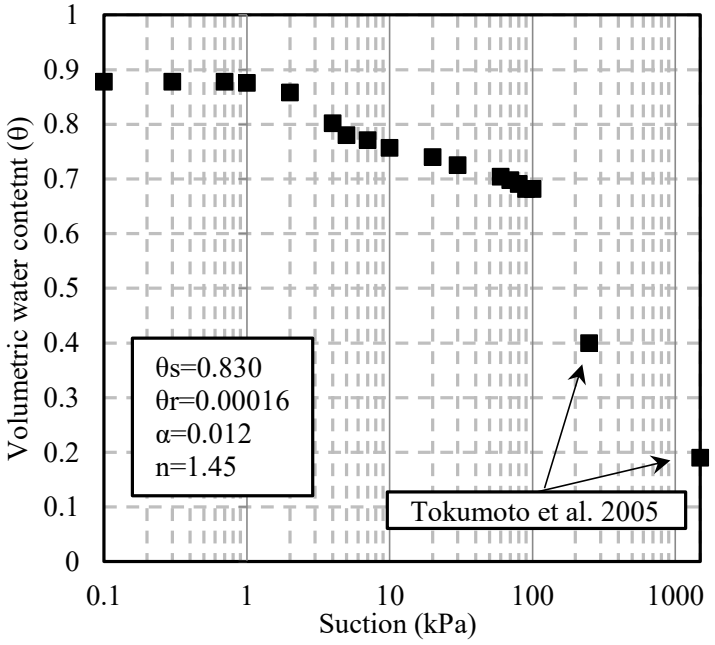

Fig 6.14 The SWCC properties of volcanic ash soil

Table 6.2. The observation points and the variety of depth layers.

Depth (m) L	Observation nodes	Distance (m) x	x/L
2	Observation node 1	0.5	0.250
	Observation node 2	1	0.500
	Observation node 3	1.5	0.750
3	Observation node 1	0.5	0.167
	Observation node 2	1	0.333
	Observation node 3	1.5	0.500
	Observation node 4	2.0	0.667
	Observation node 5	2.5	0.833
4	Observation node 1	0.5	0.125
	Observation node 2	1	0.250
	Observation node 3	1.5	0.375
	Observation node 4	2.0	0.500
	Observation node 5	2.5	0.625
	Observation node 6	3.0	0.750
	Observation node 7	3.5	0.875

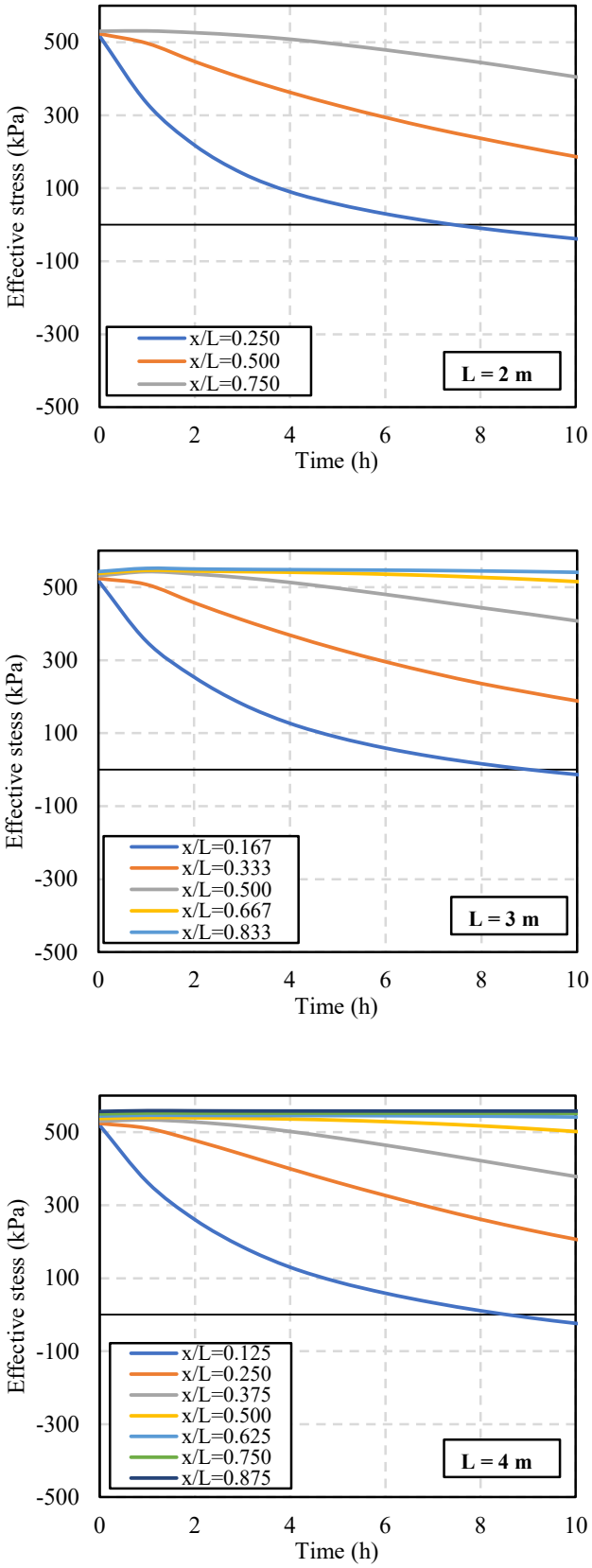

Fig 6.15 The effective stress development with time

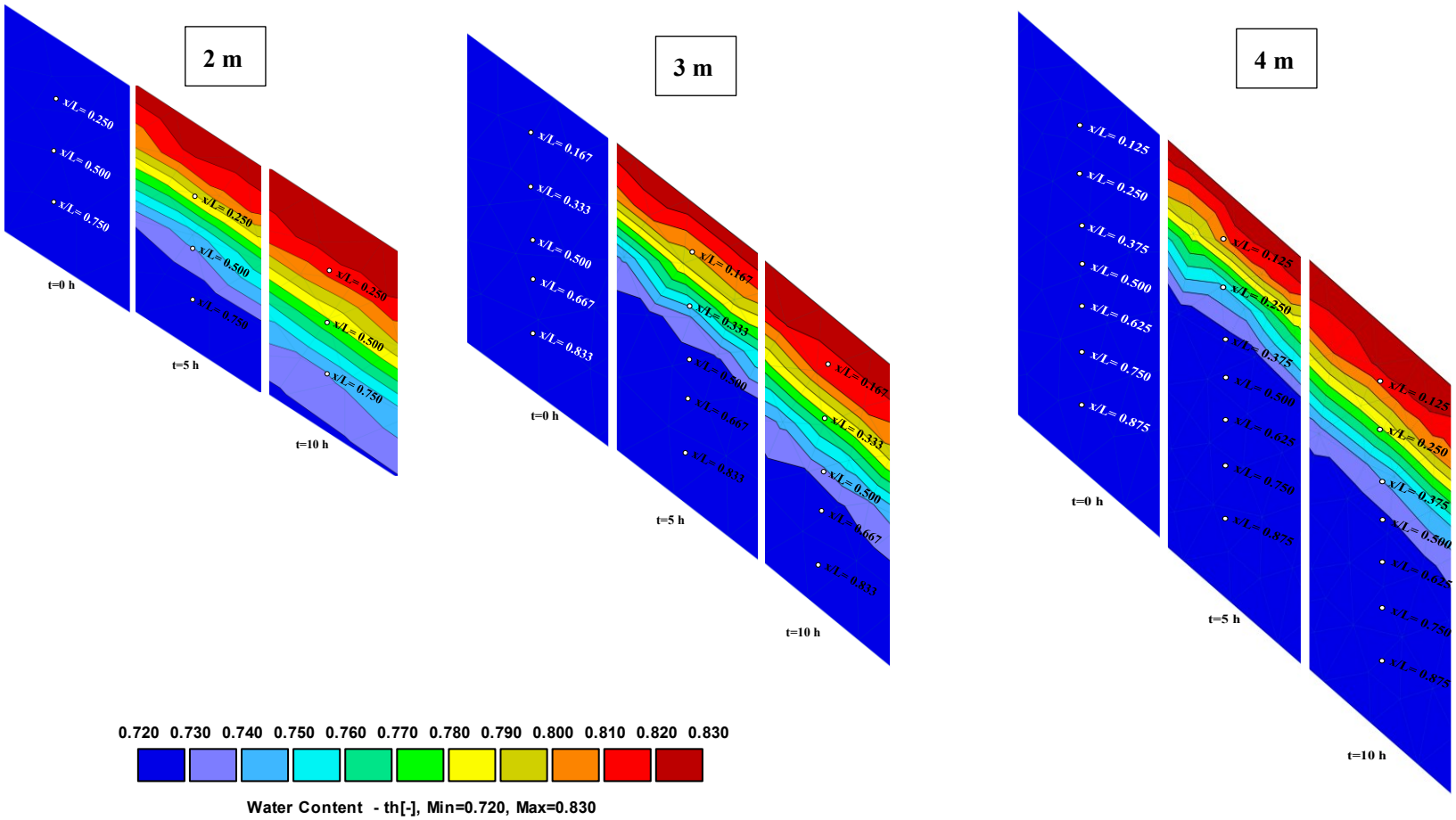

Fig 6.16 The volumetric water content development with time

Fig 6.15 show the development of effective stress with time monitored at each layer. Where *x* is the distance from the surface while *L* is the total thickness of the layer.

It can be observed that the effective stress significantly reduces during precipitation in the 2 m thickness of the volcanic ash soil. All the observation points indicate the reduction of the effective stress. Furthermore, the observation point (x/L=0.25) shows that the precipitation imposes the effective stress to 0 kPa in the 7 hours. Reduction of the effective stress related to the infiltration of water during precipitation. Where, in the 2 m thickness of the volcanic ash soil, the precipitation events significantly affected in all observation points.

Furthermore, in the 3 m thickness of the volcanic ash soil, reduction of the effective stress during precipitation clearly observed in four observation points (x/L=0.167, x/L=0.333, x/L=0.500, and x/L=0.667). On the other hand, for the (x/L= 0.833) not significant reduction of the effective stress was observed. Similar to the 2 m thickness, reduction of the effective stress related to the infiltration of water during precipitation. Where, in the 3 m thickness of the volcanic ash soil, the infiltration of water only in the observation points (x/L=0.167, x/L=0.333, x/L=0.500, and 0.667).

For the 4 m thickness of the volcanic ash soil, the reduction of the effective stress during precipitation only in four observation points (x/L=0,125, x/L=0.250, 0.375, and x/L=0.500). It can be concluded that the precipitation event only affected till 2 m depth of volcanic ash soil.

Fig 6.16 shows the development of water content with time monitored at each layer at time t = 0 h, t = 5 h, and t = 10 h. It can be observed in the 2 m thickness of the volcanic ash soil, all layers are infiltrated by precipitation events after 10 h with the maximum water content 0.830. Thus, it can be confirmed that the reduction of

effective stress on all observation points in the 2 m thickness related to the infiltration of water which confirmed with the change of water content. On the other hand, in the 3 and 4 m thickness of the volcanic ash soil, only till 2 m layers are infiltrated by precipitation events after 10 h with the maximum water content 0.830. Thus, it can be concluded that the precipitation event only affected till 2 m depth of volcanic ash soil which confirmed with the change of water content that related to the reduction of effective stress.

Fig. 6.17 illustrates the correlation safety factor of the slope before precipitation (t = 0 h) and observation point depth ratio. It must be noted that the calculation of Local Safety Factor in the Hydrus 2-D Slope Cube based on the development and evolution of effective stress under unsaturated conditions and can be determined for each observation point. This analysis is significantly different from traditionally performed under limit equilibrium methods which can determine only one safety factor. From the obtained results, it can be seen that the safety factor of slope in the x/L=0.250 approximately 3 times larger than that of x/L=0.500. It can be concluded that the safety factor of slope decreases with increasing of the depth layer. The obtained results in good agreement with the calculation in section 6.3. Where the driving force of the depth layer significantly larger in comparison to the shallow layer.

Furthermore, Fig. 6.16 illustrates the average reduction safety factor of slope and observation point depth ratio. The reduction of local safety factor can be determined as follows:

$$Reduction\ of\ LSF(\%) = \left(\frac{LSF_0 - LSF_t}{LSF_0}\right) x100 \quad (6.16)$$

Where LSF_0 is the Local Safety Factor at the initial condition and LSF_t is the Local

Safety Factor after time hours. In order to evaluate the correlation of the reduction safety factor of slope and observation point depth ratio, the average reduction from the initial till the final time of precipitation are plotted against the observation point depth ratio the whole depth layers as illustrated in Fig. 6.15. It can be observed that a shallow depth layer imposes a higher average reduction of Local Safety Factor. It can be attributed to the change of water content which related to decrease on effective stress during precipitation event. The obtained results opposite with the initial Local Safety Factor. Where the shallow depth indicates a higher Local Safety Factor. It can be concluded that the wetting process or precipitation events give a huge impact to the shallow layer of the volcanic ash soil.

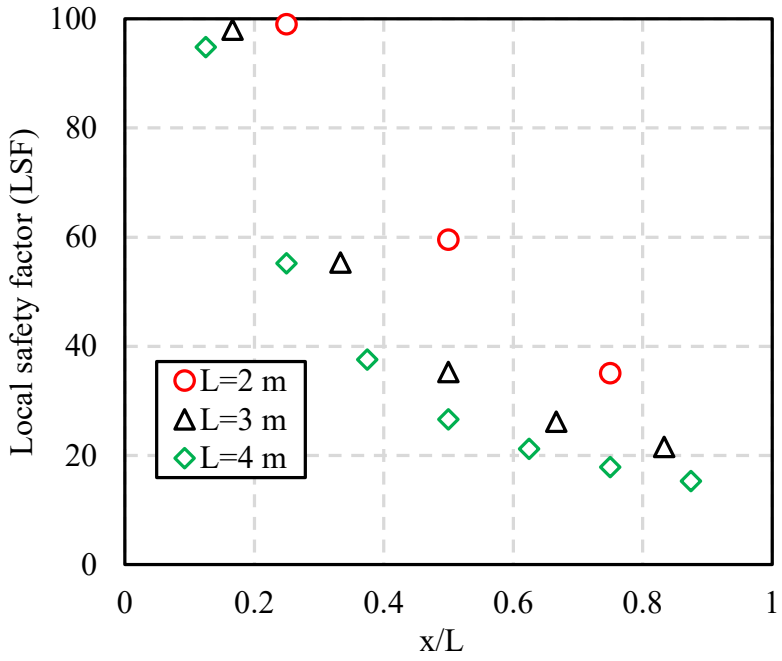

Fig 6.17 Correlation safety factor of slope before precipitation (t = 0 h) and observation point depth ratio

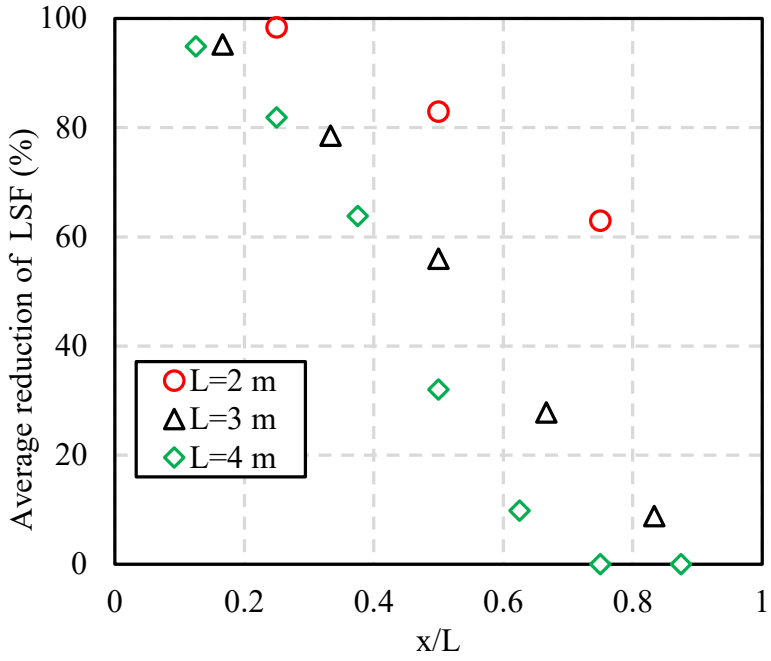

Fig 6.18 Average reduction safety factor of slope and observation point depth ratio

6.4.2 Reliability of disturbed sample shear strength properties on the slope stability

Comparison of the shear strength properties results from disturbed and undisturbed samples on the slope stability was evaluated. The soil shear strength properties from the experimental results were used as input parameter in the Hydrus 2-D Slope Cube. Where disturbed sample indicates the cohesion (c) is 11.75 kN/m^2 and the internal friction angle (ϕ) is 35°. On the other hand, the undisturbed sample shows the cohesion (c) is 24.6 kN/m^2 and the internal friction angle (ϕ) is 35.5°. Furthermore, the initial volumetric water content (θ) is 0.72 according to the natural condition. To simulate the precipitation, three types of rainfall patterns were adopted from Mojo, 2016. The rainfall patterns intensity was classified into light rain with 0.02 mm/h, medium rain 0.04 mm/h and heavy rain 0.07 mm/h. Then, the SWCC properties

was adopted from Alowaisy et al., 2019 as illustrated in Fig. 6.19.

Furthermore, 2 m depth of volcanic ash soil was adopted because of the precipitation event only affected till 2 m depth of volcanic ash soil which confirmed with the change of water content that related to the reduction of effective stress in the previous section. Fig 6.20 illustrates the detail of observation points.

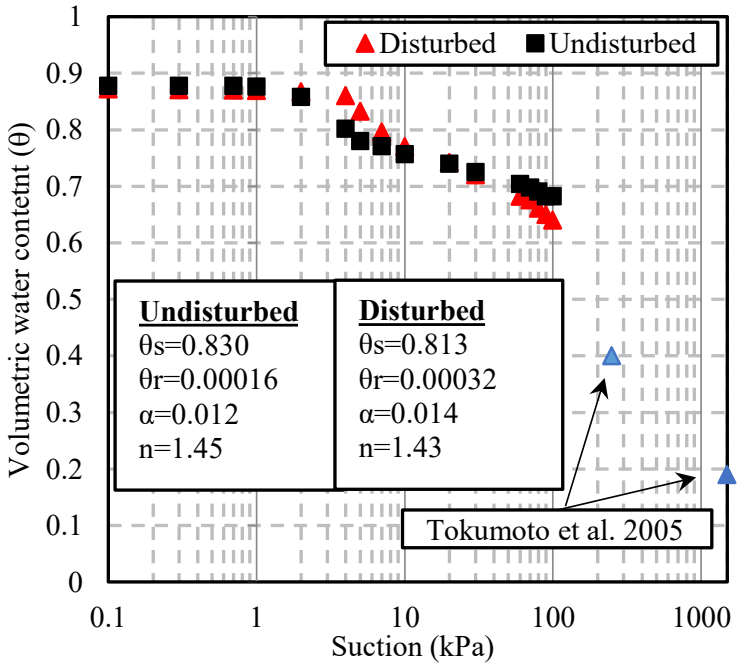

Fig 6.19 SWCC of disturbed and undisturbed samples.

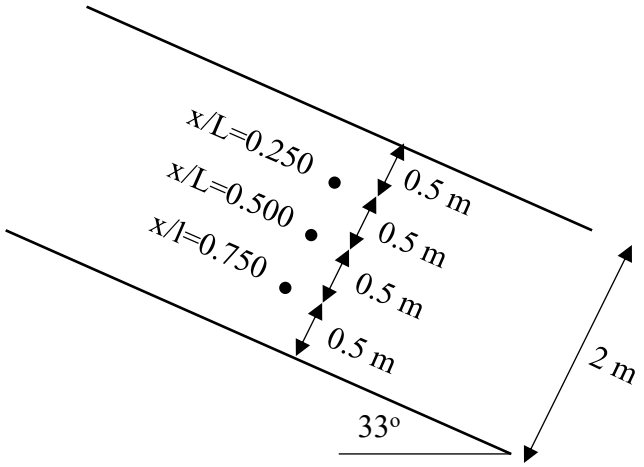

Fig 6.20 The detail of observation points.

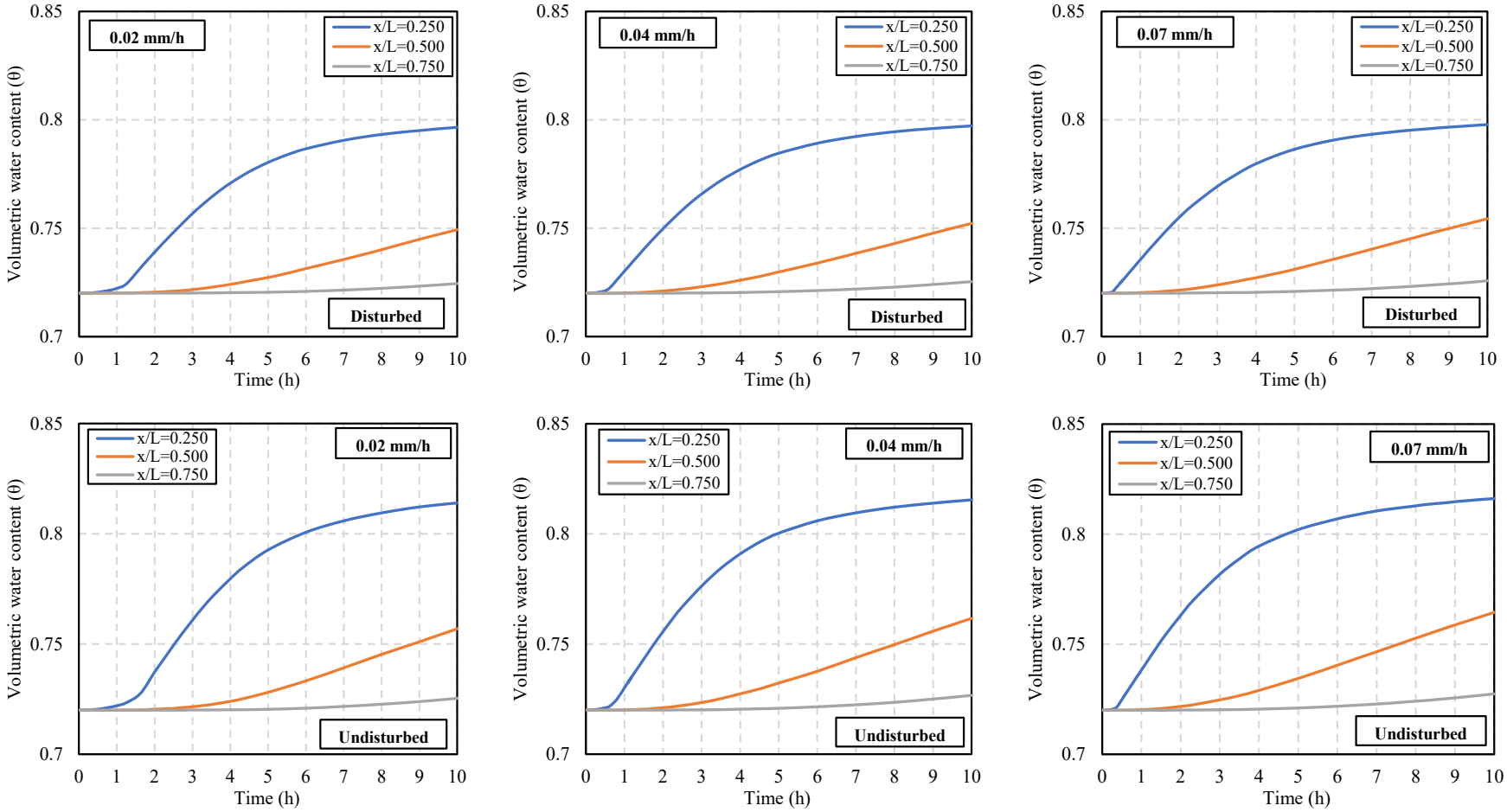

Fig 6.21 The volumetric water content development with time

Fig. 6.21 illustrates the development of the volumetric water content with time monitored at three locations (x/L=0.250, 0.500 and 0.750) under different intensity of rainfall. It can be observed that the obtained volumetric water content through the soil profile is significantly higher for the undisturbed sample in comparison to the disturbed sample. It can be attributed to the provided initial conditions and boundary conditions, where the obtained saturated volumetric water content (θs) is higher for undisturbed samples. The time needed for the maximum volumetric water content is faster in the disturbed sample in comparison to the undisturbed sample. It can be observed in the x/L=0.250, after 7 hours the volumetric water content indicates constant value. However, in the disturbed sample, till 10 hours of precipitation the volumetric water content still increasing. Furthermore, the effect of rainfall intensity clearly observed in the start increasing of volumetric water content. Where in the higher intensity of rainfall is faster in comparison to the lower intensity.

Fig 6.22 illustrates the Local Safety Factor (LSF) of the slope after 5 hours of precipitation events. It can be observed that all observation points (x/L=0.250, 0.500, and 0.750) the Local Safety Factor (LSF) of the undisturbed samples is significantly higher in comparison to disturbed samples. Furthermore, in the x/L=0.250, the Local Safety Factor (LSF) of the undisturbed sample shows more than 1 in the 0.02 m/h intensity of rainfall. However, in the 0.04 and 0.07 m/h indicate lower than 1. In other words, the slope in the unstable condition. On the other hand, the disturbed sample indicates unstable condition in the 0.02, 0.04, and 0.07 mm/h intensity of rainfall. It must be noted that the rainfall intensity effect clearly observed in all observation points, where the Local Safety Factor (LSF) of slope decreases with increasing rainfall intensity both undisturbed and disturbed samples.

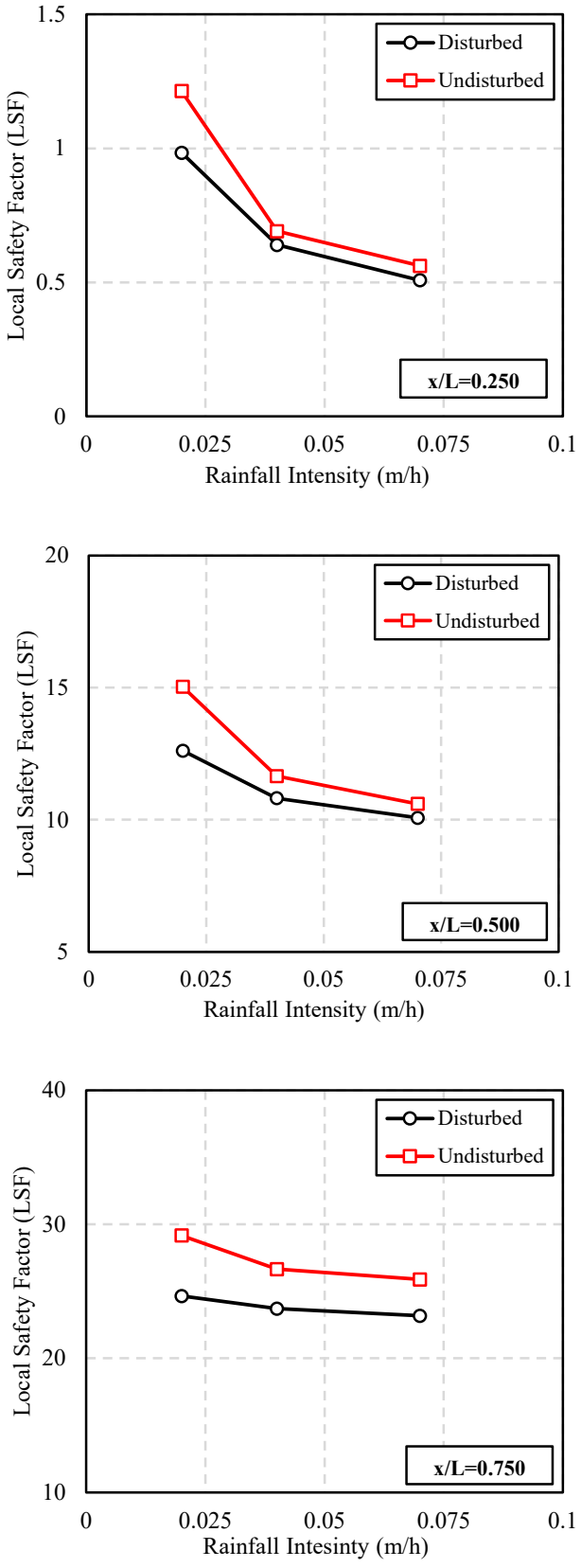

Fig 6.22 The Local Safety Factor (LSF) with rainfall intensity

In order to clearly understand, the discrepancies associated with considering the Local Safety Factor (LSF) after precipitation events between disturbed and undisturbed samples was estimated. The discrepancy index can be determined as follows:

$$Discrepancy\ index\ (\%) = \left(1 - \frac{LSF_{undisturbed}}{LSF_{disturbed}}\right) x100 \qquad (6.17)$$

Fig. 6.23 shows the Local Safety Factor (LSF) discrepancies from the disturbed and disturbed samples. It can be seen that the discrepancies 12%, 11%, and 13% corresponding to x/L=0.250, x/L=0.500, and x/L=0.750 observation points respectively under 0.02 m/h rainfall intensity. On the other hand, the discrepancies 9%, 10%, and 12% corresponding to x/L=0.250, x/L=0.500, and x/L=0.750 observation points respectively under 0.04 m/h rainfall intensity. Then, the discrepancies 11%, 7%, and 13% corresponding to x/L=0.250, x/L=0.500, and x/L=0.750 observation points respectively under 0.07 m/h rainfall intensity

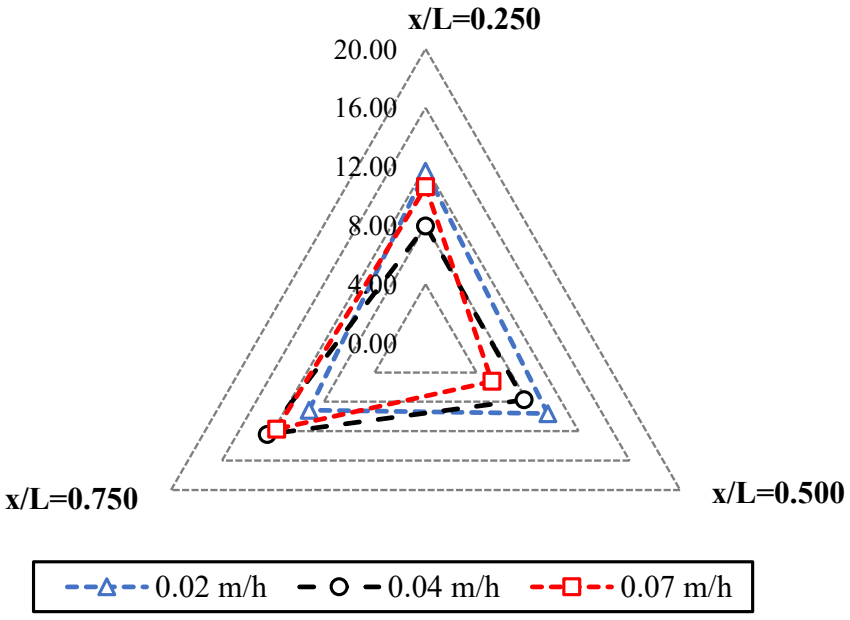

Fig 6.23 Local Safety Factor (LSF) discrepancies.

Therefore, it can be concluded that the Local Safety Factor (LSF) from disturbed samples do not properly represent the Local Safety Factor (LSF) from the undisturbed samples with significant discrepancies that should be considered when conducting the analysis especially for the reinforcement of slope stability which related to the economical consideration.

6.4.3 Influence of initial suction value on the slope stability characteristics

Table 6.3. The input shear strength properties

Initial suction (kPa)	Initial volumetric water content (θ)	Shear strength Properties
30	0.730	Cohesion = 7.92 kN/m^2 ϕ = 22^o
60	0.700	Cohesion = 10 kN/m^2 ϕ = 22^o
80	0.680	Cohesion = 14.14 kN/m^2 ϕ = 21.94^o

The obtained results of the shear strength properties from the suction-controlled direct shear box apparatus (Chapter 5) on the slope stability was evaluated. The initial volumetric water content and shear strength respect to the suction value was adopted as input parameter in the Hydrus 2-D Slope Cube as shown in Table 6.3.

Furthermore, 2 m depth of volcanic ash soil was adopted because of the precipitation event only affected till 2 m depth of volcanic ash soil which confirmed with the change of water content that related to the reduction of effective stress in the previous section. Fig 6.24 illustrates the detail of observation points.

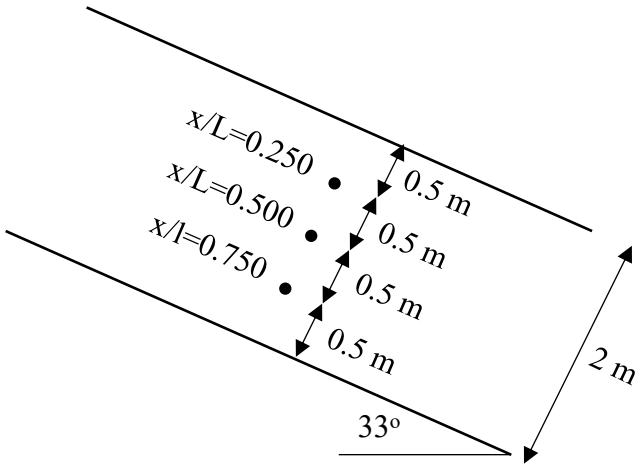

Fig 6.24 The detail of observation points.

Fig. 6.25 illustrates the development of the effective stress with time monitored at three locations (x/L=0.250, 0.500 and 0.750) under different initial suction values. It can be observed that the obtained effective stress through the soil profile is significantly higher for the 80 kPa in comparison to the 60 kPa and 30 kPa suction value. It can be attributed to the provided initial conditions and boundary conditions, where the 80 kPa suction value indicates volumetric water content (θ) is higher in comparison to 60 kPa and 30 kPa. Furthermore, the time needed for the minimum effective stress is faster in the 30 kPa in comparison to the 60 kPa and 80 kPa suction value. It can be observed in the x/L=0.250, after 8.5 hours the effective stress indicates 0 kPa. However, in the 60 kPa and 80 kPa need time around 9 and 10 hours after precipitation. On the other hand, in the final time of precipitation in the observation point x/L=0.500, the effective stress indicates 300 kPa for 80 kPa suction value, 220 kPa for 60 kPa, and 180 kPa for 30 kPa suction value. It can be concluded that the initial suction value significantly affected the reduction of suction stress during precipitation events.

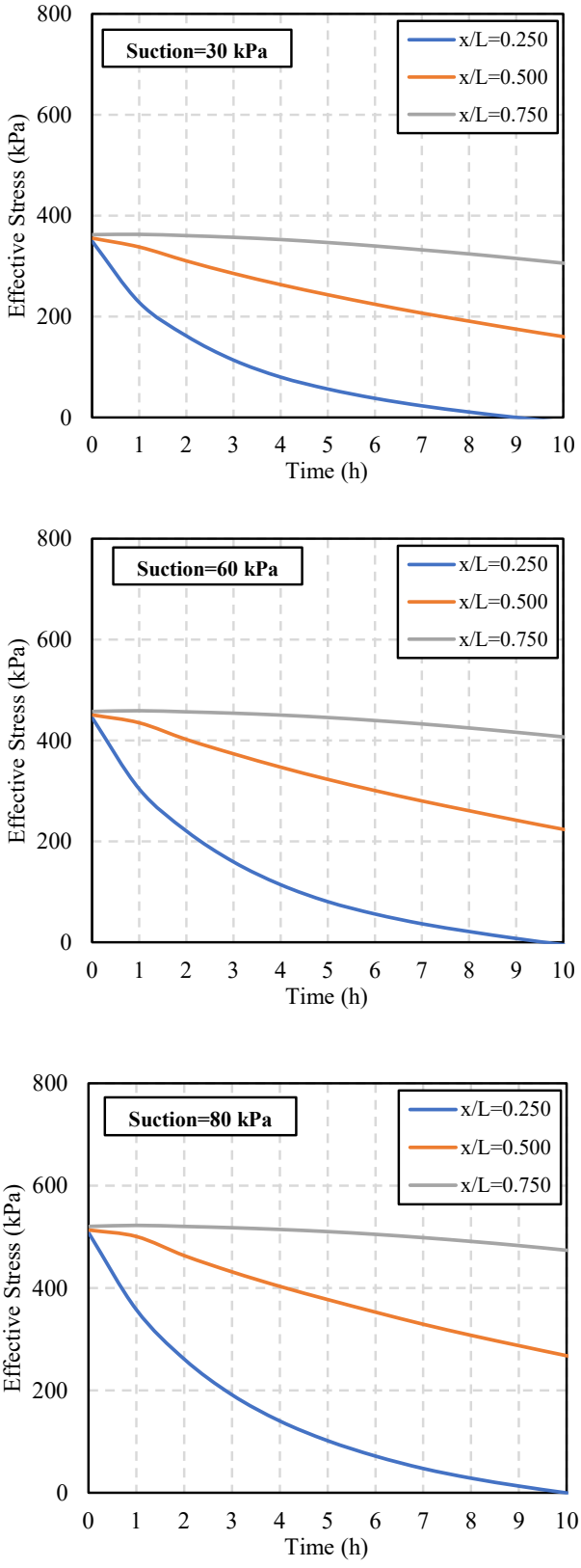

Fig 6.25 Effective stress development with time

Fig. 6.26 illustrates the Local Safety Factor of slope before precipitation (t = 0 h). From the obtained results, it can be observed that the safety factor of slope under 80 kPa suction in all observation points significantly larger in comparison to 30 kPa, and 60 kPa. Thus, it can be said that the safety factor of slope increases with increasing of suction value. Furthermore, in the observation point x/L=0.250 the safety factor of slope approximately 3 times larger than that of x/L=0.500. It can be concluded that the safety factor of slope decreases with increasing of the depth layer. The obtained results in good agreement with the calculation in section 6.3. and 6.4.1. Where the driving force of the depth layer significantly larger in comparison to the shallow layer.

Fig. 6.27 illustrates the reduction safety factor of slope and observation point depth ratio during precipitation. It can be observed that the safety factor of slope significantly reduces after precipitation. Furthermore, the observation point (x/L=0.250) shows that the precipitation imposes the safety factor of slope below 1. Reduction of the safety factor of slope related to the reduction of effective stress during precipitation. Furthermore, for the observation points (x/L= 0.500) and (x/L=0.750) reduction of the safety factor of slope also was confirmed. However, the safety factor of slope still in the stable condition. It must be noted that in all observation points, the 80 kPa suction indicates higher of safety factor in comparison to 30 kPa and 60 kPa. It can be concluded that the suction value imposes the higher resistance of the slope stability. On the other hand, it can be observed that a shallow depth layer imposes a higher reduction of Local Safety Factor. The obtained results opposite with the initial Local Safety Factor. Where the shallow depth indicates a higher Local Safety Factor. It can be concluded that the wetting process or precipitation events give a huge impact to the shallow layer of the volcanic ash soil.

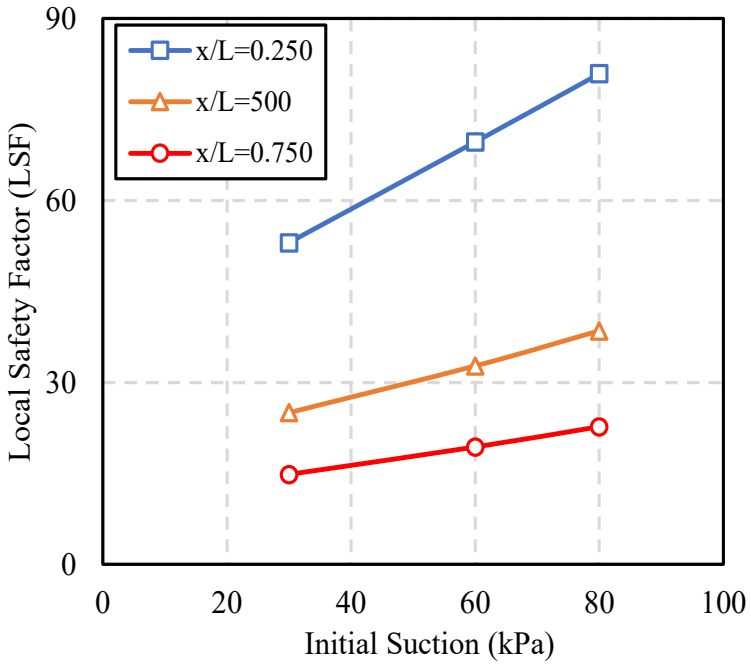

Fig 6.26 The Local Safety Factor of slope before precipitation (t = 0 h)

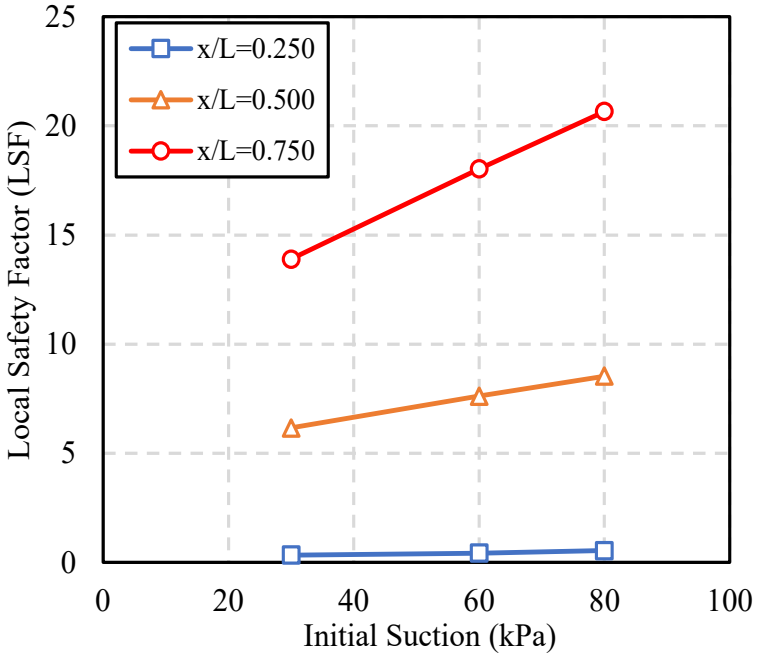

Fig 6.27 The Local Safety Factor of slope after precipitation (t = 5 h)

6.5 Summary

Through this chapter, the slope stability analysis of unsaturated volcanic ash soil was evaluated. The shear strength of the volcanic ash soil from the conventional and suction-controlled system was using as input properties in the slope stability analysis. The main conclusions are as follows:

1. The discrepancies of the soil shear strength between undisturbed and disturbed samples which related to the soil structure characteristics gives a huge impact on the safety factor of slope. Where in the disturbed sample is significantly lower both under static and seismic loading. It can be said that the disturbed samples do not properly represent the field conditions with significant discrepancies that should be carefully considered when conducting the slope stability analysis.
2. The safety factor of slope decreases with increasing of the depth layer. It can be related to the driving force of the depth layer significantly larger in comparison to the shallow layer. However, during precipitation events, the shallow depth layer imposes a higher average reduction of safety factors. It can be attributed to the change of water content which related to a decrease in effective stress during precipitation event events.
3. The safety factor of slope in the higher suction value significantly larger in comparison to the lower suction value. It can be attributed to the development of effective stress during precipitation events. Where in the higher suction value is significantly lower.

References

Alowaisy, A., Yasufuku, N., Ishikura, R., Hatakeyama, M., Kyono, S., 2019. Novel rapid measurement system of undisturbed soils water characteristics curve utilizing the continuous pressurization method. Proc. 7th International Symposium on Deformation Characteristics of Geomaterials (IS-Glasgow 2019), June 26-28, 2019, Glasgow: 92

Hung, C., Lin, G., Syu, H., Chen, C., Yen, H., 2017. Analysis of the Aso-Bridge landslide during the 2016 Kumamoto earthquakes in Japan. Bulletin of Engineering Geology and Environment.

Japan Road Association., 2012. Road Bridge Specification, V Seismic Design Edition, Maruzen Publishing Co., Ltd., December 21, 201

Kasama, K., Yamagata, S., Tanaka, H., Furukawa, Z., Yasufuku, N., 2018. Japanese Society Civil Engineers, in Japanese

Kawaguchi, Y., 2018. Kyushu University Thesis, in Japanese

Lu, N., and Likos, W. J. (2004). Unsaturated Soil Mechanics. Wiley.

Lu, N., and Likos, W. J. (2006). Suction stress characteristic curve for unsaturated soil. Journal of Geotechnical and Geoenvironmental Engineering, 132(2), 131-142.

Monjo, R., 2016. Measure of rainfall time structure using the dimensionless n-index. Climate Research, 67: 71-86

Newmark, N. M., 1965. Effects of earthquakes on dams and embankments. Géotechnique, 15 (2): 139–160

van Genuchten, M. T. (1980). A closed-form equation for predicting the hydraulic conductivity of unsaturated soils. Soil Science Society of America Journal, 44(5), 892-898.

Yamomoto, R., 2020. Kyushu University Thesis, in Japanese

CHAPTER VII

CONCLUSIONS AND FUTURE WORK

This thesis aims at the evaluation of shear strength characteristics of unsaturated-undisturbed volcanic ash soil subjected to static and cyclic loading for slope stability analysis. Furthermore, in this study, the soil was collected at Kumamoto slope failure 2016. In order to achieve the aim of this thesis, the following objectives were delineated:

1. To identify the shear strength behavior of the collected unsaturated undisturbed volcanic ash soil under static and cyclic loading.
2. To identify the effect of the soil structure disturbance on the shear strength of the volcanic ash soil by reflecting the pore size distribution differences of undisturbed and disturbed samples.
3. To develop the new suction controlled unsaturated direct shear box apparatus. The developed apparatus differs in its features and testing procedure in comparison to the conventional testing apparatus. The proposed procedure and apparatus configuration ensure easy testing, relatively short time, and low cost.
4. To analyze the stability of unsaturated slopes subjected to rainfall infiltration and earthquake loading. The analysis considers various loading and rainfall patterns and their influence on the slope stability adopting several slope stability evaluation methods.

7.1 Conclusions

The results of experimental and numerical research show that the objectives of this study have been met some limitations that need more investigation which has led to new scopes to be studied in the future as will be illustrated at the of this chapter. The main conclusions can be described as follows:

1. It was found that under static shearing, unsaturated undisturbed volcanic ash soil sample exhibits a higher the apparent cohesion and friction angle in comparison to the saturated sample condition. Furthermore, the normalized shear stress of the unsaturated undisturbed sample was found to be larger than that of the saturated sample under both one-sided and two-sided cyclic shearing. This can be attributed to the influence of the matric suction contribution in the total shear strength of soils. Then, in the post cyclic analysis, the normalized shear stress and vertical stress of volcanic ash soil dramatically reduced after cyclic loading.
2. Most of the shear strength properties determination considers remolded samples than that of undisturbed samples. Therefore, it is necessary to evaluate the effect of degree of disturbance on the volcanic ash soil which related to the soil structure characteristics. The obtained results showed the chemical composition of volcanic ash soil is comprised mainly from allophane which accounts for as high as about 94%. Furthermore, allophane behavior in response to the external load destroys the chemical structure of the allophane, consequently transforming the mineral into an amorphous mass with low strength.
3. It turned out that the undisturbed samples exhibit a unimodal pore structure and the disturbed samples exhibit a bimodal pore structure. Since the pore structure

of the disturbed sample is unstable, the static shear strength tends to be lower, and the degradation index value is around 20 % higher than that of the undisturbed sample. In other words, the cyclic normalized vertical stress of disturbed samples degrades faster under cyclic loading. It can be said that the disturbed sample do not properly represent the field conditions with significant discrepancies that should be carefully considered when conducting the slope stability analysis

4. It was found that the degradation index value in the normally consolidated samples was found to be larger than that of the over-consolidated samples. It might be associated with the increase in the pore water pressure during shearing, where the pore water pressure reduction in the over-consolidated sample is lower than that of the normally consolidated samples.
5. It turned out that the normalized vertical stress and shear stress of the unsaturated samples under static and cyclic loading is larger than that of saturated sample. This can be related to the influence of the matric suction which contributes to the total shear strength of the soil.
6. Since the conventional direct shear box apparatus considers only the initial condition for the unsaturated testing, to get more reliable and accurate results for unsaturated shear strength, the suction-controlled testing method is needed. It was found that the test for Toyoura sand as a confirmation of suction-controlled system was successfully performed in the new suction controlled direct shear box apparatus. On the other hand, the total shear strength of Toyoura sand strongly depends on the suction which can be observed with the new suction controlled direct shear box apparatus. Furthermore, the distribution of water drainage in the new suction controlled direct shear box apparatus is uniform. It

can be observed in the water content of unsaturated samples after the test.

7. It was found that in the volcanic ash soil results, the shear strength and stiffness of the soil increase with the increase in soil suction. The soil exhibits more dilative volumetric behavior as suction is increased. Similar results were observed under open valve and close valve condition for every group of three tests net normal stress (20 kPa, 40 kPa, and 60 kPa) with the four different suction values (0, 30, 60, and 80 kPa).
8. It turned out that in the open valve condition in the ceramic disc line, the shear strength is higher for every net normal stress in comparison with close valve condition. It might be attributed to the amount of water drainage during shearing process.
9. The results showed that the internal friction angle (ϕ) of volcanic ash soil is relatively independent of the increase in suction, and the apparent cohesion (c) increases with increasing the suction value.
10. The shear strength of the volcanic ash soil from the conventional and suction-controlled system was using as input properties in the slope stability analysis. It was found that the discrepancies of the soil shear strength between undisturbed and disturbed samples which related to the soil structure characteristics gives a huge impact on the safety factor of slope. Where in the disturbed sample is significantly lower both under static and seismic loading. It can be said that the disturbed samples do not properly represent the field conditions with significant discrepancies that should be carefully considered when conducting the slope stability analysis.
11. It turned out that the safety factor of slope decreases with increasing of the depth layer. It can be related to the driving force of the depth layer significantly larger

in comparison to the shallow layer. However, during precipitation events, the shallow depth layer imposes a higher average reduction of safety factors. It can be attributed to the change of water content which related to a decrease in effective stress during precipitation event events.

12. The safety factor of slope in the higher suction value significantly larger in comparison to the lower suction value. It can be attributed to the development of effective stress during precipitation events. Where in the higher suction value is significantly lower.

7.2 Future work

Although the objectives of this dissertation have been successfully achieved, further studies and research scopes are needed in order to enhance developed element testing of unsaturated soil. Some of the scopes and issues that require more investigation are listed as follows:

1. Since the distribution of volcanic ash soil covers approximately 31% of the total area of Japan, each area might be contained different characteristics. Thus, investigation of volcanic ash soil from other area is highly needed.
2. Evaluate of pore size characteristics of volcanic ash soil using Mercury Intrusion Porosimetry (MIP) is highly recommended as a comparison of pore size distribution from the SWCC.
3. The significance of discrepancies shear strength between undisturbed and disturbed samples was confirmed in this thesis, however a detailed theoretical study is highly needed.
4. The new unsaturated suction-controlled system was confirmed for low suction

and vertical stress (up to 100 kPa), where extending of the system to consider higher suction range (1500 kPa) is highly recommended.